Development of Robust Equilibrium Calculation Algorithms for Reservoir Fluids at Given Volume, Temperature and Composition

by

Chang Lu

A thesis submitted in partial fulfillment of the requirements for the degree of

Doctor of Philosophy

in

Petroleum Engineering

Department of Civil and Environmental Engineering
University of Alberta

ABSTRACT

Two-phase and three-phase equilibria can be frequently observed in the petroleum industry. To accurately predict the phase behavior of complex fluid mixtures lies at the core of the analysis and design of petroleum recovery and petrochemical processes. Normally, engineers or researchers rely on isothermal-isobaric (PT) algorithms to carry out the multiphase equilibrium computations for a given fluid mixture. In such algorithms, pressure, temperature, as well as the feed composition, are specified as inputs to the algorithm and the objective is to find out the number of phases in equilibrium, and their fractions, compositions and volumes. One alternative strategy to work out the multiphase equilibrium problem is to use volume, temperature and feed composition as known information, and find out pressure, the number of equilibrating phases and their properties. Such isothermal-isochoric (VT) equilibrium calculations are found to be more convenient in some engineering calculations (e.g., multiphase equilibrium in storage vessels) than the conventional PT equilibrium calculations. Our aim of this research is to develop more, robust, accurate and efficient algorithms to simulate phase equilibria for reservoir fluids using the Peng-Robinson EOS at specified volume, temperature and mole numbers.

Moreover, VT based phase equilibria calculation has its natural advantages to simulate the fluid phase behavior in nano-confined pores than PT-flash for that a nanopore can be considered as a volume constant system. Therefore, to give a more accurate prediction results, we develop a two-phase flash algorithm with the consideration of capillary pressure

at specified mole numbers, volume and temperature. By testing it against a number of examples, and comparing the results with the ones calculated by the pressure-temperature (PT) flash algorithm with the capillarity effect, we demonstrate the correctness and robustness of our algorithm. In addition, we examine the influence of capillary pressure on the two-phase envelope in the molar-density/temperature (cT) space. Example calculations are carried out to demonstrate the superior performance of the developed algorithm.

In addition to two-phase equilibria, three-phase equilibria are frequently encountered in a variety of petroleum engineering processes. In the second work, we develop a simple, robust VT three-phase flash calculation algorithm using a nested approach. The PT three-phase flash code is used in the inner loop, while an effective equation-solving method is applied to solve the pressure corresponding to a given volume-temperature specification. The robustness of the algorithm is safeguarded with the use of state-of-art trust-region-method-based solver in the PT three-phase flash program. By applying it to calculate the isochores of fluid mixtures, we demonstrate the robustness and efficacy of the developed algorithm in both two-phase and three-phase equilibrium calculations.

Furthermore, similar to the inaccurate liquid-density prediction issue in the isobaric-isothermal (PT) phase equilibrium calculations, an issue of inaccurate pressure prediction can also be observed in the VT phase equilibrium calculations which involves a liquid phase. In the third work, a practical methodology is proposed to incorporate a volume-translated equation of state for more accurate pressure predictions in VT phase equilibrium

calculations. By incorporating Abudour *et al.* (2012; 2013) volume-translated PR-EOS models into the VT-based phase equilibrium calculation algorithm, the accuracy of pressure prediction in the single liquid phase region for both pure substances and mixtures can be significantly improved. Lastly, we apply the proposed algorithm to the two-phase VT phase equilibrium calculations for the oil sample MY10. We found that more accurate pressure predictions can be obtained by applying the Abudour *et al.* VTPR-EOS to the VT flash results than those from the original VT-flash calculations.

PREFACE

A version of Chapter 2 has been published as Lu, C., Jin, Z., & Li, H. (2019). A two-phase flash algorithm with the consideration of capillary pressure at specified mole numbers, volume and temperature. Fluid Phase Equilibria, 485, 67-82. Lu, C. is responsible for the theoretical development, simulation results, analysis, and manuscript composition. Li, H. and Jin Z. are the supervisory authors and get involved in concept formation, theoretical development, analysis and manuscript composition.

A version of Chapter 3 was submitted to SPE Journal for publication as Lu, C., Jin, Z., Li, H. & Xu, L.* (2020) Simple and robust algorithm for isochoric-isothermal three-phase equilibrium computations. Lu, C. and Xu, L. are responsible for the theoretical development, simulation results, analysis, and manuscript composition. Li, H. and Jin Z. are the supervisory authors and get involved in concept formation, theoretical development, analysis, and manuscript composition.

A version of Chapter 4 will be submitted to *Fluid Phase Equilibria* for publication as Lu, C., Jin, Z., & Li, H. (2020). A practical methodology for incorporating the volume-translated equation of states in isochoric-isothermal phase equilibrium calculations. Lu, C. is responsible for the theoretical development, simulation results, analysis, and manuscript composition. Li, H. and Jin Z. are the supervisory authors and get involved in concept formation, theoretical development, analysis, and manuscript composition.

Chapter 1 summarizes the research background, problem statement, research objectives,

and thesis structure. Chapter 5 summarizes the conclusions reached in this thesis as well as

the recommendations for future research. Chapters 1 and 4 are originally written by Lu, C.

and have never been published elsewhere.

ACKNOWLEDGMENTS

DEDICATION

This dissertation is dedicated to my dearest parents: my mother Mrs. Yuhuan Bu and my

father Mr. Qingliang Lu.

Table of Contents

List of Tables

List of Figures

Nomenclature

a	attraction parameter, $L^2 \cdot bar \cdot mol^{-2}$
$a*$	normalized Helmholtz free energy
A	Helmholtz free energy
$AAD\%$	average percentage absolute deviation, %
b	repulsion parameter, L
c	overall mole density, mol/L
c_0	volume translation term
c_1	constant in Abudour *et al.* model [17]
C_{ij}, D_{ij}	binary interaction parameters
d	distance function, unit, cm
err	tolerance
F	volume function, L
K	equilibrium ratio
m	*number of components*
MW, Mw	molecular weight, *g/mol*
n	mole numbers, *mol*
NDP	number of data points
P	pressure, bar
P_0	initial pressure, *bar*
P_c	critical pressure, bar
P_{ca}	capillary pressure, bar
P_{cal}	calculated pressure, bar
P_{exp}	measured pressure, bar
P_t	pressure after translation
$P^{sat}(T)$	saturation pressure at temperature T, *bar*
R	Pore size, *nm*

R^g	gas constant, 8.314 J/(mol·K)
S	volume fraction
T	temperature, K
T_c	critical temperature, K
v	molar volume calculated by PR-EOS, L/mol
V	volume, L
v_c	critical volume predicted from PR-EOS, L/mol
v^{exp}_c	true critical volume, L/mol
v_t	molar volume after volume translation, L/mol
x	mole fraction of substance
z	feed composition
z_c^{exp}	experimental critical compressibility factor
z_c^{EOS}	compressibility factor calculated by PR-EOS, 0.3074
α	alpha function
β	phase fraction of vapor phase
δ	volume correction at critical temperature
θ	surface fraction of compound
μ	chemical potential, cp
ρ	molar density, mol/L
$\rho_{overall}$	overall molar density, mol/L
$\rho_{liquid}, \rho_{vapor}$	molar density of liquid/vapor phase, mol/L
σ	interfacial tension (IFT), dyne/cm
χ	parachor parameter
ω	acentric factor
Φ	volume function coefficient

Subscripts

i, j	component indicator

m	parameters for mixtures

Superscripts

L	liquid phase
V	vapor phase

CHAPTER 1 INTRODUCTION

1.1 Research Background

Phase behavior of reservoir fluids plays an important role in the recovery process of oil and gas resources. Two-phase equilibria and three-phase equilibria can be frequently observed in the upstream petroleum industry, such as CO_2 injection for enhanced oil recovery in low-temperature reservoirs, gas-liquid-liquid three-phase equilibria in the porous-media flow (Pan *et al.*, 2015) or pipe flow (Pasqualette *et al.*, 2020), gas-oil-water three-phase equilibria in steam injection process for heavy oil recovery (Gao *et al.*, 2017; Petitfrere *et al.*, 2020), etc. To accurately predict the phase behavior of complex fluid mixtures lies at the core of the analysis and design of petroleum recovery and petrochemical processes.

Computation of phase equilibria under given pressure, temperature, and chemical composition has been widely applied to simulate the phase behavior of reservoir fluids (Michelsen, 1982a; Michelsen, 1982b). It consists of the minimization of the Gibbs free energy with respect to mole numbers. In such algorithms, pressure, temperature, as well as the feed composition, are specified as inputs to the algorithm and the objective is to find out the number of phases in equilibrium, and their fractions, compositions and volumes. Even though pressure-temperature (PT) based formulation of the phase stability and flash calculation is widely used in the computational reservoir simulations, this approach has its limitations. One of the limitations of PT-based formulation using cubic equation of states

(CEOSs) is in that three roots of volume can be resulted under given pressure, temperature, and composition. This substantially increases the difficulty of choosing the correct mixture states.

One alternative strategy to work out the multiphase equilibrium problem is to use volume, temperature and feed composition as known information, and find out the pressure, the number of equilibrating phases and their properties (Michelsen, 1999). Such isothermal-isochoric (VT) equilibrium calculations are found to be more convenient in some engineering calculations (e.g., multiphase equilibrium in storage vessels) than the conventional PT equilibrium calculations (Cismondi *et al*., 2018).

Instead of minimizing the Gibbs free energy in isothermal-isobaric (PT) equilibrium calculations, an isothermal-isochoric (VT) equilibrium problem consists in the minimization of the Helmholtz free energy. Mikyška and Firoozabadi (2011) introduced two new concepts: volume function and volume function coefficient, which play the analogous roles to fugacity and fugacity coefficient in PT-flash. They firstly proposed a new numerical algorithm using the successive substitution iteration method (SSI) to solve the liquid-vapor two-phase equilibrium problem (Jindrova and Mikyska, 2013). Later, such an algorithm was successfully extended to three-phase flash calculations (Jindrova and Mikyska, 2013; Jindrova and Mikyska, 2015). Nichita (2018) developed a new unconstrained Helmholtz-free-energy minimization method used for conducting robust VT flash calculations. At a given iteration level, Nichita (2018) treats volume as a variable

dependent on mole numbers and solves such dependence by working out a nonlinear volume balance equation.

Nowadays, the unconventional reservoirs, such as shale and tight reservoirs, play very important roles in fulfilling the global energy supply. The shale/tight reservoirs have a significant amount of nanoscale pores, resulting in a much lower permeability than the conventional reservoirs. Under nano-confinement, the phase behavior of petroleum fluids is very different from the bulk due to strong interactions between fluid and pore-wall (Parsa *et al.*, 2015). Accurate modeling of the fluid phase behavior in the shale/tight reservoirs is essential for the reliable estimation of hydrocarbons in place as well as the proper understanding of the mechanisms governing the oil/gas production from these reservoirs. One of the approaches is using an equation of state to simulate the liquid-vapor two-phase equilibrium by considering capillary pressure. A number of works have been done to model the reservoir fluid properties and phase behaviors by considering the effect of capillary pressure at specified pressure and temperature (Nojabaei *et al*., 2013; Sandoval *et al*., 2016; Stimpson *et al*., 2016). However, VT-flash has its natural advantages to simulate the fluid phase behavior in nano-confined pores than PT-flash for that the pores can be considered as a volume constant system. However, the two-phase equilibrium simulation by considering the effect of capillary pressure at specified volume and temperature (VT-flash) were rarely studied.

In addition to the development of a two-phase equilibrium calculation algorithm, the

development of a robust VT flash algorithm for three-phase equilibria is rather important. However, it is a non-trivial task to set up the VT flash code based on the Helmholtz-free-energy minimization approach. Meanwhile, different from the Helmholtz-free-energy minimization approach, Michelsen (1999) proposed another so-called nested optimization approach for phase equilibrium computations at a variety of flash specifications (such as pressure-enthalpy (PH) specification and VT specification). In the nested approach, a PT flash is solved in the inner loop, while the pressure and/or temperature are solved by maximizing the Q function in the outer loop. The advantage of such nested approaches lies in that they are very easy to implement, and their robustness can be well assured if the inner PT flash code is robust.

Moreover, different from PT-flash algorithms, pressure becomes one of the outputs in the VT-based phase behavior calculations, which is calculated at specified volume, temperature and composition. As using VT-based formulations to predict the reservoir fluid phase behavior becomes increasingly attractive, the accuracy of pressure prediction becomes an emerging issue. Subject to the limitations of the two-parameter nature of the cubic equation of state (CEOS), the predicted relation between pressure and volume at a given temperature and composition by CEOS is not accurate (Martin, 1967). Similar to the inaccurate liquid density prediction issue in the PT-based phase behavior calculations, pressure may fail to be predicted accurately by VT-based phase behavior calculations. Due to the large slope of the pressure-volume/density curve in the liquid phase, a small

volume/density error may lead to a very inaccurate pressure prediction by CEOS in VT-based calculations. This issue has been overlooked in previous studies.

1.2 Problem Statement

Normally, engineers or researchers rely on PT algorithms to carry out the multiphase equilibrium computations for a given fluid mixture, which is relatively well-developed. VT algorithms for multiphase equilibrium calculations are competitive alternatives to PT algorithms, although much more research is needed to develop robust, reliable and efficient VT algorithms. We are still lacking robust and efficient VT two-phase and three-phase equilibrium calculation algorithms which can be reliably integrated with compositional simulators. The main research problems to be addressed in this dissertation include the following:

- Robust algorithms of two-phase VT-flash computations applicable to confined pores are rarely developed. Only Kou and Sun (2018) proposed a dynamic algorithm to simulate the phase equilibria by considering the capillarity at specified moles, volume and temperature; such an algorithm is developed based on the convex-concave splitting of the Helmholtz energy density. They depicted phase molar density, phase saturation and pressure at equilibrium along with the change of temperature or overall molar densities. But they did not present an entire two-phase envelope with the consideration of the effect of capillarity. Meanwhile, the influence of capillary pressure on the two-phase envelope in molar-

density/temperature (cT) space is not discussed.

- There are several robust VT equilibrium calculation algorithms developed based on the Helmholtz-free-energy minimization approach. However, it's not a trivial task to configure the VT flash code using such a Helmholtz-free-energy minimization approach. In comparison, the nested approach using the PT flash code in the inner loop is much easier to configure. Due to the fact that the PT equilibrium calculation algorithms are relatively well developed, can we develop an easy-to-implement and robust three-phase VT flash code by using the nested approach?

- The prediction accuracy of pressure is inferior in the VT-based phase equilibrium calculations. How to improve it? Can we use the state-of-art volume translation model, which is recently developed to correct the liquid density predictions in PT-based formulations, to correct the pressure predictions in VT-based phase equilibrium calculations? If so, how to incorporate the volume translation in VT-based formulations. And, finally, how effective is the incorporation?

1.3 Objective

The objective of this research is to develop more robust, accurate and efficient algorithms to simulate two-phase and three-phase equilibria for reservoir fluids using the Peng-Robinson (PR) EOS (Peng and Robinson, 1976) at specified volume, temperature and mole numbers. The detailed objectives are listed as follows:

6

- Develop an accurate and robust two-phase flash algorithm with the consideration of capillary pressure at specified volume, temperature and mole numbers which can simulate the two-phase equilibrium in nanopore-rich porous media.

- Develop a simple and robust algorithm for VT three-phase equilibrium computations by using the nested approach, which can be easily implemented and configured by practicing engineers to carry out VT three-phase equilibrium computations if a reliable PT flash code is available.

- Develop a practical methodology for incorporating volume-translated equation of states in VT phase equilibrium calculations, which can provide more accurate pressure predictions in both single liquid-phase region and two-phase equilibrium region.

1.4 Thesis Structure

There are five chapters in this dissertation. In Chapter 1, we introduce the research background, the problem statement, and the major research objectives. Chapter 2 presents the development of the two-phase flash algorithm with the consideration of capillary pressure at specified volume, temperature and mole numbers. Chapter 3 depicts a simple and robust algorithm for VT three-phase equilibrium computations that is developed by using the nested approach. Chapter 4 develops a practical methodology for incorporating volume-translated equation of states in VT phase equilibrium calculations. Finally, Chapter 5 summarizes the conclusions of the thesis research and the recommendations for future

work.

1.5 References

Cismondi, M., Ndiaye, P.M., and Tavares, F.W. (2018). A new simple and efficient flash algorithm for T-v specifications. *Fluid Phase Equilibria*, **464**, 32-39.

Gao, J., Okuno, R., and Li, H. (2017). An experimental study of multiphase behavior for n-butane/bitumen/water mixtures. *SPE Journal*, **22**(3), 783-798.

Jindrova, T., and Mikyska, J. (2013). Fast and robust algorithm for calculation of two-phase equilibria at given volume, temperature, and moles. *Fluid Phase Equilibria*, **353**, 101-114.

Jindrova, T. and Mikyska, J. (2015). General algorithm for multiphase equilibria calculation at given volume, temperature, and moles. *Fluid Phase Equilibria*, **393**, 7-25.

Kou, J., and Sun, S. (2018). A stable algorithm for calculating phase equilibria with capillarity at specified moles, volume and temperature using a dynamic model. *Fluid Phase Equilibria*, **456**, 7-24.

Martin, J. J. (1967). Equations of state—Applied thermodynamics symposium. *Industrial & Engineering Chemistry*, **59**(12), 34-52.

Michelsen, M. L. (1982a). The isothermal flash problem. Part I. Stability. *Fluid Phase Equilibria*, **9**(1), 1-19.

Michelsen, M. L. (1982b). The isothermal flash problem. Part II. Phase-split calculation. *Fluid Phase Equilibria*, **9**(1), 21-40.

Michelsen, M. L. (1999). State function based flash specifications. *Fluid Phase Equilibria*, **158-160**, 617-626.

Mikyska, J. and Firoozabadi, A. (2011). A new thermodynamic function for phase-splitting at constant temperature, moles, and volume. *AIChE Journal*, **57**(7), 1897-1904.

Nichita, D.V. (2018). New unconstrained minimization methods for robust flash calculations at temperature, volume and moles specifications. *Fluid Phase Equilibria*, **466**, 31-47.

Nojabaei, B., Johns, R. T., and Chu, L. (2013). Effect of capillary pressure on phase behavior in tight rocks and shales. *SPE Reservoir Evaluation & Engineering*, **16**(3), 281-289.

Pan, H., Chen, Y., Sheffield, J., Chang, Y. B., and Zhou, D. (2015). Phase-behavior modeling and flow simulation for low-temperature CO_2 injection. *SPE Reservoir Evaluation & Engineering*, **18**(02), 250-263.

Parsa, E., Yin, X., and Ozkan, E. (2015). Direct observation of the impact of nanopore confinement on petroleum gas condensation. In *SPE Annual Technical Conference and Exhibition*. Society of Petroleum Engineers.

Pasqualette, M.D., Carneiro, J., Johansen, S.T., Lovfall, B.T., Fonseca Jr., R., and

Ciambelli, J. (2020). A numerical assessment of carbon-dioxide-rich two-phase flows with dense phases in offshore production pipelines. *SPE Journal*, **25**(2), 712-731.

Peng, D. Y., and Robinson, D. B. (1976). A new two-constant equation of state. *Industrial & Engineering Chemistry Fundamentals*, **15**(1), 59-64.

Petitfrere, M., Nichita, D.V., Voskov, D., Zaydullin, R., and Bogdanov, I. (2020). Full-EoS based thermal multiphase compositional simulation of CO_2 and steam injection processes. *Journal of Petroleum Science and Engineering*, **192**, 107241.

Sandoval, D. R., Yan, W., Michelsen, M. L., and Stenby, E. H. (2016). The phase envelope of multicomponent mixtures in the presence of a capillary pressure difference. *Industrial & Engineering Chemistry Research*, **55**(22), 6530-6538.

Stimpson, B. C., and Barrufet, M. A. (2016). Thermodynamic modeling of pure components including the effects of capillarity. *Journal of Chemical & Engineering Data*, **61**(8), 2844-2850.

CHAPTER 2 A TWO-PHASE FLASH ALGORITHM WITH THE CONSIDERATION OF CAPILLARY PRESSURE AT SPECIFIED MOLE NUMBERS, VOLUME AND TEMPERATURE

A version of this chapter has been published in *Fluid Phase Equilibria*.

Abstract

In this work, we develop an alternative two-phase flash algorithm with the consideration of capillary pressure at specified mole numbers, volume, and temperature. This algorithm is built upon the volume-temperature (VT) two-phase flash algorithm as proposed by Mikyška and Firoozabadi (2012), which relies on the use of the newly defined volume function and volume function coefficient. Our algorithm contains two loops: an inner loop and an outer loop. In the inner loop, the interior point method is used to solve the vapor-phase fraction by minimizing the objective function. In the outer loop, the volume fraction of the vapor phase is updated by solving the pressure equilibrium equation which simultaneously considers the capillary pressure between the two phases; herein, we first divide the interval (0, 1) to 1000 subintervals and then apply the bisection method in each subinterval. This method is used to robustly solve the pressure equilibrium equation. The capillary pressure is calculated using the Young-Laplace equation on the basis of the interfacial tension predicted by the parachor model. Eventually, knowing the volume fractions enables one to update the equilibrium ratios in the outer loop. We demonstrate the correctness and robustness of our algorithm by testing it against four fluid mixtures, including binary and ternary mixtures. The two-phase envelope obtained from the VT-flash algorithm with capillarity effect has shown excellent agreement with the pressure-temperature (PT) flash algorithm with capillarity effect. In addition, we examine the influence of capillary pressure on the two-phase envelope in the molar-density/temperature

(cT) space.

Keywords: VT flash; Phase split calculation; Capillary pressure; Nanopore; Confinement

effect

2.1 Introduction

Nowadays, unconventional reservoirs, such as shale oil/gas and tight oil/gas reservoirs, play very important roles in fulfilling the global energy supply. Shale reservoirs have significant amount of nanoscale pores, resulting in much lower permeability than the conventional reservoirs. Tight sandstone reservoirs consist of pores with diameters ranging between about 30 nm and 2 μm [1], while shale reservoirs consist of micropores smaller than 2 nm and mesopores with diameters ranging between 2 nm and 50 nm [2]. Under nano-confinement, phase behavior of petroleum fluids is very different from the bulk due to strong interactions between fluid and pore-wall [3]. The deviation of phase behavior of fluid in nano-confined pores from the bulk has been shown by many experimental works [4-6]. Accurate modeling of the fluid phase behavior in tight/shale reservoirs is essential for the reliable estimation of hydrocarbons in place as well as the proper understanding of the mechanisms governing the oil/gas production from these reservoirs [7].

Besides experimental works, many theoretical and modeling studies have been conducted to simulate the effect of confinement on fluid phase behaviour in confined spaces. For example, equation of sate by considering capillary pressure [8], GCMC simulations [9] and DFT simulations [7] have been used to predict the phase behavior of fluid in confined pores for mixtures. In particular, the method of incorporating the capillarity effect into an equation of state (EOS) can be readily implemented in a reservoir simulator due to its high computational efficiency. A number of works have been done to model the reservoir fluid

properties and phase behaviors by considering the effect of capillary pressure at specified

pressure and temperature [8, 11-13]. Young-Laplace [10] equation is widely applied to

characterize the capillary pressure in sufficiently narrow pores, in which the Bond number

of the fluid is relatively low. Nojabaei *et al.* [8] used Young-Laplace equation with equal

principle radii of curvature to model the capillary pressure, and coupled with Peng-

Robinson equation of state (PR-EOS) [14] to examine the effect of capillary pressure on

the phase behaviour in nano-scale pores. They demonstrated that the capillary pressure

induced by the pore sizes ≤ 50 nm significantly alters the phase boundary. They also found

that, due to the capillarity, the bubble point pressures and lower dew point pressures

decrease, while the upper dew point pressures increase. The existence of capillary pressure

also affects the mass densities, saturations and viscosities of the equilibrating phases.

Sandoval *et al.* [11] modeled phase behaviors for multicomponent mixtures at different

capillary radii using PR-EOS, and found out that in addition to the shift of bubble and dew

points due to the capillarity, the cricondentherm is shifted to a higher temperature.

Stimpson and Barrufet [12] estimated phase boundaries and fluid properties of a single

component in a single pore using PR-EOS at specified pressure and temperature. They

considered different radii of curvature in Young-Laplace equation and corrected the molar

volume using volume shift parameter. Their thermodynamic modeling approaches have

shown good agreement with molecular simulation data for light components such as carbon

dioxide and methane in a confined pore with a diameter equal to 4 nm, when the condition

is away from the bulk critical point. Sherafati and Jessen [13] proposed effective and robust

algorithms for stability testing based on the tangent plane distance criteria by considering the capillary pressures for multicomponent reservoir fluid mixtures over a wide range of temperatures, pressures and pore radii.

Vapor-liquid phase equilibrium can be computed under constant pressure and temperature conditions (PT-flash), as well as under other specifications including specified volume and temperature conditions (VT-flash) and specified pressure and enthalpy conditions (PH-flash) [15]. When temperature, volume and mole numbers are known, VT-flash should be applied to determine the vapor-liquid phase equilibrium. The VT-flash algorithms at given volume, temperature and mole numbers are implemented based on minimizing the total Helmholtz free energy [15]. The advantage of VT-flash is that it provides a unique pressure in the majority of physically admissible conditions for a given volume, which contrasts with the PT flash where three roots of volume are obtained by solving a cubic equation of state. Both of the nested optimization approach and the Newton approach are used by Michelsen [15] to solve the VT-flash. In 2011, Mikyška and Firoozabadi [16] proposed a new numerical algorithm using successive substitution iteration method (SSI) to solve the VT-flash problem. They introduced two new concepts - volume function and volume function, to make the formulation more convenient. In their algorithm, volume function and volume function coefficient play the analogous roles to fugacity and fugacity coefficient in PT-flash [16]. In the algorithm, a polynomial of degree 5 should be solved in the outer loop. They illustrated that only one root would be found in the interval (0,1) in

their tested examples. In 2013, Jindrová and Mikyška [17] solved the VT-flash by minimizing the Helmholtz free energy with Newton method. In 2018, Dan Vladimir Nichita [18] provided a new method for phase equilibrium calculations at constant temperature, volume and mole numbers (VTN flash). But it is noted that all the above works are dedicated to the VT-flash under bulk condition without the presence of capillarity. In 2017, Kou and Sun [18] proposed a dynamic algorithm to simulate the phase equilibrium by considering the capillarity at specified moles, volume and temperature; such algorithm is developed based on the convex-concave splitting of the Helmholtz energy density. Both pure-substance and binary mixtures were used to test the robustness of their algorithm. They depicted phase molar density, phase saturations and pressure at equilibrium along the change of temperature or overall molar densities. But, they did not present an entire two-phase phase envelope that is drawn by considering the effect of capillarity.

In this work, we propose an alternative algorithm to incorporate the effect of capillary pressure into the VT-flash calculation in order to study the effect of confinement on the phase behavior of hydrocarbon fluid mixtures. Our algorithm is based on the framework of volume function proposed by Mikyška and Firoozabadi in 2011 [16]. The problem of properly selecting the correct root out of a polynomial of degree 5 is solved in our work. Two loops are contained in our algorithm. The interior point method is used in the inner loop to solve the vapor-phase fraction by minimizing the objective function proposed [20-

21]. Capillarity between two phases is taken into consideration when we update the volume fraction of vapor phase in the outer loop. Young-Laplace equation [10] is used to simulate the capillary pressure, while the interfacial tension (IFT) is predicted by the parachor model [22] that considers the dependence on both composition and phase mole density. Four examples are used to calibrate our algorithm and test its robustness. We also compare our algorithm against the PT-flash algorithm with capillarity. Then, we use the VT-flash with capillarity to formulate the entire envelope in the overall molar density/temperature (cT) space.

This chapter is structured as follows. In section 2.2, we present the mathematical formulations governing the vapor-liquid equilibrium with the consideration of the effect of capillary pressure at specified volume, temperature and mole numbers. We use PR-EOS [10] to model the phase behavior of multicomponent mixtures. In section 2.3, we describe the numerical implementation of the two-phase VT-flash algorithm considering the effect of capillary pressure. In section 2.4, four examples are used to calibrate our algorithm and test its robustness of our model. Firstly, we compare our results with those given by PT-flash with capillarity. Then, we discuss the influence of capillary pressure on the phase boundaries in the cT space, and the variations in the equilibrium pressure, mass density, saturation and mole fraction of each component in the vapor and liquid phases as a function of overall molar density at a given temperature. In section 2.5, we discuss the potential insights and implications of our work.

2.2 Mathematical Formulations

In this work, we use the capillary pressure to account for the effect of confinement on vapor/liquid equilibrium. A mixture of m components with mole numbers $n_1, n_2, \ldots$ in a constant volume V at a given temperature T reaches the equilibrium state when the total Helmholtz energy of the mixture is at minimum. Assume that the mixtures are split into liquid/vapor two phases with volumes of V^L and V^V, respectively, and mole numbers of each component in each phase are n_i^L and n_i^V ($i = 1, 2, \ldots$), respectively. Considering the effect of capillary pressure P_{ca}, the necessary condition for the phase equilibrium is [18],

$$P^V \left(V^V, T, n_1^V, n_2^V, \ldots \right) \qquad \ldots \qquad (2.1)$$

and

$$\mu_i^V \left(V^V, T, n_1^V, n_2^V, \ldots \right) \qquad \ldots \qquad \ldots \qquad , \qquad (2.2)$$

in which P^V and P^L depict the vapor and liquid phase pressures, respectively, and μ_i^V and μ_i^L represent the chemical potentials of i-th component in the vapor phase and liquid phase, respectively. In order to solve Eq. (2.2) at specified volume, temperature and mole numbers, Mikyška and Firoozabadi [16] proposed a new concept: volume function F. This concept is introduced for the purpose of making the formulation of VT-flash more convenient. The volume function of i-th component $F_i = F_i(V, T, n_1, n_2 \ldots)$ can be expressed by the following properties [16],

$$\mu_i\left(V_2,T,n_1,n_2,\ldots\right) \qquad \ldots \qquad \frac{F_i\left(V_2,T,n_1,n_2\ldots\right)}{F_i\left(V_1,T,n_1,n_2\ldots\right)} \tag{2.3}$$

and

$$\lim_{V\to+\infty}\frac{F_i\left(V,T,n_1,n_2\ldots\right)}{V} \qquad = \ldots \tag{2.4}$$

Furthermore, they also related ideal fluid volume to volume function through the dimensionless volume function coefficient Φ_i by [16],

$$\Phi_i\left(V,T,n_1,n_2\ldots\right) \qquad \frac{F_i\left(V,T,n_1,n_2\ldots\right)}{V} \qquad . \tag{2.5}$$

In term of volume function coefficient, Eq. (2.2) can be equivalently expressed as [16],

$$\frac{n_i^V}{V^V\Phi_i^V\left(V^V,T,n_1^V,n_2^V,\ldots\right)} \qquad - \qquad n_i^L \qquad \ldots \qquad . \tag{2.6}$$

The volume function F_i and volume function coefficient Φ_i play similar roles with fugacity and fugacity coefficients which are widely used in the PT flash. The volume function coefficient Φ_i can be calculated by the following equation [16]:

$$\ln\Phi_i\left(V,T,n_1,n_2\ldots\right) \qquad \int_V^{+\infty}\left[\frac{1}{V}-\frac{1}{R^gT}\frac{\partial P}{\partial n_i}\right] \qquad \ldots \tag{2.7}$$

where R^g is the universal gas constant; Φ_i is a function of phase volume and composition.

We use the Young-Laplace equation [10] to calculate the capillary pressure, assuming equal principle radii of curvature and zero contact angle,

20

$$P_{ca} = \frac{2\sigma}{R} \tag{2.8}$$

where R is the pore radius, and σ is the bulk vapor-liquid IFT. Weinaug and Katz provided the following equation to calculate the IFT between the liquid phase and vapor phase [22]:

$$\sigma = \left[\sum_{i}^{m} \chi_i \left(x_i^L c^L - x_i^V c^V \right) \right]^4 \tag{2.9}$$

where χ_i represents the Parachor number of component i, c^L and c^V are the molar density of the liquid phase and vapor phase, respectively, x_i^L and x_i^V are the mole fractions of component i in the liquid phase and vapor phase, respectively.

2.3 Numerical Implementation of Two-phase VT Flash with Capillarity

To solve the two-phase split problem at constant volume, temperature and mole numbers, it is convenient to use molar density, phase volume faction and mole fraction to express the phase equilibrium conditions [16]. Mikyška and Firoozabadi provided the following definitions [16]: $c = n/V$ is the overall molar density; $c^V = n^V/V^V$ and $c^L = n^L/V^L$ are the molar densities of the vapor phase and liquid phase, respectively; $S^V = V^V/V$ and $S^L = V^L/V$ are the phase volume fractions of the vapor phase and liquid phase, respectively. The overall mole fraction of the i-th component is $z_i = n_i/n$ and the mole fractions of the vapor phase and liquid phase are $x_i^L = n_i^L/n^L$ and $x_i^V = n_i^V/n^V$, respectively.

Rachford-Rice (RR) equation is solved in the inner loop of the two-phase split algorithm [23].

$$\sum_{i=1}^{m}\left(x_i^V - x_i^L\right) = \sum_{i=1}^{m}\frac{\left(K_i - 1\right)z_i}{1 + \left(K_i - 1\right)\beta} = 0 \quad, \tag{2.10}$$

where $K_i = x_i^V/x_i^L$ is the equilibrium ratio, and $\beta = c^V S^V/c$ is the mole fraction of the vapor phase. In this work, we solve the RR equation based on a minimization method by imposing a more realistic feasible region [19-20, 24]. This feasible region is derived based on the consideration that the mole fractions of each component in both phases lie within the range of [0,1]. The mathematical formulations of the objective function and constraint are shown as below [19-20, 24],

$$\begin{cases} \min : F(\beta) = \sum_{i=1}^{m} -z_i \ln\left[1 - \beta(1 - K_i)\right] \\ \text{subject to} : \beta\left(1 - K_i\right) \leq \min\left\{1 - z_i, 1 - K_i z_i\right\}, i = 1, 2, \ldots \end{cases} \tag{2.11}$$

The above formula contains $m + 1$ variables including $\{K_i\}$ and β. The equilibrium ratio K_i should be firstly initialized using Wilson correlation and then updated in the outer loop. The Wilson correlation is given as [25],

$$\ln K_i = 5.37(1 - \omega_i)\left[1 - \frac{T_{ci}}{T}\right] + \ln\frac{P_{ci}}{P_0} \tag{2.12}$$

where ω is acentric factor, T_c is critical temperature, P_c is critical pressure and P_0 is the initial pressure. Unlike PT-flash calculation, the initial pressure is unknown in VT-flash calculation. Mikyška and Firoozabadi [26] proposed a method for initializing the VT-flash

algorithm based on the saturation pressure $P_i^{sat}(T)$ of each component i at temperature T. Eqs. (2.13) and (2.14) are used to estimate the initial vapor phase pressure P_0 for the conditions near the bubble point and dew point, respectively [26]:

$$P_0 = \sum_{i=1}^{m} P_i^{sat}(T)z_i, i = 1,2,\ldots \tag{2.13}$$

$$\left\{ \begin{array}{l} P_0 = \displaystyle\sum_{i=1}^{m} P_i^{sat}(T)x_i^0, i = 1,2,\ldots \\[2em] x_i^0 = \dfrac{z_i / P_i^{sat}(T)}{\displaystyle\sum_{j=1}^{m} z_i / P_j^{sat}(T)}, i = 1,2,\ldots \end{array} \right\}. \tag{2.14}$$

Once β and the mole fractions of each component in both phases are obtained in the inner loop, we proceed to the outer loop to update the equilibrium ratios K_i based on volume function coefficient Φ_i. To calculate the volume function coefficients of both phases, phase molar densities are needed. Phase molar densities can be obtained from the pressure equilibrium equation as given by Eq. (2.1). In terms of overall molar density, vapor phase volume fraction and mole fraction, molar volumes of vapor and liquid phases v^V and v^L can be rewritten as [16],

$$v^V = \frac{S^V}{c\beta} \text{ and } v^L = \frac{1-S^V}{c(1-\beta)}. \tag{2.15}$$

The molar densities of both phases c^V and c^L are given as [16],

$$c^V = \frac{c\beta}{S^V} \text{ and } c^L = \frac{c(1-\beta)}{1\text{-}S^V} . \tag{2.16}$$

Then, Eq. (2.1) can be expressed as

$$P^V \left[\frac{S^V}{c\beta}, T, x_1^V, x_2^V, \ldots \right] \quad \left[\ldots \right] \quad \ldots \quad \left[\ldots , \frac{c(1-\beta)}{1\text{-}S^V} \right]. \tag{2.17}$$

The only unknown term in Eq. (2.17) is the volume fraction of the gas phase S^V. Once the gas phase volume fraction is obtained, phase molar densities, volume fraction of liquid phase and volume function coefficients can be calculated. To solve the phase volume fraction S^V by considering the capillarity, we rewrite the Eq. (2.17) as a function of S^V:

$$f(S^V) = P^V \left[\frac{S^V}{c\beta}, T, x_1^V, x_2^V, \ldots \right] \quad \left[\ldots \right] \quad \ldots \quad \left[\ldots , \frac{c(1-\beta)}{1\text{-}S^V} \right] \tag{2.18}$$

The roots of S^V can be found by making $f(S^V)$ equal to zero.

Mikyška and Firoozabadi [16] illustrated that only one root of S^V for Eq. (2.18) can be found in the interval (0,1) in their tested examples, leading to Eq. (2.18) being readily solved by the bisection method. However, since either Eq. (2.17) or the counterpart equation given by Mikyška and Firoozabadi [16] (which does not consider capillary pressure) is a polynomial of degree 5, multiple real roots might appear in the interval (0,1). Based on our tests, although in most cases, only one root is found in the interval (0,1), three

or five real roots can actually appear near the dew points at relatively low temperatures. We take the binary mixture of methane (C_1) and normal pentane (nC_5) with a feed composition of (54.7413 mol% C_1, 45.2587 mol% nC_5) to illustrate the possible number of real roots appearing in Eq. (2.18). At a relatively high temperature of $T=371$K, we determine the number of real roots (S^V) at three different molar densities corresponding to a bubble point, a two-phase equilibrium and a dew point. At a relatively low temperature of $T=280$K, we determine the number of real roots (S^V) at four different molar densities corresponding to a bubble point, a two-phase equilibrium near the bubble point, a two-phase equilibrium in the middle of the two-phase region, and a dew point.

To test if the capillary pressure, which is also a function of S^V, will influence the number of real roots, we determine the number of real roots in Eq. (2.18) for the C_1-nC_5 mixture in a confined pore ($R=15$ nm) under different conditions. **Table 2-1** shows the number of real roots obtained. **Figures 2-1 and 2-2** show the variation of $f(S^V)$ vs. S^V calculated at $T=371$K under bulk conditions and under confined conditions ($R=15$ nm), respectively. The molar densities tested under bulk condition are $c=0.525, 5.000$ and 8.700 mol/L which correspond to mole fractions of the vapor phase $\beta=0.9989, 0.4566$ and 0.0120, while the molar densities tested under confined condition are $c=0.525, 5.000$ and 8.670 mol/L which correspond to mole fractions of the vapor phase $\beta=0.9837, 0.4510$ and 0.0073. We can observe from Figures 2-1 and 2-2 that, at the relatively high temperature of $T=371$K, only a single root can be detected; this is true for both bulk and confined conditions. **Figure 2-**

3 and 2-4 show the variation of $f(S^V)$ vs. S^V calculated at T=280K under bulk conditions and under confined conditions (R=15 nm), respectively. The molar densities tested under bulk condition are c=0.040, 0.100, 5.000 and 12.500 mol/L which correspond to mole fractions of the vapor phase β= 0.9149, 0.6943, 0.3904 and 0.0011, while the molar densities tested under confined condition are c=0.040, 0.100, 5.000 and 12.500 mol/L which correspond to mole fractions of the vapor phase β= 0.8922, 0.6951, 0.3961 and 0.0035. It can be seen from Figures 2-3 and 2-4, at the relatively low temperature of T=280K, 5 or 3 real roots can be detected near the dew point regardless of considering the capillarity effect or not; when the molar density increases to the bubble point, only single root can be detected. By comparing Figures 2-1 to 2-4, we can find that the capillary pressure P_{ca} will only shift the value of S^V but will not affect the number of real roots, albeit P_{ca} being also a function of S^V. In summary, considering that more than single root might be detected in some cases, the traditional bisection method becomes unreliable and cannot be used. To address this issue, we first divide the interval (0, 1) to 1000 subintervals and then apply the bisection method in each subinterval. As such, all the real roots of S^V can be securely found. Also, a total of 1000 subintervals are used to reach an accuracy of 0.001 for S^V.

Table 2-1 The number of real roots in Eq. (2.18) at different conditions.

T=371K						T=280K					
Bulk			R=15 nm			Bulk			R=15 nm		
c, mol/L	β	roots No.	c, mol/L	β	roots No.	c, mol/L	β	roots No.	c, mol/L	β	roots No.
0.525	0.9989	1	0.525	0.9837	1	0.040	0.9149	5	0.040	0.8922	5
5.000	0.4566	1	5.000	0.4510	1	0.100	0.6943	3	0.100	0.6951	3
8.700	0.0120	1	8.670	0.0073	1	5.000	0.3904	1	5.000	0.3961	1
-	-	-	-	-	-	12.500	0.0011	1	12.500	0.0035	1

T=371 K
c=0.525 mol/L
β=0.9989
S=0.99992 L/L

(a)
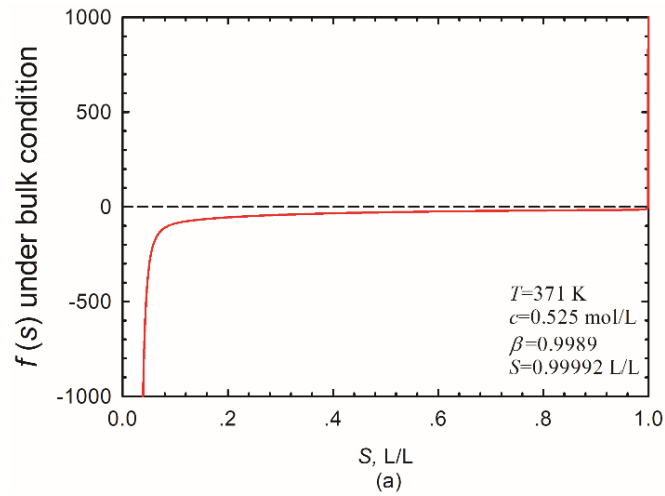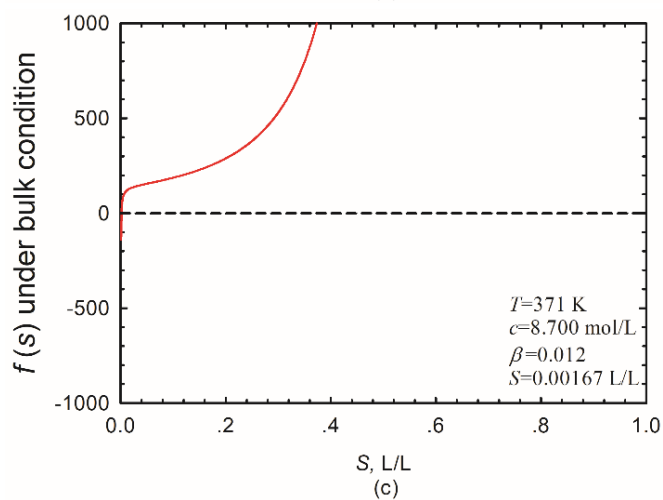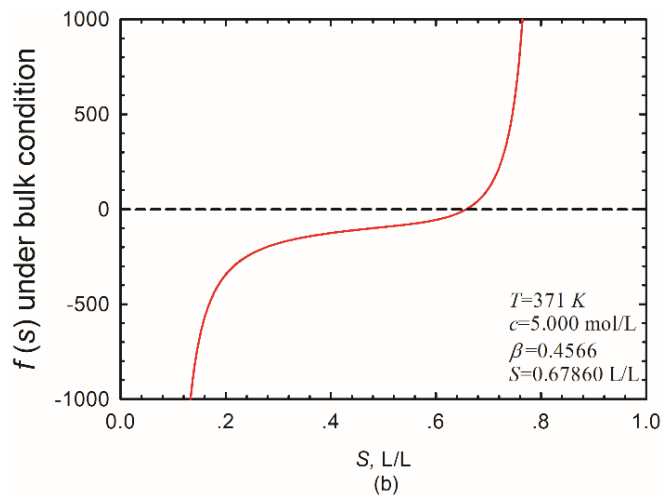
Figure 2-1 Variation of $f(S^V)$ vs. S^V under bulk condition (T=371K). The subplots (a), (b) and (c) show the calculated results at c=0.525, c=5.000 and c=8.700 mol/L (the corresponding mole fractions of the vapor phase are 0.9989, 0.4566 and 0.0120), respectively.
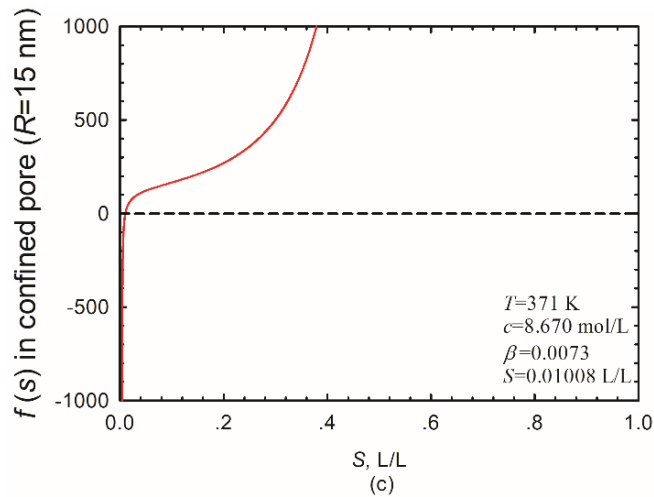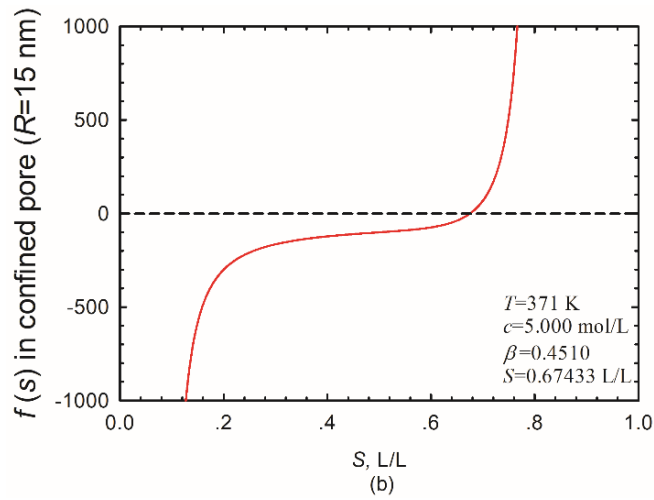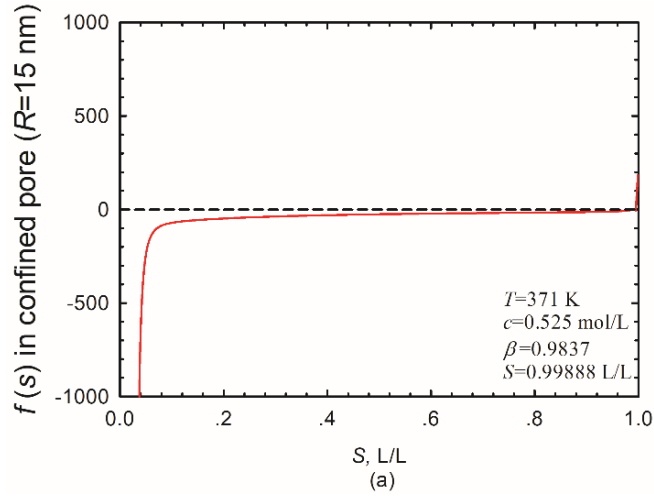
Figure 2-2 Variation of $f(S^V)$ vs. S^V in confined pore (R=15 nm) (T=371K). The subplots (a), (b) and (c) show the calculated results at c=0.525, c=5.000 and c=8.670 mol/L (the corresponding mole fractions of the vapor phase are 0.9837, 0.4510 and 0.0073), respectively.

T=280 K
c=0.040 mol/L
β=0.9149
S1=0.00346 L/L
S2=0.00670 L/L
S3=0.91750 L/L
S4=0.99672 L/L
S5=0.99963 L/L

(a)

T=280 K
c=0.100 mol/L
β=0.6943
S1=0.71675 L/L
S2=0.96946 L/L
S3=0.99666 L/L

(b)

T=280 K
c=5.000 mol/L
β=0.3904
S=0.71302 L/L

(c)
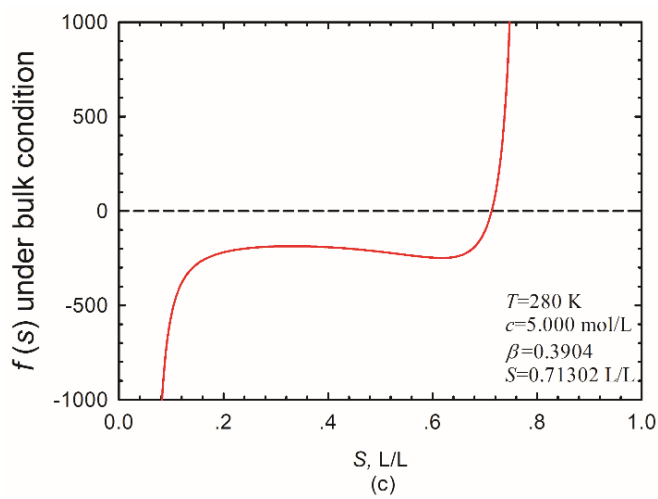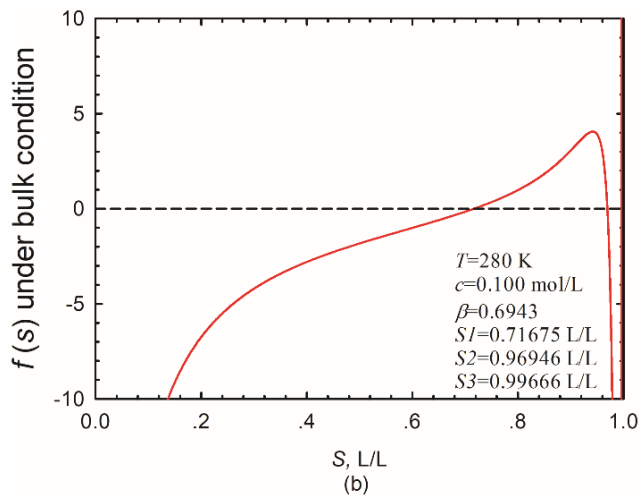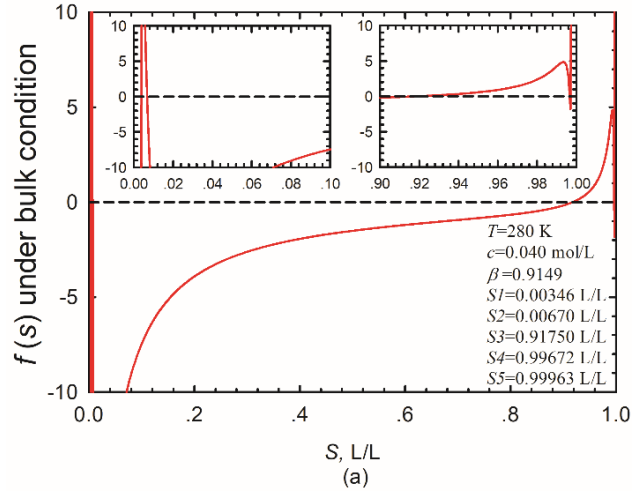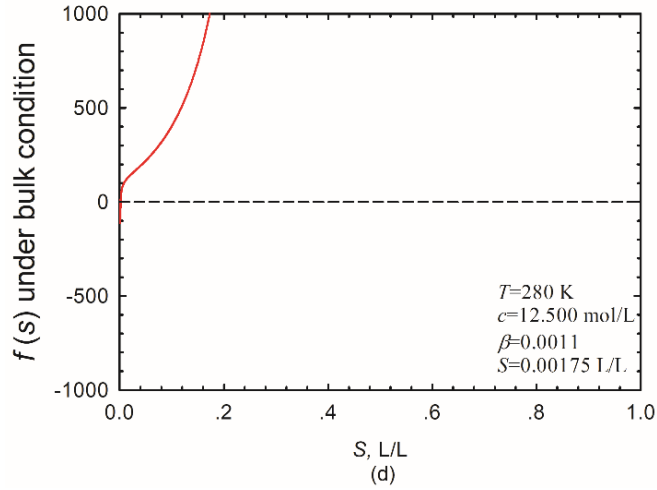
Figure 2-3 Variation of $f(S^V)$ vs. S^V under bulk condition (T=280K). The subplots (a), (b), (c) and (d) show the calculated results at c=0.040, c=0.100, c=5.000 and c=12.500 mol/L (the corresponding mole fractions of the vapor phase are 0.9149, 0.6943, 0.3904 and 0.0011), respectively.
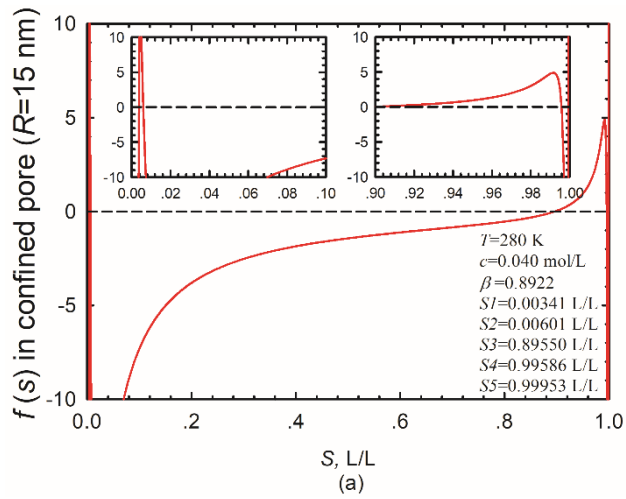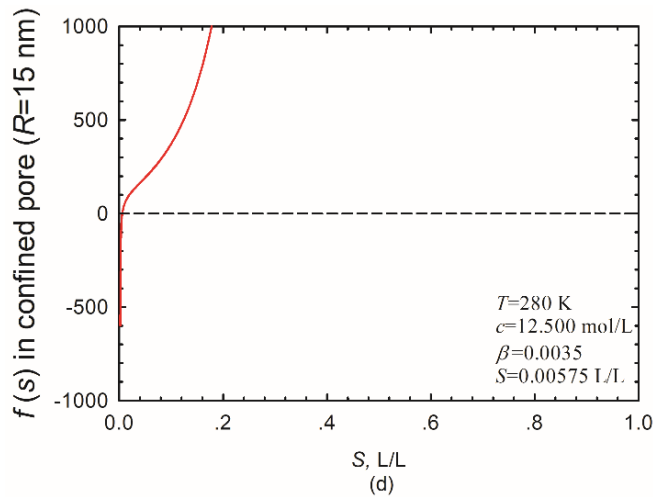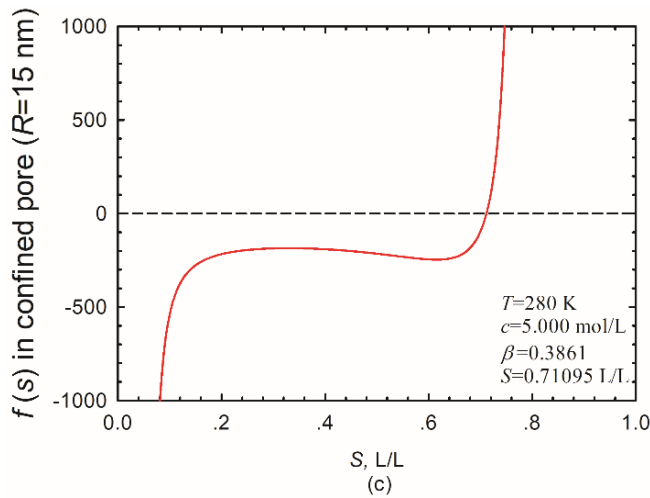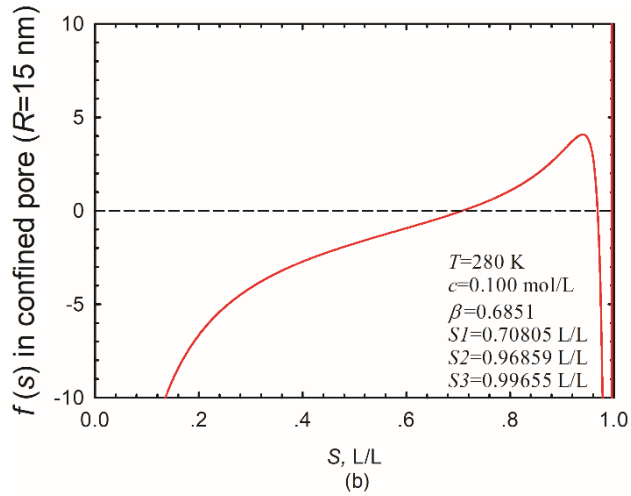
Figure 2-4 Variation of $f(S^V)$ vs. S^V in confined pore (R=15 nm) (T=280K). The subplots (a), (b), (c) and (d) show the calculated results at c=0.040, c=0.100, c=5.000 and c=12.500 mol/L (the corresponding mole fractions of the vapor phase are 0.8922, 0.6851, 0.3861 and 0.0035), respectively.

After knowing all the possible real roots of S^V, selecting the correct one becomes critical.

The correct root can be determined by minimizing the following Helmholtz free energy,

$$A = A^V(V^V, T, n_1^V, \ldots \qquad \ldots \qquad (2.19)$$

where,

$$\begin{cases} A^V(V^V, T, n_1^V, \ldots & -P^V V^V + \sum_{i=1}^{m} n_i^V \mu_i^V \\[4mm] A^L(V^L, T, n_1^L, \ldots & -P^L V^L + \sum_{i=1}^{m} n_i^L \mu_i^L \end{cases} \qquad (2.20)$$

The Helmholtz free energy can be rewritten in terms of phase volume fractions S^V and

S^L, composition and temperature T, yielding the following expression,

$$\begin{cases} A^V = -P^V(\dfrac{S^V}{c\beta}, T, x_1^V, x_2^V, \ldots & \ldots \\[4mm] A^L = -P^L(\dfrac{1\text{-}S^V}{c(1-\beta)}, T, x_1^L, x_2^L, \ldots & \ldots \end{cases}$$

$$(2.21)$$

Finally, K_i values are updated by the following equation [16],

$$K_i^{n+1} = \frac{x_i^V}{x_i^L} = \frac{c^L \Phi_i^V (1/c^V, T, x_1^V, x_2^V, \ldots}{c^V \Phi_i^L (1/c^L, T, x_1^L, x_2^L, \ldots} \qquad . \qquad (2.22)$$

The iterations stop whenever $error = \max\left[\ln K_i^{n+1} - \ln K_i^n\right] \le 10^{-6}, i = 1, 2, \ldots$.

Using Eq. (2.22) to track the phase boundary under low temperature and high overall molar

density conditions may yield inappropriate K_i values, leading to convergence issue. We

take the binary mixture of methane (C_1) and normal pentane (nC_5) with a feed composition

of (54.7413 mol% C_1, 45.2587 mol% nC_5) at temperature of T=340K as an example to illustrate the convergence issue. To detect the bubble point, we conduct the VT-flash from a molar density smaller but close to the bubble point (c=10.045 mol /L), and gradually increase the molar density with the step size c=0.05 mol/L until the one which makes β approach 0 (or 1 in the retrograde condensation zone). However, bubble point may fail to be detected if the step size used for updating K_i (as given by Eq. (2.22)) is too large. Table 2 shows the converged β values at different molar densities for the binary C_1-nC_5 mixture at T=340K. As can be seen from Table 2, β converges to the value of 0.0173 at c=10.145 mol/L, while β does not converge at c=10.195 mol/L. In this case, the bubble point can be regarded to occur at c=10.145 mol/L. But in fact, bubble point should occur at a higher c value. Multiple trials lead us to realize that the issue of premature detection of the bubble point lies in the improper updating of the K_i values by the use of Eq. (2.22) in the flash algorithm. Based on extensive testing, we find out that the following equation can be pragmatically used to update K_i values in order to avoid the non-convergence of the algorithm at conditions close to the bubble point:

$$K_i^{n+1} = \frac{K_i^{n+1} + K_i^n}{2}$$
(2.23)

Use of Eq. (2.23) can ensure the flash algorithm converges to the true solution at conditions close to the bubble point. As shown in Table 2, the true bubble point is found to occur at c=10.245 mol/L.

Table 2-2 The converged β values given by the flash algorithm at different molar densities for the binary C_1-nC_5 mixture (T=340 K). A step size of 0.05 mol/L of c is used in this example.

c, mol/L	10.045	10.095	10.145	10.195	10.245	10.295
β solved using Eq. (2.22)	0.0334	0.0255	0.0173	Non-convergence	Non-convergence	Non-convergence
β solved using Eq. (2.23)	0.0334	0.0255	0.0173	0.0090	0.0004	Non-convergence

We use the PR-EOS to calculate the pressures and volume function coefficients of both phases and the related formulas are presented in the Appendix. The flow chart of this algorithm is shown in **Figure 2-5** and the procedure of the algorithm is briefly explained as follows:

1) Assume a unit total volume $V = 1L$ for given c, $z_1, \ldots$, and T. Then, evaluate P_0 by following the method proposed by Mikyška and Firoozabadi's [16]. Initialize equilibrium ratios K_i using Wilson correlation shown in Eq. (2.12) and set the number of iterations to 0.

2) Calculate mole fraction of vapor phase β by minimizing the objective function [19-20]. The interior point method is used for such purpose. Then, the composition of both phases can be calculated.

3) Use the bisection method to calculate the vapor phase volume fraction S^V by solving Eq. (2.17). Then, update the molar densities of both phases using Eq. (2.16) and the liquid volume fraction $S^L = 1 - S^V$.

4) Update equilibrium ratios using Eq. (2.22) or Eq. (2.23), and check for the tolerance $\max\left[\ln K_i^{n+1} - \ln K_i^n\right] \leq 10^{-6}, i = 1, 2, \ldots$. If the termination condition is not satisfied, increase the number of iterations and go back to step 2; otherwise, output the results.
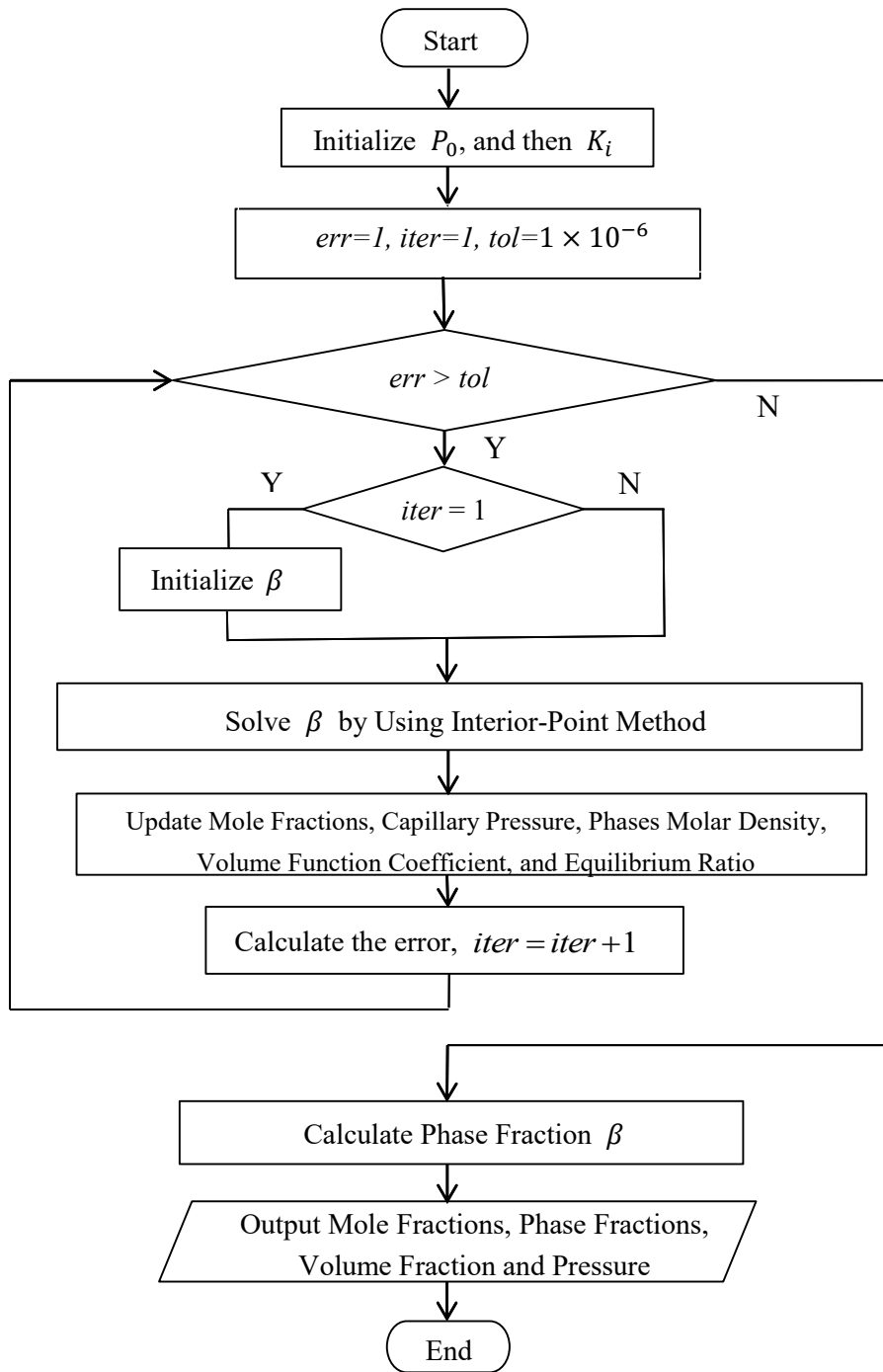
Figure 2-5 Flow chart of the two-phase VT-Flash algorithm with the effect of capillary pressure.

2.4 Results and Discussion

In this section, in order to verify the correctness and robustness of our algorithm, we test our VT-flash algorithm with capillarity by considering four binary and ternary mixtures under different conditions. The algorithm of VT- flash with effect of capillary pressure is used to detect the boundary between single-phase and two-phase region, i.e., the phase boundary can be detected when the phase fraction β becomes 0 or 1. In the first example, we compare the results calculated from the VT-flash with capillarity against those calculated by the PT-flash with capillarity. The remaining three examples are selected from the work by Jindrová and Mikyška [17]. The related parameters for all the used components are presented in **Table 2-3**, while the binary interaction parameters used in PR-EOS are presented in **Table 2-4**.

Table 2-3 Physical properties of the compounds used in the example calculations [17, 27].

Component	Tc (K)	Pc (bar)	ω	Mw (g/mol)	χ
CO_2	304.14	73.75	0.239	44	78
C_1	190.56	45.99	0.011	16	77.33
nC_5	469.7	33.7	0.251	72.2	231.5
nC_6	507.4	30.12	0.296	86.2	271
nC_{10}	617.7	21.1	0.489	142.28	433.5

Table 2-4 Binary interaction parameters (BIP) used in the equation of state models [17].

BIP	CO_2	C_1	nC_5	nC_6	nC_{10}
CO_2	0	-	-	-	0.150
C_1	-	0	0.041	0.005	0.052
nC_5	-	0.041	0	-	-
nC_6	-	0.005	-	0	0
nC_{10}	0.150	0.052	-	0	0

2.4.1 Example 1 - binary mixture of methane (C_1) and hexane (nC_6)

In the first example, we study the two-phase equilibria for a binary mixture of C_1 and nC_6 with or without the presence of confinement; the feed composition is (70 mol% C_1, 30 mol% nC_6). We calibrate our model by comparing it to PT-flash with or without capillary pressure effect. **Figure 2-6** shows the bulk two-phase boundary as well as the two-phase boundary in a confined nanopore with a radius of R=10 nm. The VT-flash algorithm developed in this work, together with PT-flash with capillarity [8, 28], have been used in these calculations. The equilibrium pressure refers to the vapor phase pressure in confined pores. The solution can be found with 20 to 50 iterations for most points along the phase envelope including the critical point region or the retrograde condensation region. However, at conditions close to the bubble points at the low temperatures, it may take up to 100 iterations to locate the solution. It can be seen that the two-phase boundary calculated by the VT flash algorithm (with or without capillarity) agrees well with those calculated by

the PT flash algorithm. **Figure 2-7** provides a zoomed view on the phase boundaries in the proximity of the cricondentherm point. Under the effect of capillary pressure, the bubble point and lower dew point decreases, while the upper dew point increases; the bubble point and dew point meet at the critical point due to zero capillary pressure. The cricondentherm point increases due to the capillary pressure effect, which is in line with previous findings [11].
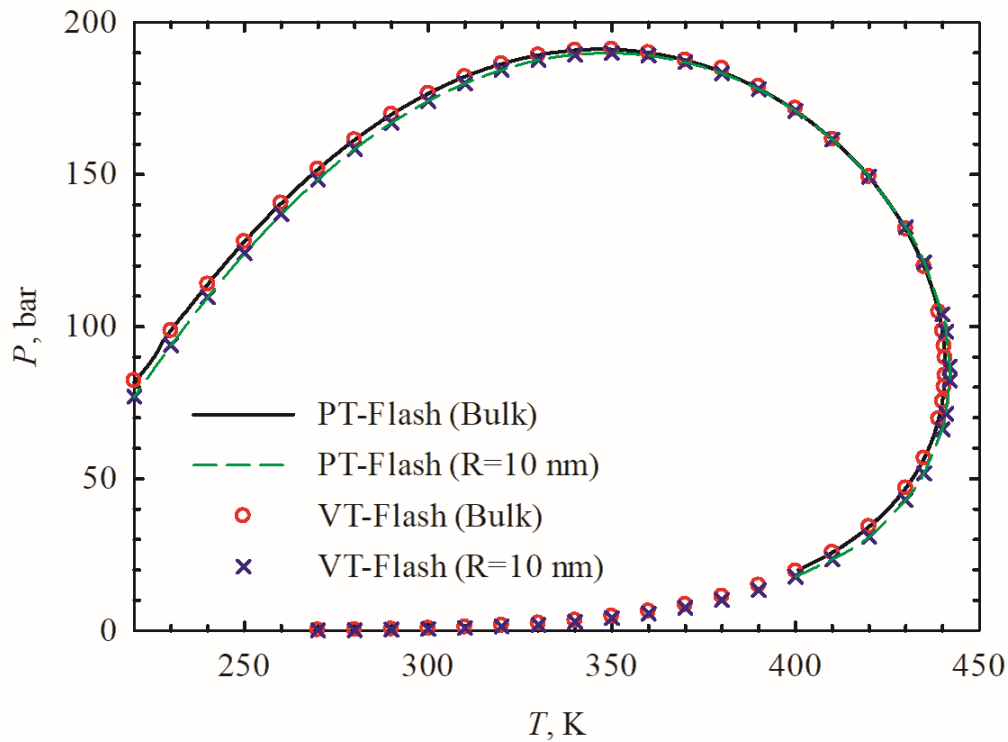
Figure 2-6 Phase envelope in PT-space modeled by PT-flash [8, 28] and VT-flash in bulk system, and VT-flash in confined pores with R=10 nm. The calculations are made for Example 1: C_1-nC_6 mixture (z_{C1}=0.7 and z_{nC6}=0.3).
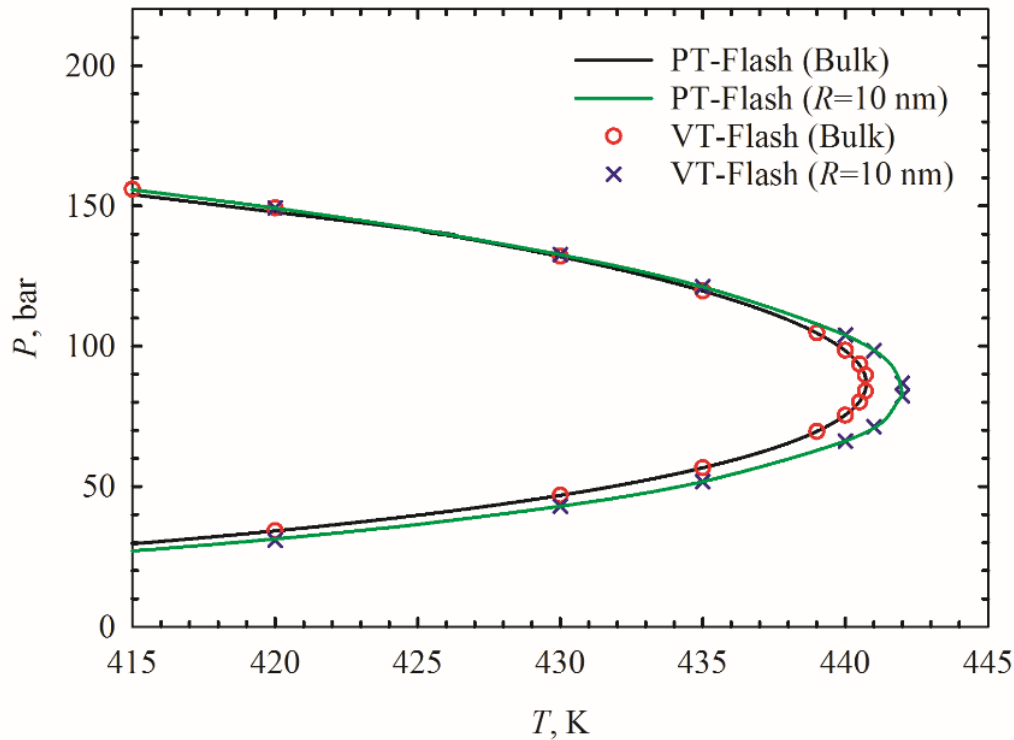
Figure 2-7 Phase envelope in PT space near the cricondentherm point as modeled by PT-flash [28] and VT-flash in bulk and confined pores with $R=10$ nm. The calculations are made for Example 1: C1-nC6 mixture ($z_{C1}=0.7$ and $z_{nC6}=0.3$).

2.4.2 Example 2 - binary mixture of methane (C_1) and pentane (nC_5)

In the second example, we study the two-phase equilibria for a binary mixture of C_1 and nC_5 with or without confinement effect; the feed composition is (54.7413 mol% C_1, 45.2587 mol% nC_5). **Figure 2-8** shows the cT (overall molar density/temperature) envelope of C_1-nC_5 mixture calculated with the consideration of the capillary-pressure effect under different pore sizes ($R=15$ nm and $R=30$ nm), and compares them with the cT envelope calculated under the bulk condition. Similar to the first example, up to 100 iterations may be needed to find the solution near the bubble points at low temperatures. For other region, 20 to 50 iterations are sufficient. For clarity, the topography of envelope adjacent to the

dew point, cricondentherm point, critical point and bubble point are also presented. At a fixed temperature, the bubble point occurs at a larger overall molar density under the effect of capillary pressure, but the dew point occurs at either a larger or smaller overall molar density, depending on the location of the phase envelope. When the overall molar density is larger than the one at the cricondentherm point, the dew point occurs at a larger overall molar density; otherwise, the dew point occurs at a smaller overall molar density. The difference in the overall molar density between the bulk and confined fluids tends to increase as the pore size decreases. A higher cricondentherm point due to capillarity can be found on the cT envelope, which is in line with the PT flash calculation. The cT envelopes calculated with different pore sizes intersect with the bulk envelope at the critical point, where the capillary pressure is zero due to zero IFT.

Furthermore, we study the influence of capillarity on the equilibrium pressures, mass densities, saturations and compositions during an isothermal compression process. At a constant temperature (i.e., T=371K), we plot all the calculated results as a function of the overall molar density c for the bulk and confined scenarios. **Figure 2- 9** shows the confined and bulk equilibrium pressure as a function of the overall molar density at T=371K. The equilibrium pressure presented in Figure 2-9 corresponds to the vapor-phase pressure in nanopores. The capillarity effect results in a smaller equilibrium pressure at the same overall molar density, as seen from the inset figure in Figure 2-9. A smaller pore size, corresponding to a large capillarity, leads to larger deviation from the bulk equilibrium

pressure. **Figure 2-10 (I)** and **Figure 2-10 (II)** present the mass densities and saturations

(volume fractions) of both phases as functions of the overall molar density in bulk

condition as well as in a confined nanopore with a radius of $R=15$ nm, respectively. At the

same overall molar density, the mass densities of both phases decrease with the presence

of capillarity. Under confinement effect and at a given overall molar density, the vapor-

phase saturation increases. **Figure 2-11** shows the compositions of both phases. It can be

seen from Figure 2-11 that, at a given overall molar density, capillarity leads to higher mole

fractions of the lighter component in both phases.

(I)

(II)

(III)

(IV)
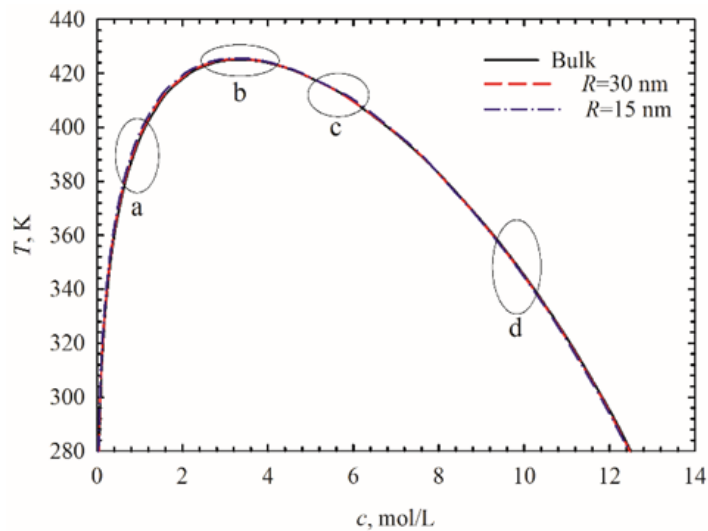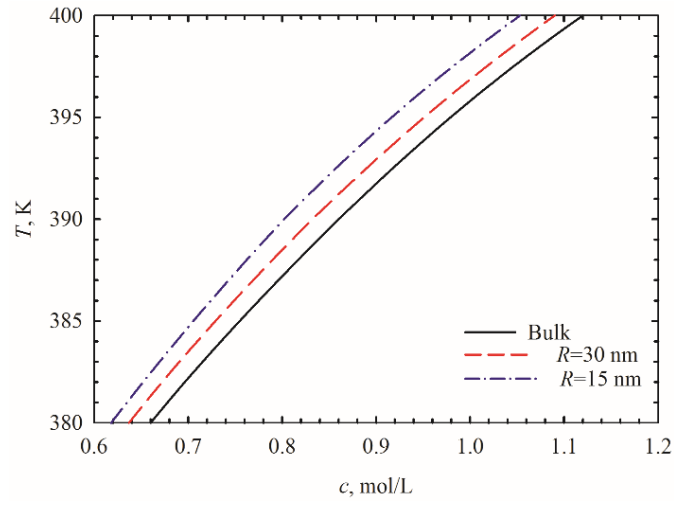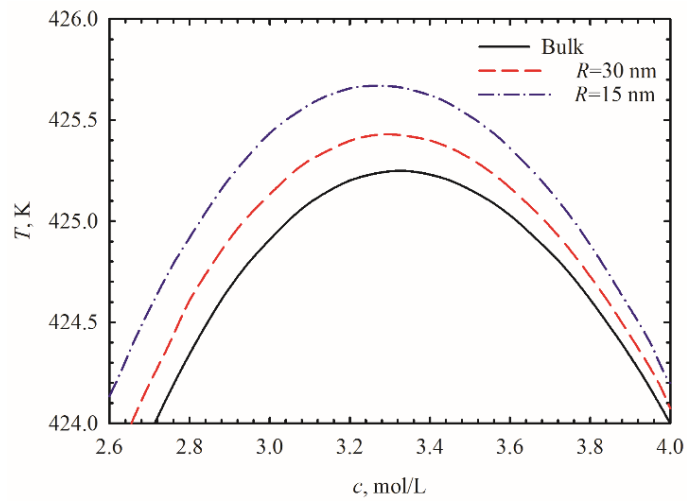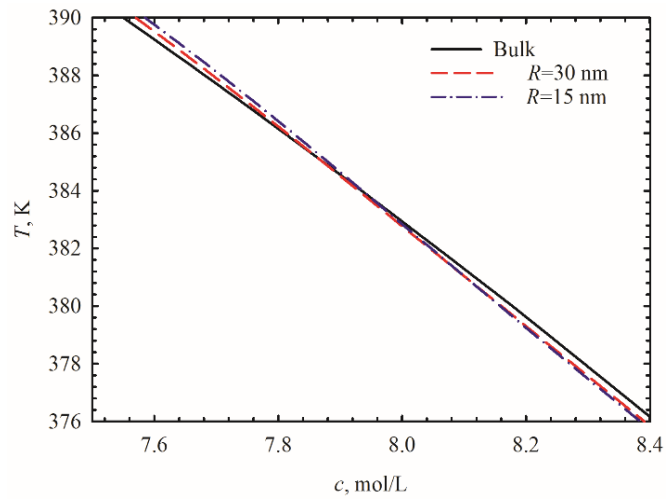
(V)
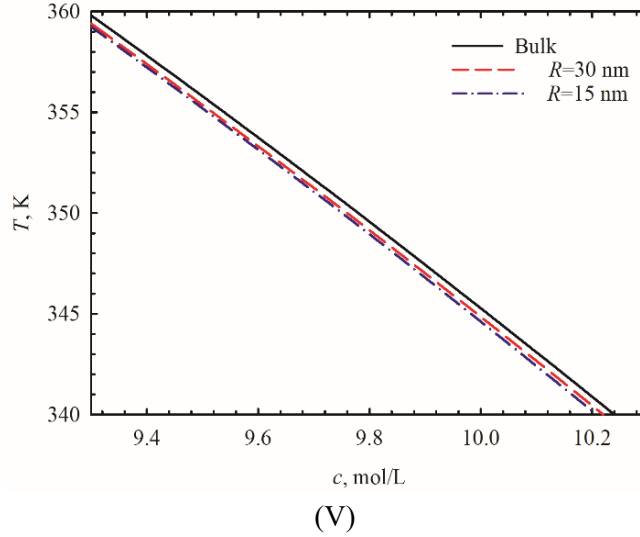
Figure 2-8 Phase boundary under the effect of capillary pressure for the C_1-nC_5 mixture (z_{C1}=0.547413 and z_{nC5}=0.452587) in the cT-space. The subplot (I) shows the overall cT envelope; (II) gives an enlarged view of the region 'a' marked in subplot (I), showing a part of the dew point line; (III) gives an enlarged view of the region 'b' near the cricondentherm point, as marked in subplot (I); (IV) gives an enlarged view of the region 'c' near the critical point, as marked in subplot (I); (V) gives an enlarged view of the region 'd' circled marked in subplot (I), showing a part of the bubble point line.
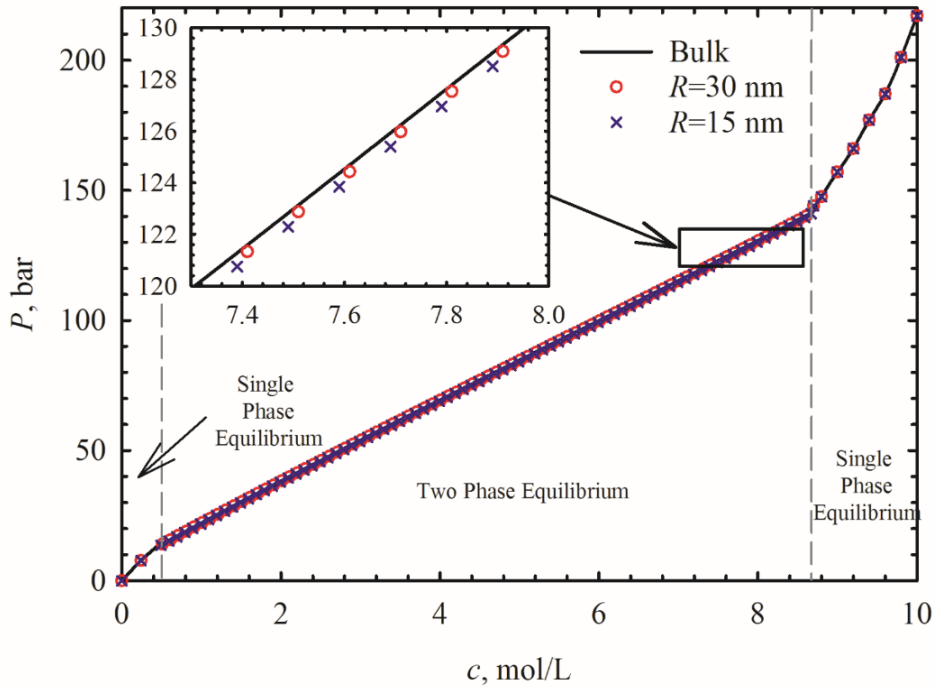
Figure 2-9 Equilibrium pressure under the effect of capillary pressure as a function of overall molar density at 371 K for the C_1-nC_5 mixture (z_{C1}=0.547413 and z_{nC5}=0.452587).

45
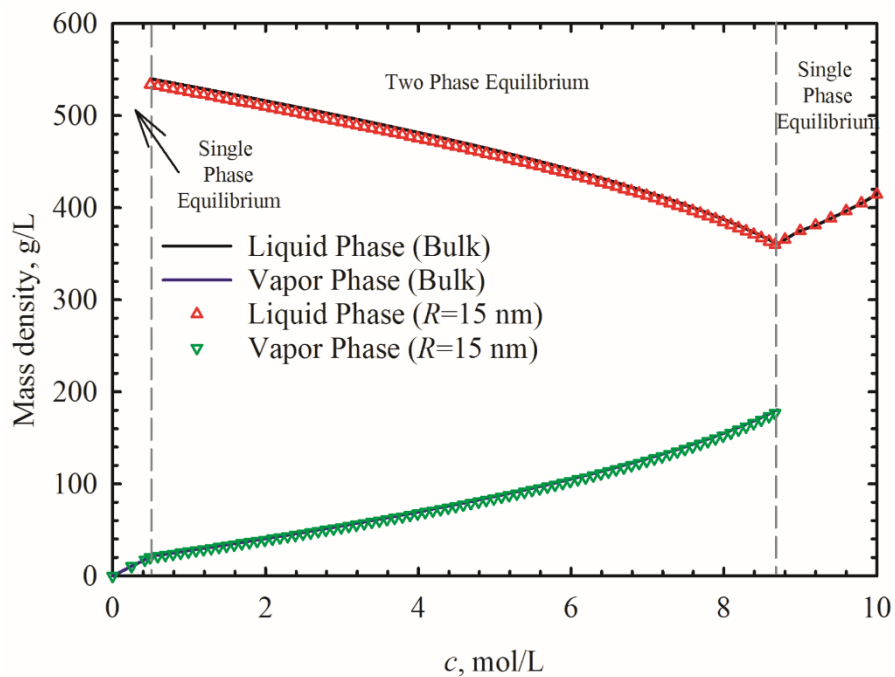
(I)
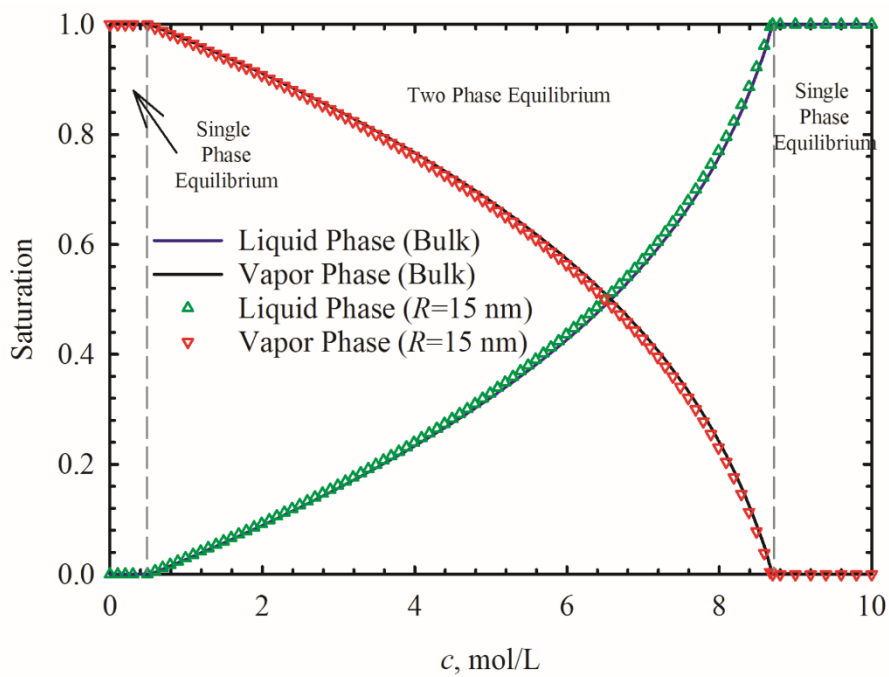
(II)

Figure 2-10 Mass density (I) and saturations (II) of both phases under the effect of capillary pressure as a function of overall molar density at 371 K for the C_1-nC_5 mixture (z_{C1}=0.547413 and z_{nC5}=0.452587).
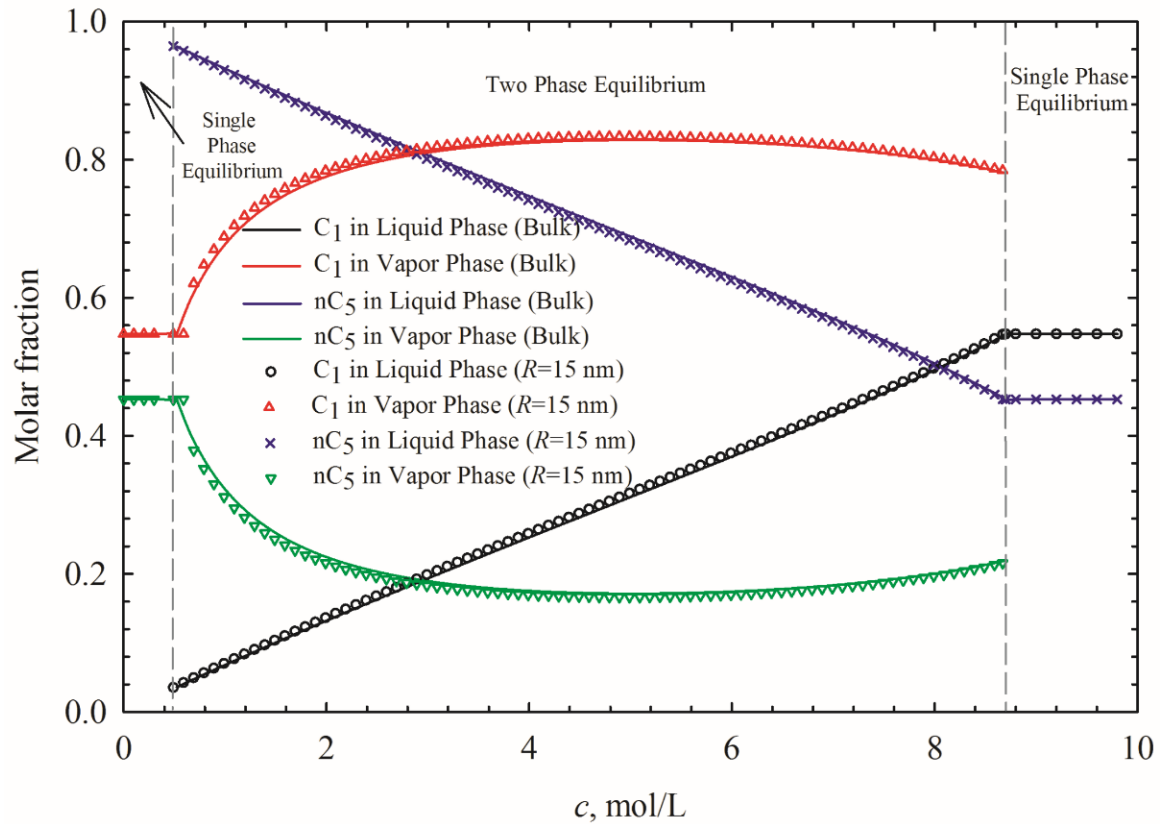
Figure 2-11 Molar fractions of components in vapor and liquid phases under the effect of capillary pressure as a function of overall molar density at 371 K for the C_1-nC_5 mixture (z_{C1}=0.547413 and z_{nC5}=0.452587).

2.4.3 Example 3 - binary mixture of carbon dioxide (CO₂) and normal decane (nC₁₀)

In the third example, we study the two-phase equilibria for a binary mixture of CO_2 and n-C_{10} with or without the presence of confinement; the feed composition is (54.7413 mol% CO_2, 45.2587 mol% nC_{10}). **Figure 2-12** shows the cT phase envelope of CO_2-nC_{10} mixture under bulk condition as well as in confined nanopores of R=15 nm and R=30 nm. There are two two-phase regions covered by the cT phase envelope. These two two-phase regions are separated by the valley marked by "e". The left two-phase region corresponds to vapor-liquid two-phase equilibria. The right two-phase region corresponds to liquid-liquid two-

phase equilibria which exist under the conditions of high molar density and low temperature. The solution can be found in 40 to 80 iterations in most vapor-liquid equilibria region, but more than 200 iterations may be needed near the bubble point region at low temperatures as well as in the liquid-liquid equilibria region. We also provide zoomed views on the phase boundary in cT space in the proximity of the dew point, cricondentherm point, critical point, bubble point, as well as the liquid-liquid equilibrium region. From **Figure 2-12**, we can observe similar behavior with regard to the influence of capillary pressure on the dew points, bubble points, cricondentherm point, and critical point as seen in Example 2. As for the liquid-liquid phase boundary, we hardly see noticeable effect of the capillary pressure on the phase boundary due to small IFT between these two liquid phases.

We also study the influence of capillarity on the equilibrium pressure, mass densities, saturations and compositions during an isothermal compression process. **Figure 2-13** presents the equilibrium pressures of vapor-liquid (I) and liquid-liquid (II) equilibria in bulk and confined pores as functions of the overall molar density at 311K; the pressure of the vapor phase or the lighter liquid phase is taken as the equilibrium pressure in confined pores. As for the vapor-liquid two-phase equilibria, it is obvious that the equilibrium pressure in the confinement deviates more from the bulk as overall molar density increases due to the increased capillary pressure. As for the liquid-liquid two-phase equilibria, the

equilibrium pressures in the bulk and confined pores overlap due to the negligible effect of capillary pressure.

(I)

(II)

49
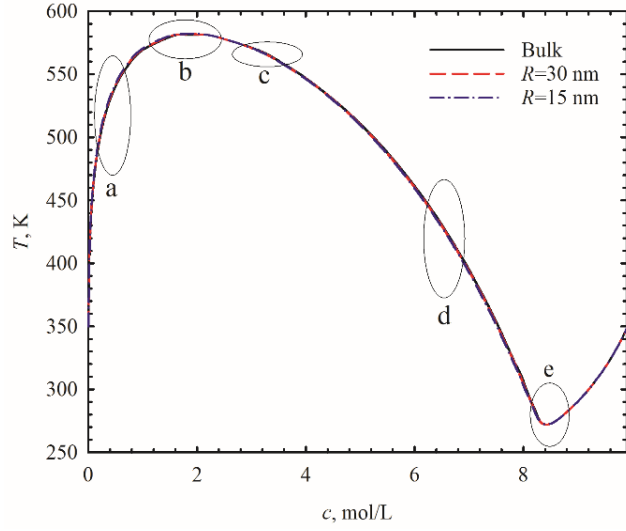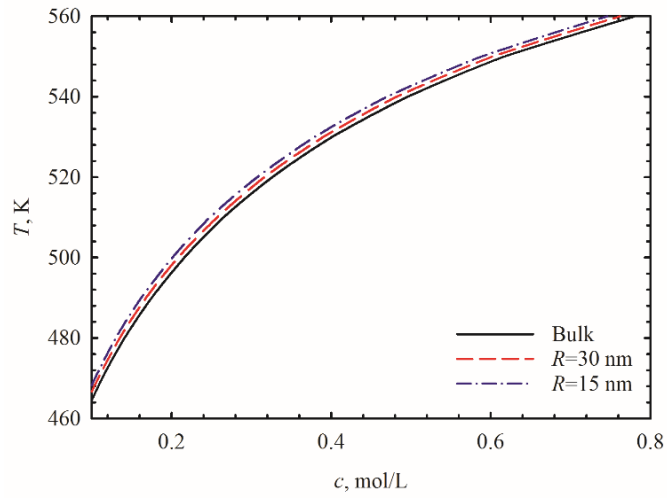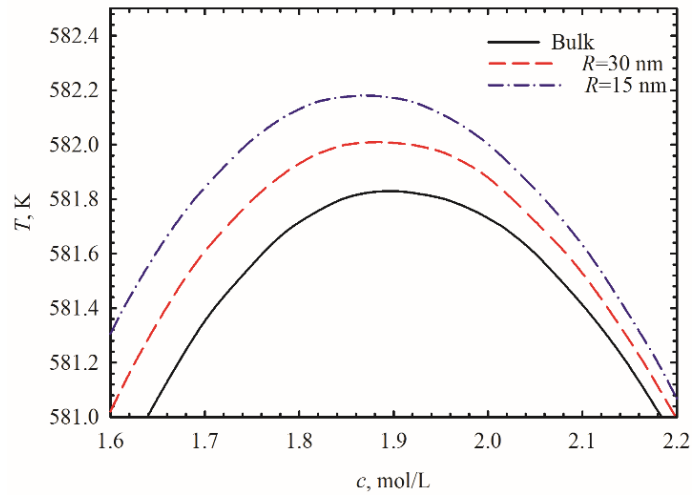
(III)
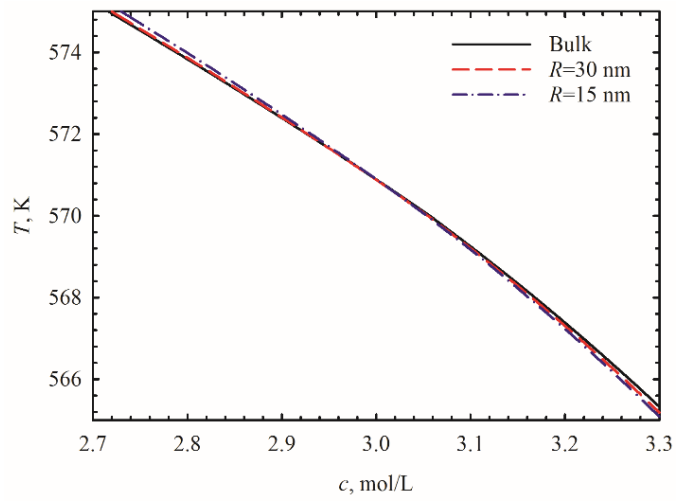
(IV)
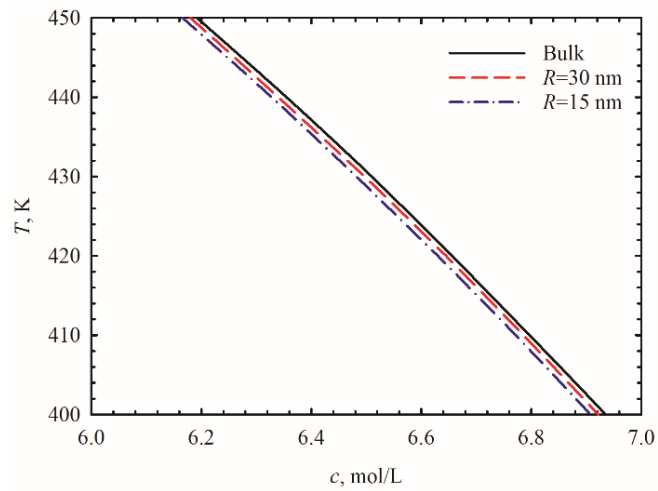
(V)
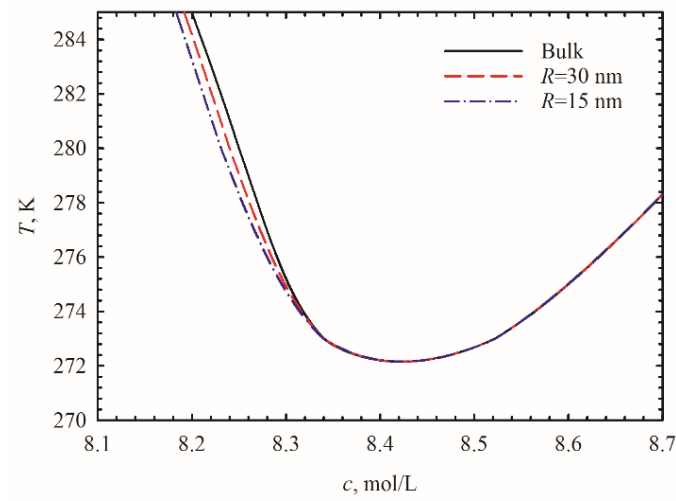
(VI)

Figure 2-12 Phase boundary under the effect of capillary pressure for the CO_2-nC_{10} mixture (z_{CO2}=0.547413 and z_{nC10}=0.452587) in the cT-space. The subplot (I) shows the overall cT envelope; (II) gives an enlarged view of the region 'a' marked in subplot (I), showing a part of the dew point line; (III) gives an enlarged view of the region 'b' near the cricondentherm point, as marked in subplot (I); (IV) gives an enlarged view of the region 'c' near the critical point, as marked in subplot (I); (V) gives an enlarged view of the region 'd' circled marked in subplot (I), showing a part of the bubble point line; (VI) gives an enlarged view of region 'e' marked in sub plot (I), showing the transition from vapor-liquid equilibrium region to liquid-liquid equilibrium region.
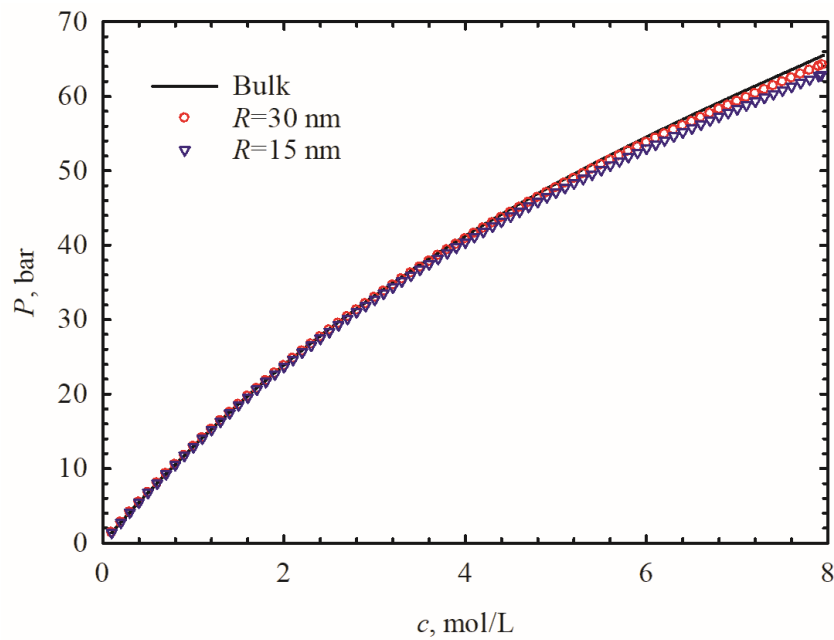
(I)
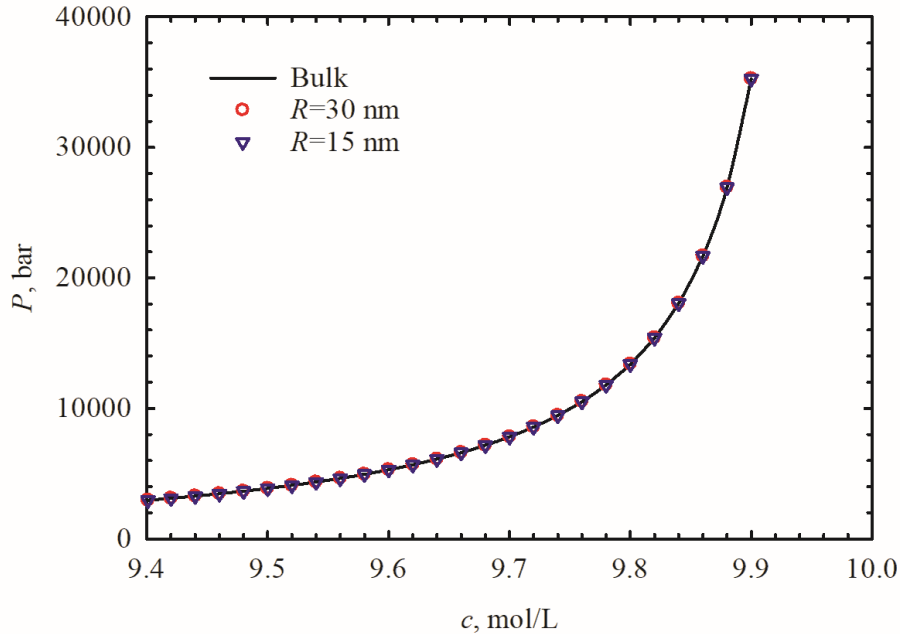
(II)

Figure 2-13 Equilibrium pressure under the effect of capillary pressure as a function of overall molar density at 311K for CO_2-nC_{10} mixture (z_{CO2}=0.547413 and z_{nC10}=0.452587). Subplot (I) shows the equilibrium pressure of the vapor-liquid phase equilibrium; Subplot (II) shows the equilibrium pressure of the liquid-liquid phase equilibrium.

Figure 2-14 shows the mass densities and saturations of vapor-liquid or liquid-liquid phases that are calculated under bulk or confined conditions as function of the overall molar density. It is worthwhile to note from **Figure 2-14[I]** that at higher molar density, the capillary pressure causes a more obvious reduction in the vapor-phase mass density. **Figure 2-14[II]** shows that as molar density increases, the mixture sequentially experiences vapor-liquid two phase equilibria, single liquid phase equilibria and liquid-liquid two phase equilibria. The capillary pressure tends to only exert minor effect on the phase saturations.

Figure 2-15 shows the compositions of vapor-liquid or liquid-liquid phases under bulk or confined conditions as function of the overall molar density. As for the vapor-liquid two-phase equilibria, at a given overall molar density, capillarity leads to higher mole fractions

of the lighter component CO_2 but lower mole fractions of the heavier component nC_{10} in both phases. As for the liquid-liquid two phase equilibria, the effect of the capillary pressure on composition is negligible.
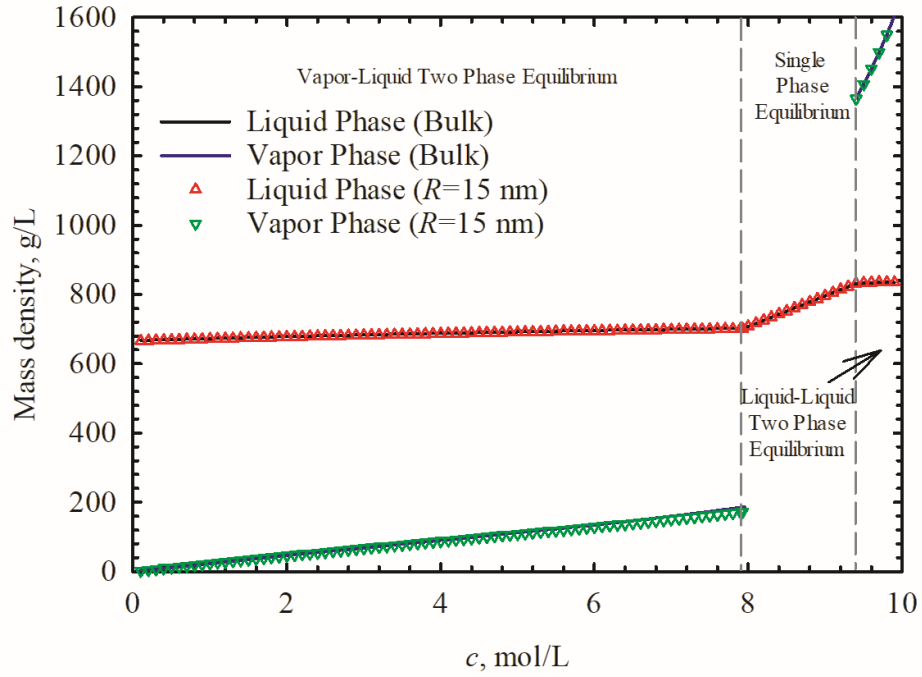
(I)
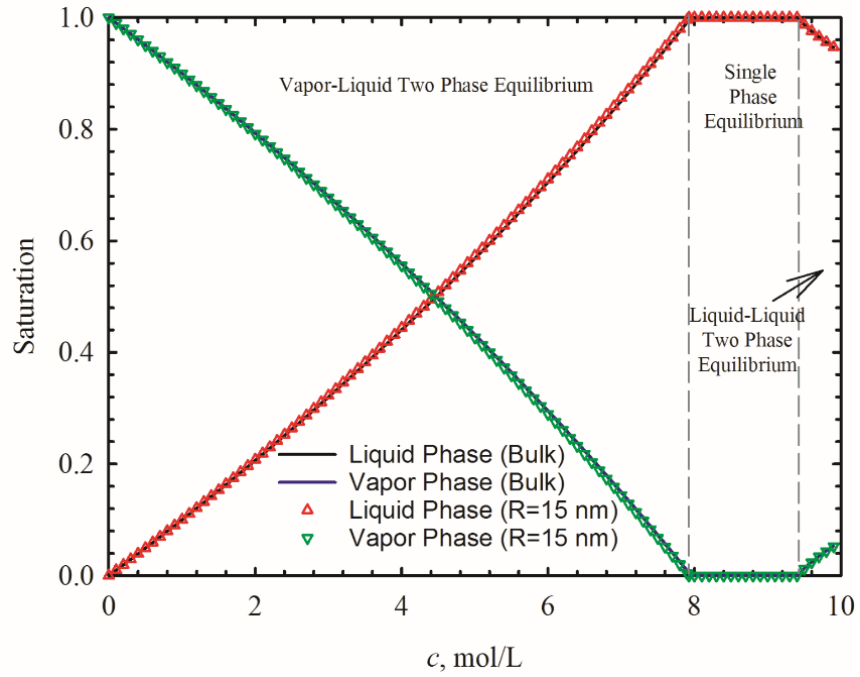
(II)

Figure 2-14 Mass density (I) and saturations (II) in vapor-liquid two phase and liquid-liquid two phase region under the effect of capillary pressure as a function of overall molar density at constant temperature at 311K for CO_2-nC_{10} mixture (z_{CO2}=0.547413 and z_{nC10}=0.452587).
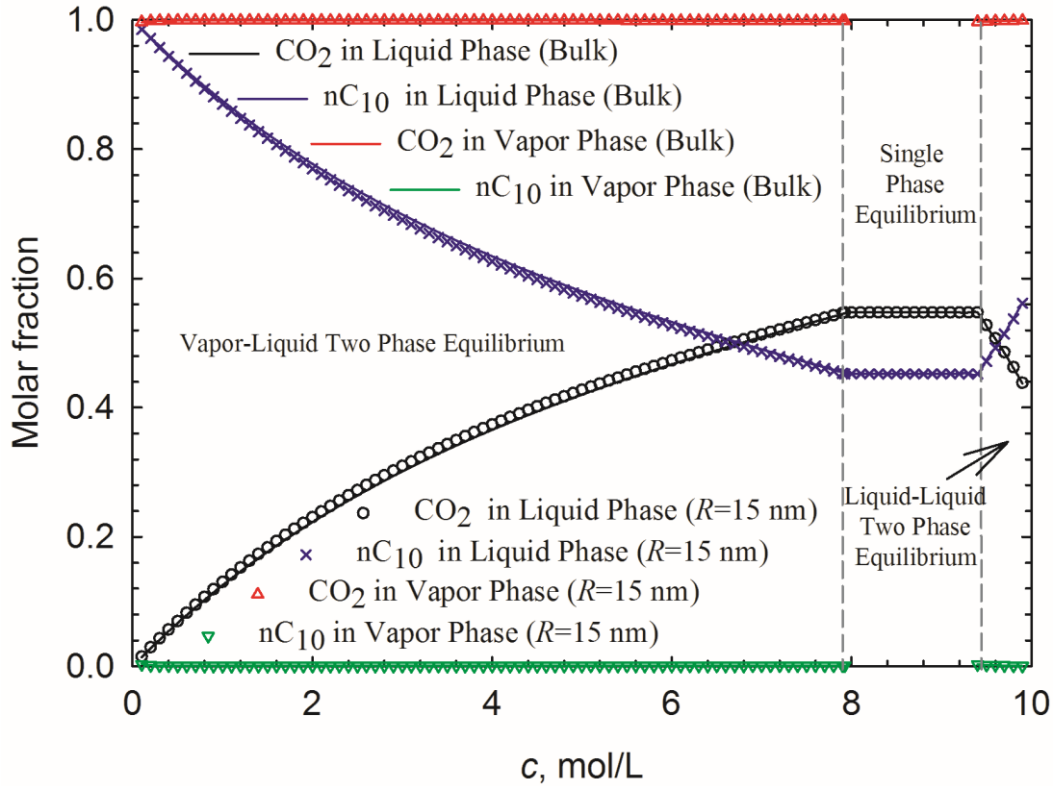
Figure 2-15 Molar fractions of components in the vapor-liquid phases and liquid-liquid phases under the effect of capillary pressure as a function of overall molar density at constant temperature at 311K for CO_2-nC_{10} mixture (z_{CO2}=0.547413 and z_{nC10}=0.452587).

2.4.4 Example 4 – ternary mixture of methane (C_1), hexane (nC_6) and decane (nC_{10})

The fourth example examines the two-phase equilibria for a ternary mixture comprised of

C_1, nC_6 and nC_{10} with or without the presence of confinement; the feed composition is

(40.5946 mol% C_1, 29.7027 mol% nC_6 and 29.7027 mol% nC_{10}). **Figure 2-16** shows the

cT envelope calculated with the consideration of the capillary pressure effect under

different pore sizes. The topography of cT envelope adjacent to the dew point,

cricondentherm point, critical point, and bubble point are shown in Figure 2-16 as well.

We also investigate the effect of capillarity on equilibrium pressure, mass density,

saturation and mole fraction of each component in vapor and liquid phases as a function of

55

overall molar density at a given temperature (T=420K), following the same procedure as adopted in Examples 2 and 3. The corresponding calculation results are presented in **Figures 2-17**, **2-18** and **2-19**. Overall, we can make similar observations with regard to the effect of capillarity on the phase equilibria as seen in Example 2. More than 100 iterations will be needed to find the solution near the bubble point at low temperatures, while 20 to 60 iterations are needed in other regions.

(I)

(II)

(III)

(IV)

(V)

57
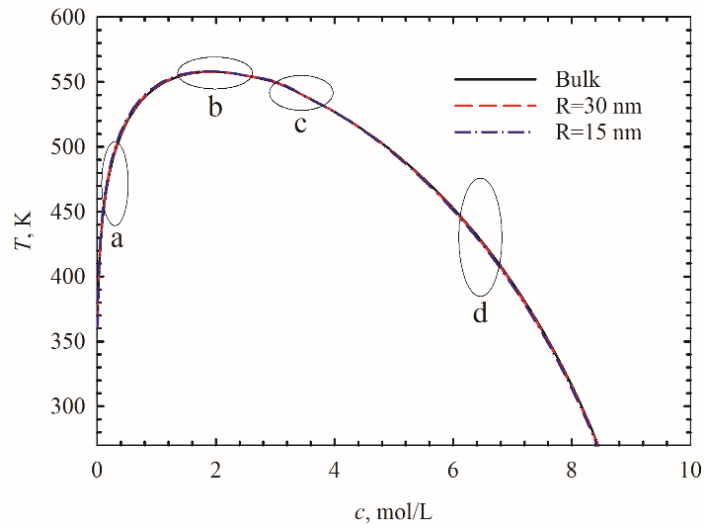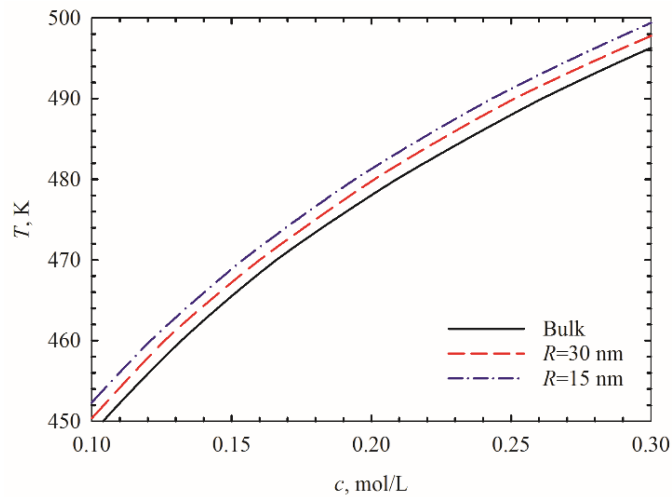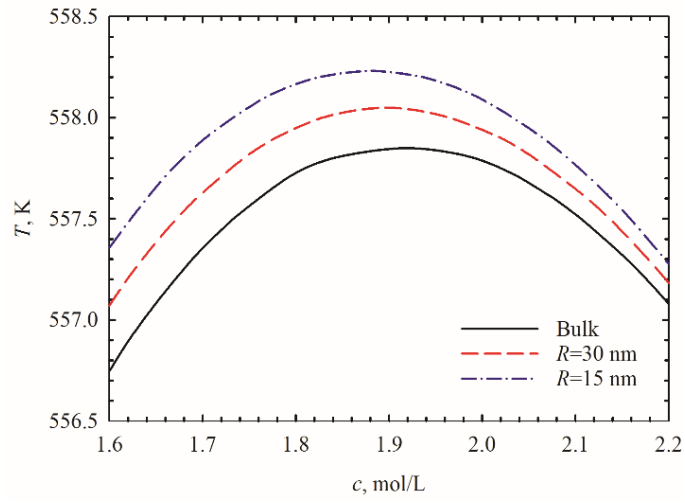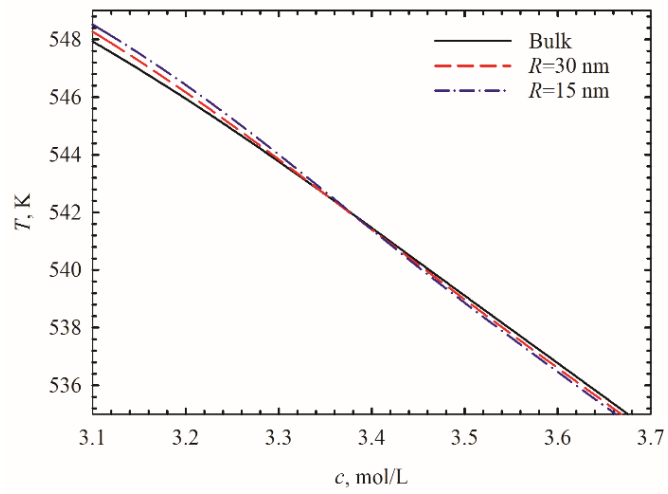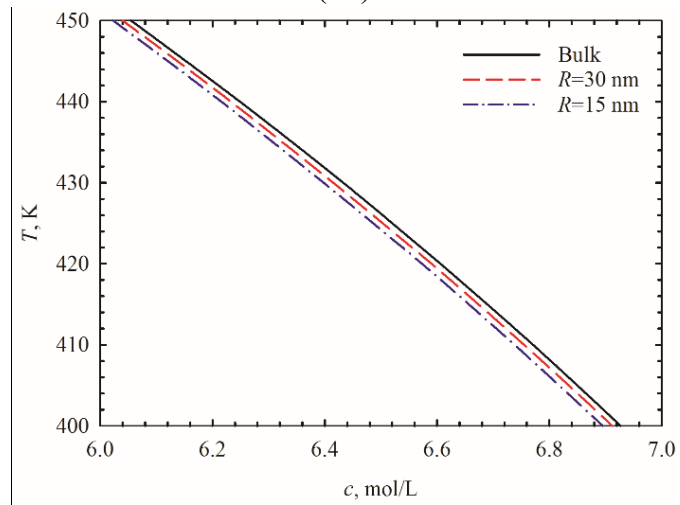
Figure 2-16 Phase boundary under the effect of capillary pressure for the ternary C_1-nC_6-nC_{10} mixture (z_{C1}=0.405946, z_{nC6}=0.298027 and z_{nC10}=0.297027) in the cT-space. The subplot (I) shows the overall cT envelope; (II) gives an enlarged view of the region 'a' marked in subplot (I), showing a part of the dew point line; (III) gives an enlarged view of the region 'b' near the cricondentherm point, as marked in subplot (I); (IV) gives an enlarged view of the region 'c' near the critical point, as marked in subplot (I); (V) gives an enlarged view of the region 'd' circled marked in subplot (I), showing a part of the bubble point line.
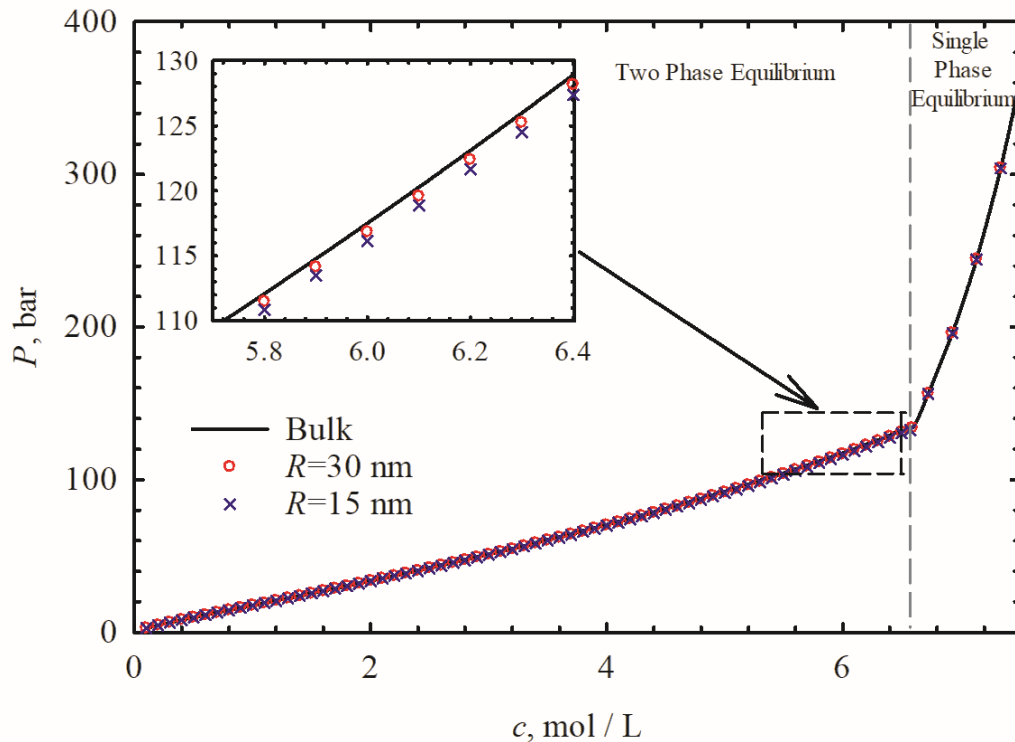
Figure 2-17 Equilibrium pressure under the effect of capillary pressure as a function of overall molar density at 420K for ternary C1-nC6-nC10 mixture (z_{C1}=0.405946, z_{nC6}=0.298027 and z_{nC10}=0.297027).
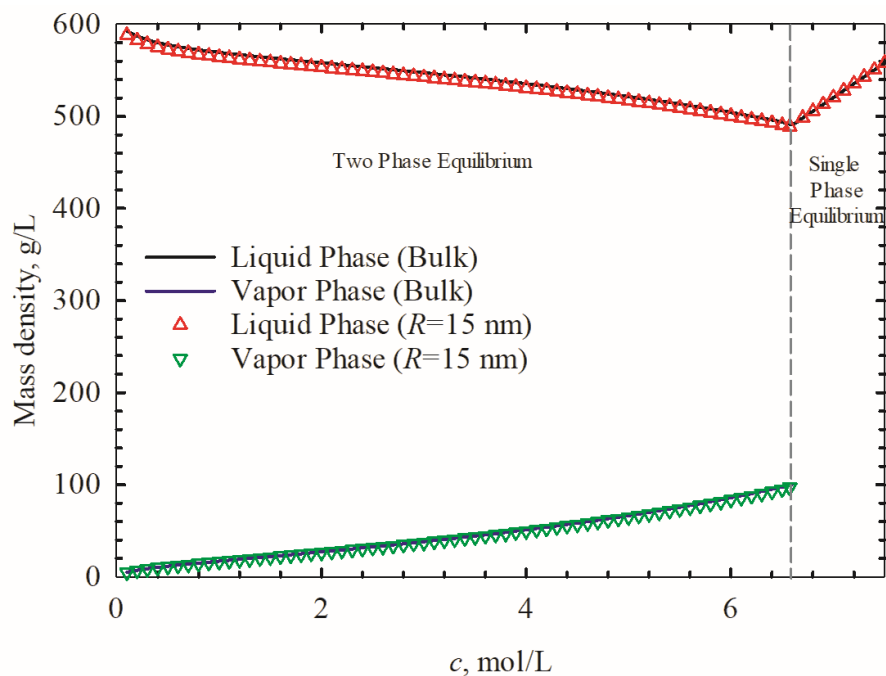
(I)
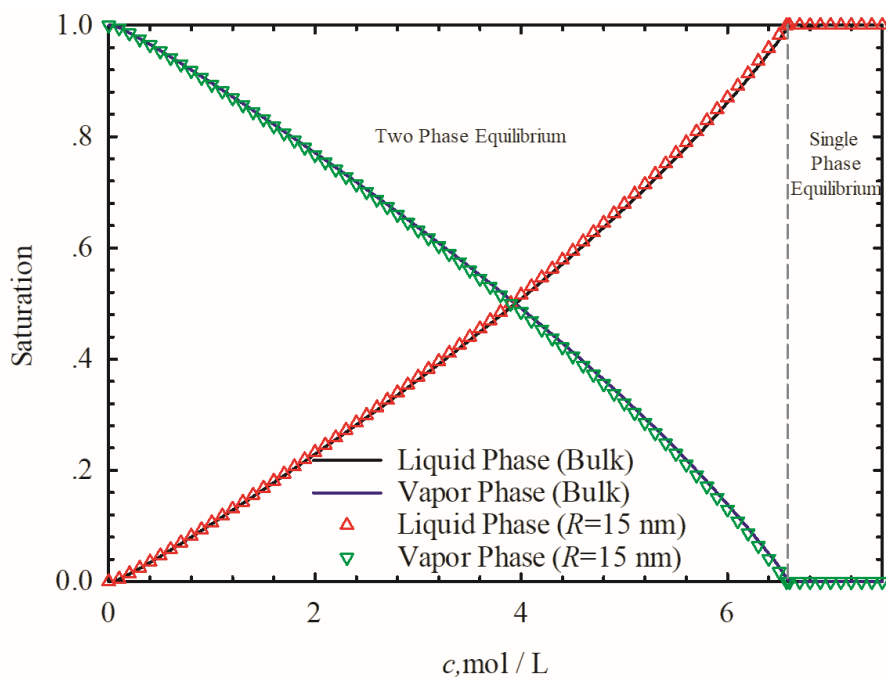
(II)

Figure 2-18 Mass density (I) and saturations (II) of the vapor and liquid phases under the effect of capillary pressure as a function of overall molar density at 420K for ternary C_1-nC_6-nC_{10} mixture (z_{C1}=0.405946, z_{nC6}=0.298027 and z_{nC10}=0.297027).
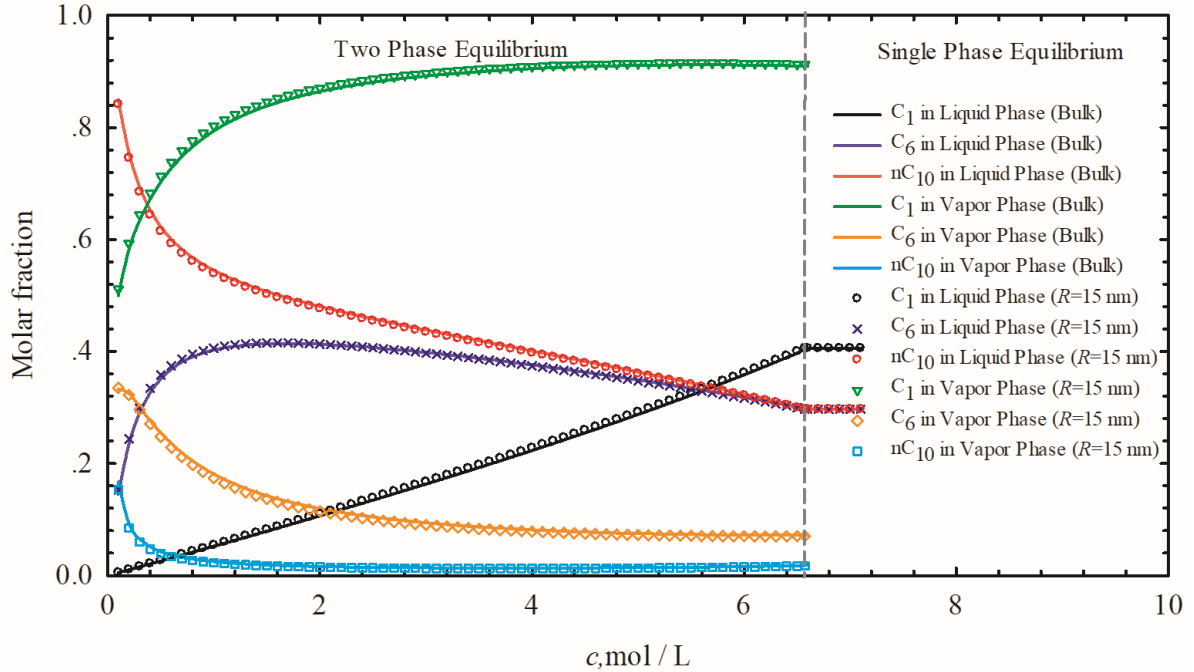
Figure 2-19 Molar fractions of all components in both phases under the effect of capillary pressure as a function of overall molar density at 420K for ternary C_1-nC_6-nC_{10} mixture (z_{C1}=0.405946, z_{nC6}=0.298027 and z_{nC10}=0.297027).

2.5 Conclusions

In this work, we develop an alternative two-phase split algorithm by considering the effect of capillary pressure at constant volume, temperature and mole numbers of components. To improve the robustness of our algorithm, the following measures are proposed:

1) Firstly, we propose a method to determine the correct root of volume fraction by selecting the one leading to the minimum Helmholtz free energy, which ensures the robustness of our algorithm near the dewpoint at low temperatures.

2) Secondly, an improved scheme of updating K_i values is adopted to resolve the convergence issue that is encountered when conducting two-phase VT under low temperature and high overall molar density conditions.

We use four examples to test the robustness and correctness of our algorithms, leading to the following conclusions:

1) Using the first example, it is shown that our VT flash algorithm with capillarity can give the same flash results as the PT flash algorithm with capillarity;

2) As for the vapor-liquid phase boundary, under the effect of capillarity, the bubble point occurs at a larger overall molar density, but the dew point occurs at either a larger or smaller overall molar density, depending on the location of the phase envelope. The phase envelopes calculated under different pore sizes intersect with the bulk phase envelope at the critical point, where the capillary pressure is zero due to zero IFT. We can also detect a higher cricondentherm point in the *c-T* plot when capillarity is considered in the VT flash.

3) As for the vapor-liquid equilibria, the capillarity effect results in a smaller equilibrium pressure, smaller mass densities of both phases, a smaller liquid-phase saturation and a larger vapor-phase saturation. Capillarity also leads to higher mole fractions of the relatively lighter component, but lower mole fractions of the relatively heavier component in both phases.

4) Our algorithm can be also used to model the liquid-liquid equilibrium. However, in our example, due to the small IFT between the two liquid phases, we hardly see noticeable effect of the capillary pressure on the phase boundary and the fluid properties.

Acknowledgements

Nomenclature

$a^* = $ normalized Helmholz free energy

$A = $ Helmholz free energy

$c = $ overall mole density, *mol/L*

$F = $ volume function, *L*

$K = $ equilibrium ratio

$m = $ number of components

$M_w = $ molar weight, *g/mol*

$n = $ mole numbers, *mol*

$P = $ pressure, *bar*

$P_0 = $ initial pressure, *bar*

$P_c = $ critical pressure, *bar*

$P_{ca} = $ capillary pressure, *bar*

$P^{sat}(T) = $ saturation pressure at temperature T, *bar*

$R = $ pore radius, *nm*

$R^g = $ gas constant, $8.314459848 \times 10^{-2} L \cdot bar \cdot K^{-1} \cdot mol^{-1}$

$S =$ volume fraction

$T =$ temperature, K

$T_c =$ critical temperature, K

$v =$ molar volume, L/mol

$V =$ volume, L

$x =$ mole fraction

$z =$ feed composition

$\beta =$ phase fraction of vapor phase

$\mu =$ chemical potential, cp

$\sigma =$ interfacial tension (IFT), $dyne/cm$

$\omega =$ acentric factor

$\chi =$ parachor parameter

$\Phi =$ volume function coefficient

Superscripts

$L =$ liquid phase

$V =$ vapor phase

Subscripts

$i =$ component index

2.6 References

[1]   P. H. Nelson, "Pore-throat sizes in sandstones, tight sandstones, and shales," *Am. Assoc. Pet. Geol. Bull.*, vol. 93, no. 3, pp. 329-340, 2009.

[2]   U. Kuila and M. Prasad, "Specific surface area and pore-size distribution in clays and shales," *Geophys. Prospect.*, vol. 61, no. 2, pp. 341-362, 2013.

[3]   Z. Jin and A. Firoozabadi, "Thermodynamic modeling of Phase Behavior in Shale Media," *SPE J.*, vol. 21, no. 1, pp. 1-18, 2016.

[4]   S. Z. Qiao, S. K. Bhatia, and D. Nicholson, "Study of Hexane Adsorption in Nanoporous MCM-41 Silica," *Langmuir*, vol. 20, no. 2, pp. 389-395, 2004.

[5]   E. Parsa, X. Yin, and E. Ozkan, "Direct Observation of the Impact of Nanopore Confinement on Petroleum Gas Condensation," in *SPE Annual Technical Conference and Exhibition*, 28-30 September, Houston, Texas, USA, 2015.

[6]   M. Alfi, H. Nasrabadi, and D. Banerjee, "Experimental investigation of confinement effect on phase behavior of hexane, heptane and octane using lab-on-a-chip technology," *Fluid Phase Equilib.*, vol. 423, pp. 25-33, 2016.

[7]   Z. Jin, "Bubble/dew point and hysteresis of hydrocarbons in nanopores from molecular perspective," *Fluid Phase Equilib.*, vol. 458, pp. 177-185, 2018.

[8]   B. Nojabaei, R. T. Johns, and L. Chu, "Effect of capillary pressure on phase behavior in tight rocks and shales," *SPE Reserv. Eval. Eng.*, vol. 16, no. 03, pp. 281–289, 2013.

[9] J. P. R. B. Walton and N. Quirke, "Capillary condensation: a molecular simulation study." *Molecular Simulation*., vol. 2, pp.361-391,1989.

[10] T. Young, "An Essay on the Cohesion of Fluids," *Philos. Trans. R. Soc. London*, vol. 95, no. 0, pp. 65–87, 1805.

[11] D. R. Sandoval, W. Yan, M. L. Michelsen, and E. H. Stenby, "The phase envelope of multicomponent mixtures in the presence of a capillary pressure difference," *Ind. Eng. Chem. Res.*, vol. 55, no. 22, pp. 6530–6538, 2016.

[12] B. C. Stimpson and M. A. Barrufet, "Thermodynamic modeling of pure components including the effects of capillarity," *J. Chem. Eng. Data*, vol. 61, no. 8, pp. 2844–2850, 2016.

[13] M. Sherafati and K. Jessen, "Stability analysis for multicomponent mixtures including capillary pressure," *Fluid Phase Equilib.*, vol. 433, pp. 56–66, 2017.

[14] D. Y. Peng and D. B. Robinson, "A new two-constant equation of state," *Ind. Eng. Chem. Fundam.*, vol. 15, no. 1, pp. 59–64, 1976.

[15] M. L. Michelsen, "State function based flash specifications," pp. 617–626, 1999.

[16] J. Mikyška and A. Firoozabadi, "A new thermodynamic function for phase-splitting at constant temperature, moles, and volume," *AIChE J.*, vol. 57, no. 7, pp. 1897–1904, 2011.

[17] T. Jindrová and J. Mikyška, "Fast and robust algorithm for calculation of two-phase

equilibria at given volume, temperature, and moles," *Fluid Phase Equilib.*, vol. 353, pp. 101–114, 2013.

[18] D. V. Nichita, "New unconstrained minimization methods for robust flash calculations at temperature, volume and moles specifications," *Fluid Phase Equilibria*, vol. 466, 2018.

[19] J. Kou and S. Sun, "A stable algorithm for calculating phase equilibria with capillarity at specified moles, volume and temperature using a dynamic model," *Fluid Phase Equilib.*, vol. 456, pp. 7–24, 2018.

[20] M. L. Michelsen, "Calculation of multiphase equilibrium," *Comput. Chem. Eng.*, vol. 18, no. 7, pp. 545–550, 1994.

[21] C. F. Leibovici and J. Neoschil, "A new look at the Rachford-Rice" *Fluid Phase Equilib.* vol. 14, pp. 303–308, 1992.

[22] C. F. Weinaug and D. L. Katz, "Surface tensions of methane-propane mixtures," *Ind. Eng. Chem.*, vol. 35, pp. 239–246, 1943.

[23] H. H. Rachford Jr. and J. D. Rice, "Procedure for use of electronic digital computers in calculating flash vaporization hydrocarbon equilibrium," *Pet. Trans. AIME*, vol. 195, pp. 327–328, 1952.

[24] R. Okuno, R. Johns, and K. Sepehrnoori, "Three-phase flash in compositional simulation using a reduced method," *SPE J.*, vol. 15, no. 3, pp. 689–703, 2010.

[25] G. M. Wilson, "A modified Redlich-Kwong equation of state, application to general physical data calculations," in 65th *National AIChE Meeting*, Cleveland, OH, USA, 1969.

[26] J. Mikyška and A. Firoozabadi, "Investigation of mixture stability at given volume, temperature, and number of moles," *Fluid Phase Equilib.*, vol. 321, pp. 1–9, 2012.

[27] O. R. Quayle, "The parachors of organic compounds. An interpretation and catalogue," *Chem. Rev.*, vol. 53, no. 3, pp. 439–589, 1953.

[28] Y. Liu, Z. Jin, and H. Li, "Comparison of PR-EOS with capillary pressure model with engineering density functional theory on describing the phase behavior of confined hydrocarbons," *SPE J.*, vol. 23, no. 5., pp. 1784-1797, 2018.

CHAPTER 3 SIMPLE AND ROBUST ALGORITHM FOR ISOCHORIC-ISOTHERMAL THREE-PHASE EQUILIBIRUM COMPUTATIONS

A version of this chapter has been submitted to *SPE Journal* for possible publication.

Abstract

Two-phase and three-phase equilibria are frequently encountered in a variety of industrial processes, such as CO_2 injection for enhanced oil recovery in low-temperature reservoirs, multiphase separation in surface separators, and multiphase flow in wellbores and pipelines. Simulation and engineering design of these processes using isothermal-isochoric flash calculations are sometimes more convenient than that using isothermal-isobaric flash calculations. This work develops a robust isothermal-isochoric three-phase flash calculation algorithm using a nested approach. The proposed algorithm is simple since the isothermal-isobaric three-phase flash code is used in the inner loop without any further modifications, while an effective equation-solving method is applied to solve the pressure corresponding to a given volume-temperature specification. The robustness of the algorithm is safeguarded with the use of state-of-art trust-region-method-based solver in the isothermal-isobaric three-phase flash program. We demonstrate the robustness and efficacy of the developed algorithm by applying it to calculate the isochores of fluid mixtures that exhibit both two-phase and three-phase equilibria.

Keywords: Isothermal-isochoric flash; Isobaric-isothermal flash; Three-phase flash; Multiphase equilibria; Algorithm development

3.1 Introduction

In addition to two-phase equilibria, three-phase equilibria can be also frequently observed in the upstream petroleum industry. For example, when CO_2 injection is applied to low-temperature reservoirs for enhanced oil recovery, gas-liquid-liquid three-phase equilibria can appear in the porous-media flow (Pan *et al.*, 2015) or pipe flow (Pasqualette *et al.*, 2020). In the steam injection process for heavy oil recovery, a different type of three-phase equilibria (*i.e.*, gas-oil-water three-phase equilibria) can take place in the reservoir over a wide temperature/pressure range (Gao *et al.*, 2017; Petitfrere *et al.*, 2020). Hence it is important to consider such three-phase equilibria in the compositional simulations of these processes (Pang and Li, 2017; Connolly *et al.*, 2019; Li and Li, 2019a; Petitfrere *et al.*, 2020). Normally, engineers or researchers rely on isothermal-isobaric (PT) algorithms to carry out the multiphase equilibrium computations for a given fluid mixture. In such algorithms, pressure, temperature, as well as the feed composition, are specified as inputs to the algorithm and the objective is to find out the number of phases in equilibrium, and their fractions, compositions and volumes.

One alternative strategy to work out the multiphase equilibrium problem is to use volume, temperature and feed composition as known information, and find out pressure, the number of equilibrating phases and their properties (Michelsen, 1989). Such isothermal-isochoric (VT) equilibrium calculations are found to be more convenient in some engineering calculations (*e.g.*, multiphase equilibrium in storage vessels) than the conventional PT

equilibrium calculations (Cismondi *et al.*, 2018). The natural way to solve the VT flash is to recast the phase equilibrium problem as a minimization of the Helmholtz free energy and solve the minimization problem using optimization routines. Mikyska and Firoozabadi (2011) defined new thermodynamic functions and developed a new VT flash algorithm using the new thermodynamic functions. Later, such algorithm was successfully extended to three-phase flash calculations (Jindrova and Mikyska, 2013; Jindrova and Mikyska, 2015) and two-phase flash calculations with the consideration of capillary pressure (Lu *et al.*, 2019). Nichita (2018) developed a new unconstrained Helmholtz-free-energy minimization method used for conducting robust VT flash calculations. At given iteration level, Nichita (2018) treats volume as a variable dependent on mole numbers and solves such dependence by solving a nonlinear volume balance equation. The developed algorithm is shown to be fast and robust. But, overall, it is a not trivial task to set up the VT flash code based on the Helmholtz-free-energy minimization approach. In view of the complexity of the Helmholtz-free-energy minimization approach, Cismondi *et al.* (2018) developed a simple but efficient VT flash code for both vapor-liquid and liquid-liquid equilibria. Their VT flash algorithm is similar to the popular PT flash framework proposed by Michelsen (1982a and 1982b) and the only difference is that under a guessed pressure, it solves the phase molar volumes by solving a pressure-equality equation. But the efficacy of their algorithm has not been demonstrated for three-phase equilibrium computations.

Different from the Helmholtz-free-energy minimization approach, Agarwal *et al.* (1991)

developed a nested approach to conduct isenthalpic flash calculations using PT flash. In such approach, PT flash is solved in the inner loop while temperature is solved in the outer loop to satisfy the energy balance equation. Michelsen (1999) proposed a formal framework to formulate a variety of flash specifications (such as pressure-enthalpy (PH) specification and temperature-volume (VT) specification) for phase equilibrium computations. One of the two methods proposed by Michelsen (1999) is the so-called nested optimization approach where a PT flash is solved in the inner loop while the pressure and/or temperature are solved by maximizing the Q function. The advantage of such nested approaches lies in that they are very easy to implement, and their robustness can be well assured if the inner PT flash code is robust (Li and Li, 2017). The stage-wise PT-based multiphase equilibrium calculations proposed by Petitfrere and Nichita (2014) and Pan *et al.* (2019) is employed in our algorithm. The trust-region-based (TR) optimization method is used for solving both the stability tests and the flash calculation, which is found to be the most robust and efficient solution method.

The motivation of this work is to develop an easy-to-implement three-phase VT flash code that does not make any changes to the existing three-phase PT flash code and directly calls the three-phase PT flash code whenever needed. Such algorithm can be easily configured by practicing engineers to carry out VT flash computations, provided a reliable PT flash code is available. Through testing the three-phase PT flash code on many example fluid mixtures that exhibit three-phase equilibria, we prove the robustness of the three-phase VT

flash code. In the section of "Numerical Algorithm", we introduce the methodology and flowchart of the three-phase VT flash algorithm developed to solve for isochores for a given fluid mixture. In the section of "Results and Discussion", we present calculation results for one example reservoir fluid mixture that exhibits single-phase, two-phase (including vapor-liquid and liquid-liquid) and three-phase (*i.e.*, vapor-liquid-liquid) equilibria. We draw conclusions in the section of "Conclusions".

3.2 Numerical Algorithm

Without the direct calculation of Helmholtz free energy, we establish an algorithm to iteratively find the pressure corresponding to a specified volume. The continuous function (f) is given by,

$$f(P,T,z) = V(P,T,z) - V_{spec}, P^L < P < P^U \qquad (3.1)$$

where V_{spec} is the specified molar volume, V is the molar volume calculated from a robust PT solver, P^L and P^U are the pre-specified lower and upper pressure limits, respectively. P^L and P^U are set as 1 bar and 1000 bar in this study, respectively. The function values corresponding to P^L and P^U are represented by f^L and f^U, respectively. The zero of function (f) is solved by a root finding method discussed below.

As one derivative-free root finding method, the secant method has been successfully used in isenthalpic flash algorithms (Agarwal *et al.*, 1994; Li and Li, 2017). One advantage of the secant method is that no derivative calculations are involved, although its speed is also

73

compromised by this advantage. The secant method is applicable to our study because the isotherms in pressure-volume (PV) space are monotonic for multi-component fluids represented by a cubic equation of state (CEOS) (Firoozabadi, 2015; Cismondi *et al.*, 2018). However, the secant method can become unstable when an inferior initial guess is used. To avoid this problem, Dekker (1969) proposed a new root finding method combining the bisection method and the secant method. Then Brent (1971) modified this method to be a more stable and adaptable version. The algorithm proposed by Brent (1971) yields guaranteed convergence for finding the zero of a function. It is a combination of the bisection method, the secant method, and the inverse quadratic interpolation.

Considering the robustness of the Brent algorithm (Brent, 1971), it is adopted in this study. We thereby solve the root finding problem defined in Eq. 1 by the Brent algorithm (Brent, 1971). **Figure 3-1** shows the flowchart of the Brent algorithm (Brent, 1971) in the context of our VT flash problem. In Figure 3-1, the parameters $a, b, c, d,$ and e are values of the independent variables, which are pressure values in our problem. The parameters $fa, fb,$ and fc are function values calculated at $a, b,$ and c using Eq. 3.1. The parameters $m, p, q, r,$ and s are intermediate variables. The finally calculated value of b is the root of our problem. As shown in Figure 3-1, two error tolerances, namely tol_1 and tol_2, are used. tol_1 is defined for b in the original algorithm by Brent (1971). tol_2 is a user-defined tolerance that directly corresponds to the function value fb. The termination criterion of the whole algorithm is $abs(fb) \leq tol_2$. Herein, we set $tol_2 = 1 \times 10^{-6}$ and

tol_1 is given by Brent (1971) as: $tol_1 = 2 \times eps \times |b| + 10^{-14} \ll tol_2$ (where eps is

the machine precision).
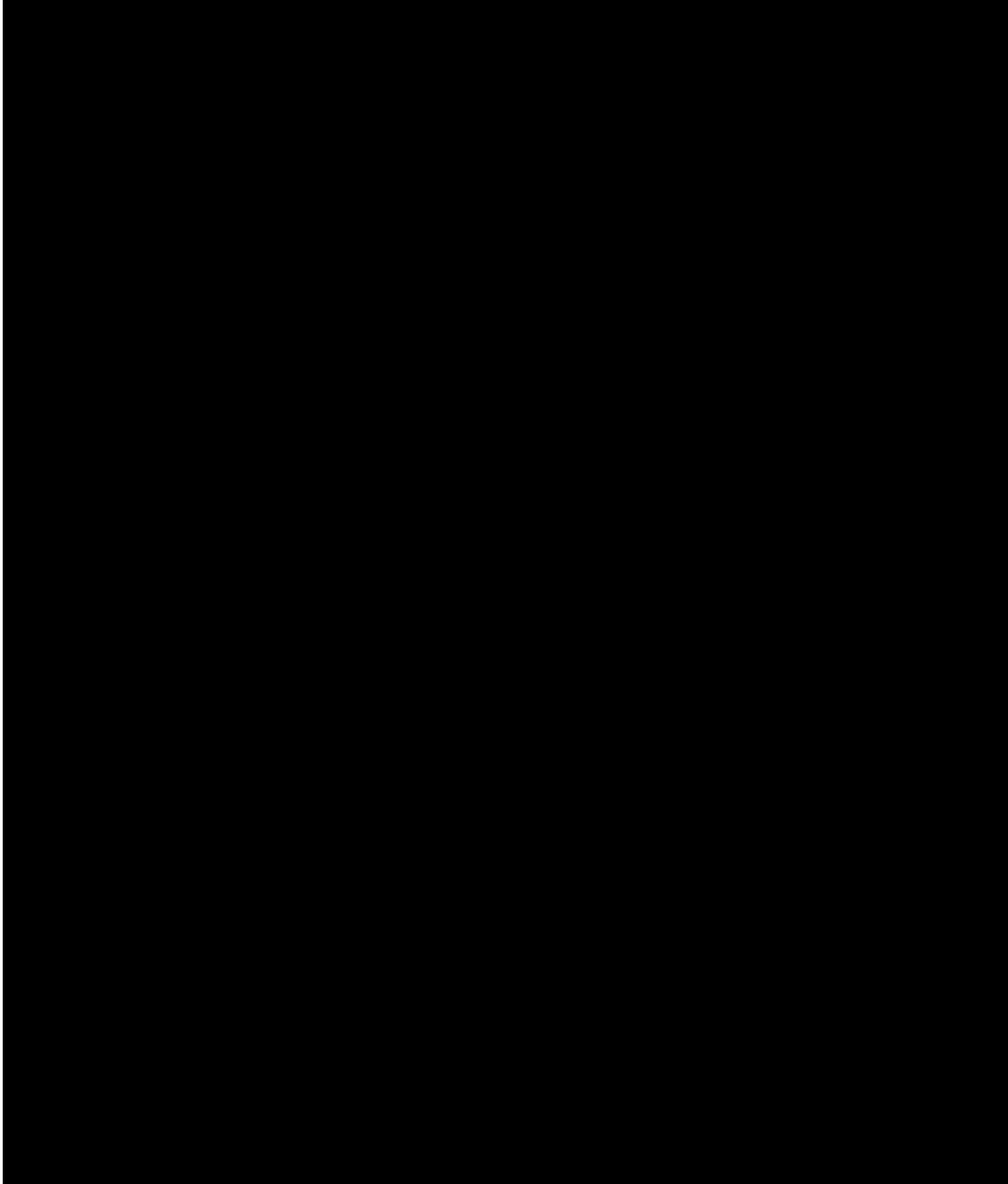
Figure 3-1 Flowchart of Brent's equation solving method (Brent, 1971)

Presented below is the stepwise procedure executed in the VT flash algorithm:

1) Input T, V, feed composition (z), and other fluid properties (critical temperature (T_c), critical pressure (P_c), acentric factors (ω), and binary interaction parameters (BIP)).

2) Set the lower and upper boundaries of P (P^L and P^U).

3) Call the PT solver to calculate f^L and f^U.

4) Assuming the fluid remains as one-phase, calculate the initial guess P^0 using PR-EOS (Peng and Robinson, 1976).

5) If $P^L < P^0 < P^U$ is true, go to step 7. If not, two options are available: If $P^0 < P^L$, set $P^0 = (P^L + P^U)/2$, go to step 7; if $P^0 > P^U$, go to step 6.

6) Set $P^U = P^U + 100$ bar and go back to step 3.

7) Calculate f^0 using Eq. 1 and check if $abs(f^0) > 1 \times 10^{-6}$. If true, go to step 8; if not, P^0 is the solution and go to step 11.

8) Check if $f^0 f^L < 0$. If true, $P^U = P^0$ and $f^U = f^0$; if not, $P^L = P^0$ and $f^L = f^0$.

9) Set $a = P^L$, $b = P^U$, $fa = f^L$, $fb = f^U$ as the input parameters for Brent's algorithm.

10) Call Brent's algorithm, and record f and other essential parameters at the converged pressure $P = b$.

11) Output f, P, phase compositions, phase fractions and phase compressibilities.
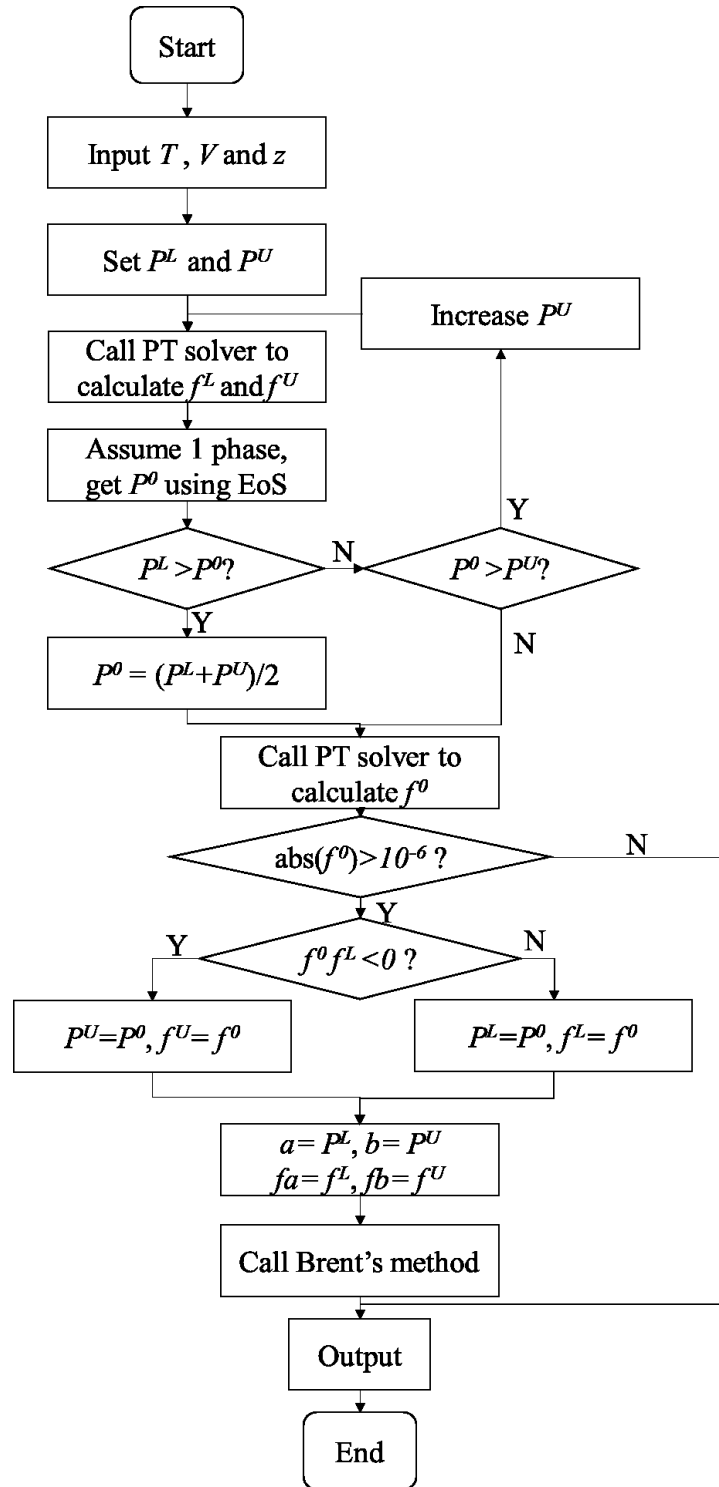
Figure 3-2 Flowchart of the three-phase VT flash calculation algorithm developed based on the three-phase PT flash subroutine.

Figure 3-2 shows the flowchart of the above three-phase VT flash calculation algorithm based on the three-phase PT flash subroutine. In recent studies by Petitfrere and Nichita (2014) and Pan *et al.* (2019), the TR-based optimization method is employed to solve the PT based multiphase equilibrium problem. The TR algorithm comprises two major steps: a) updated the TR radius; b) compute the step size for the restricted step within the TR radius. TR algorithm is used for both the stability tests and the flash calculation. The hybrid algorithm combining the successive substitution iteration (SSI), the Newton method, and the TR optimization method (Petitfrere and Nichita, 2014; Pan *et al.*, 2019) is implemented in the three-phase PT flash solver. Moreover, the multiphase Rachford-Rice problems (Rachford and Rice, 1952) are also solved by the TR method in the inner loop when the SSI method is applied. A detailed coverage of how to apply the TR optimization method (Nocedal and Wright, 2006) in the stagewise multiphase equilibrium calculations can be found in the papers by Petitfrere and Nichita (2014) and Pan *et al.* (2019). In particular, an extensive test has been done by Pan *et al.* (2019) on nine CO_2-reservoir fluids. The TR optimization method shows an excellent performance even in the stability test limit locus region in stability testing and in the critical region for two-phase and three-phase flashes, which are the most challenging problems during the phase equilibrium calculations. There is no single failure encountered during the construction of pressure-temperature and pressure-composition (*PX*) phase diagrams involving both two-phase and three-phase equilibria in the case studies by Pan *et al.* (2019). Moreover, the sequential SSI-Newton-TR algorithm performs much more efficiently compared with other algorithms (such as by

the combination of SSI and Newton method). Thus, to a certain extent, the efficiency and the robustness of our three-phase VT flash calculation algorithm can be safeguarded by using the PT-based phase equilibrium calculation algorithm proposed by Petitfrere and Nichita (2014) and Pan *et al.* (2019). The algorithms shown in Figures 3-1 and 3-2 are implemented in Matlab. We have compared the calculated phase diagrams for all the reservoir fluids tested in the studies by Petitfrere and Nichita (2014) and Pan *et al.* (2019) against those yielded by our algorithm. The comparison indicates an excellent agreement.

3.3 Results and Discussion

We show the calculation results for two case studies. The first case study is focused on the three-phase equilibrium calculations for the NWE oil sample mixed with 70 mol% of an impure CO_2 mixture (i.e., CO_2-CH_4 mixture), while the second case study is focused on the three-phase equilibrium calculations for the JEMA oil sample mixed with 75 mol% of pure CO_2. Both mixtures exhibit three-phase vapor-liquid-liquid equilibria at low temperatures (Khan *et al.*, 1992). **Table 3-1** shows the fluid properties of the NWE oil sample and injection gas (Khan *et al.*, 1992; Okuno *et al.*, 2010). **Table 3-A1** shows the fluid properties of the JEMA oil sample and injection gas (Khan *et al.*, 1992; Okuno *et al.*, 2010). In this section, we only show the calculation results for the NWE oil, while the appendix shows the calculation results for the JEMA oil.

Table 3-1 The fluid properties of the NWE oil sample and injection gas (Khan *et al.*, 1992; Okuno *et al.*, 2010).

Components	Oil composition (mol%)	Gas composition (mol%)	Molecular weight	T_c, K	P_c, bar	ω	BIP with CO_2*
CO_2	0.77%	95.0	44.01	304.20	73.76	0.225	0
C_1	20.25%	5.0	16.04	190.60	46.00	0.008	0.12
C_{2-3}	11.80%	0.0	38.4	343.64	45.05	0.130	0.12
C_{4-6}	14.84%	0.0	72.82	466.41	33.50	0.244	0.12
C_{7-14}	28.63%	0.0	135.82	603.07	24.24	0.600	0.12
C_{15-24}	14.90%	0.0	257.75	733.79	18.03	0.903	0.12
C_{25+}	8.81%	0.0	479.95	923.20	17.26	1.229	0.12

*All the other BIPs are zero.

Figure 3-3 shows the *PX* phase diagram which is generated using the trust-region-optimization-based PT flash solver for the NWE oil sample mixed with the injection gas at 301.48 K. The composition of the injection gas is 95 mol% CO_2 and 5 mol% CH_4. The graph is generated by carrying out multiphase equilibrium calculations over a mole-fraction interval of 0.0025 and a pressure interval of 0.175 bar. A total of 160000 times of PT flash calculations are involved. No single failure is found during these computations. It can be observed from Figure 3-3 that the phase boundaries have pretty smooth and consistent shapes. A large three-phase (i.e., three-phase vapor-liquid-liquid equilibria) region appears at the lower right part of the diagram. In such a three-phase vapor-liquid-liquid equilibrium for CO_2-oil mixtures, the first liquid phase is lighter phase rich in CO_2, while the second liquid phase is heavier phase rich in oil.
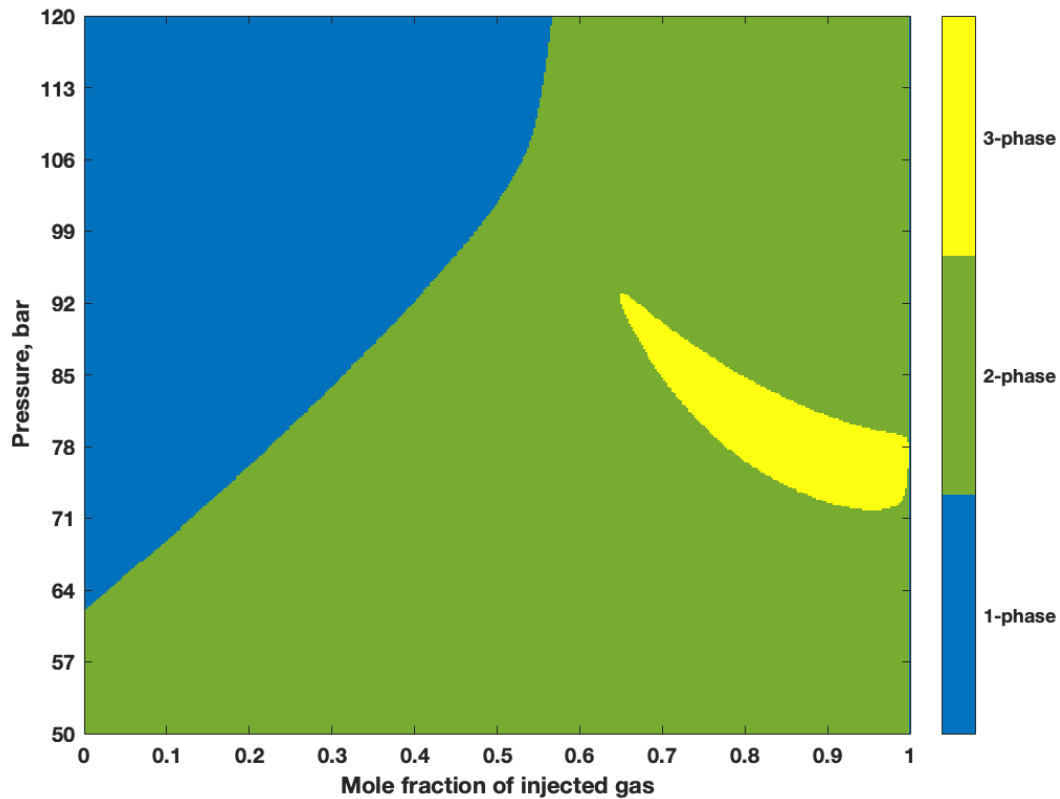
Figure 3-3 *PX* diagram generated using the PT flash solver for the NWE oil sample mixed with the injection gas at 301.48 K. The graph is generated by multiphase equilibrium calculations over a mole-fraction interval of 0.0025 and a pressure interval of 0.175 bar. A total of 160000 equilibrium calculations are involved.

Next, we calculate the PT phase diagram for the NWE oil mixed with 70 mol% injection gas using the PT flash solver. **Figure 3-4** shows the calculation results. As temperatures reduces (see Figure 3-4), the bubble-point curve of the two-phase envelope is uplifted to the extremely-high-pressure side of the phase diagram, instead of showing a downward trend as exhibited by the commonly seen reservoir fluids. This is reminiscent of a liquid-liquid immiscibility phenomenon (Michelsen, 1982b). Due to the liquid-liquid immiscibility, one tiny three-phase vapor-liquid-liquid equilibrium region appears at the lower-left corner of the diagram. In Figure 3-4 are also drawn the isochoric lines at constant

molar volumes (ranging from 80 cm^3/mol to 500 cm^3/mol) that are computed with the proposed VT flash algorithm. These isochoric lines are generated by repetitively carrying out the VT calculations under a constant molar volume but gradually reducing temperatures. As a part of Figure 3-4, **Figure 3-5** shows an enlarged view of the three-phase boundary together with the isochoric lines passing through the three-phase region. Liquid-liquid equilibria reside above the three-phase boundary, while vapor-lqiuid equilibria prevail below the three-phase boundary. As can be seen from Figures 3-4 and 3-5 that, starting from the one-phase equilibria at higher pressures, all the isochoric lines tend to first ecounter the two-phase envelope, and then pass through the three-phase envelope. Another interesting observation from Figure 3-5 is that the slope change of the isochoric lines transitioning from a liquid-liquid equilibrium to a vapor-liquid-liquid equilibrium is much more abrupt than that exhibited by the isochoric lines transitioning from one vapor-liquid equilibrium to a vapor-liquid-liquid equilibrium.
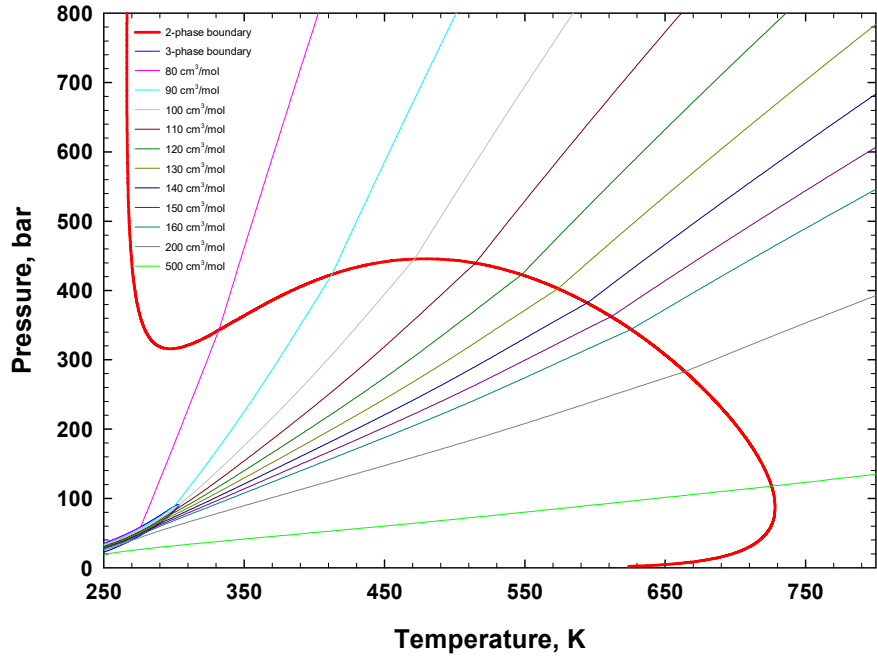
Figure 3-4 Two-phase and three-phase envelopes calculated for the NWE oil mixed with 70 mol% injection gas as shown in Table 3-1. The isochoric lines, calculated with the proposed VT flash algorithm, are also shown in this figure.
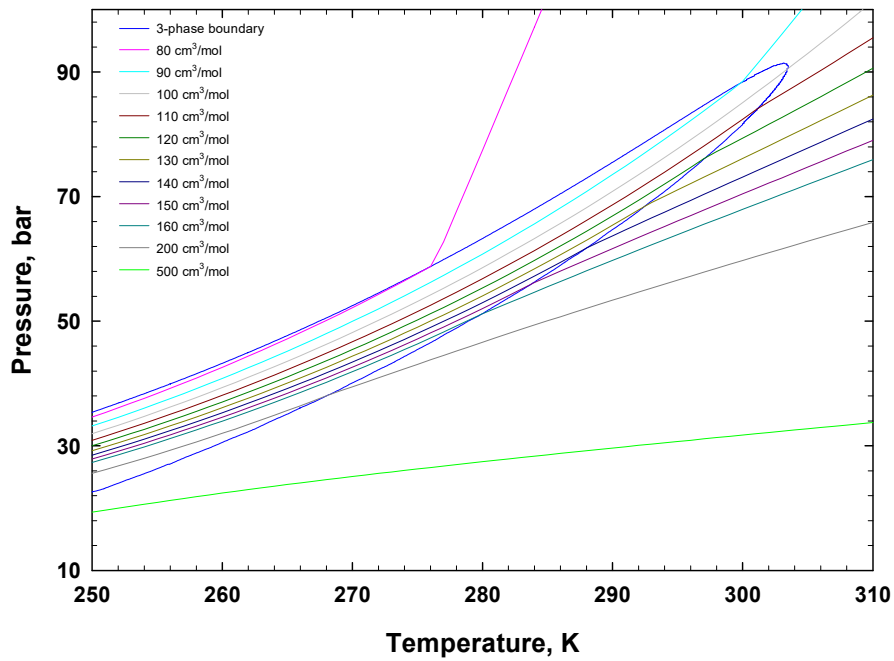
Figure 3-5 A close-up view showing the three-phase boundary together with the isochoric lines passing through the three-phase region for the NWE oil mixed with 70 mol% injection gas.

In addition, one can observe an interesting feature exhibited by Figures 3-4 and 3-5, i.e., all the isochores tend to trace back to the three-phase region. This implies that if one conducts VT flash calculations along a given isochore, one could very likely encounter single-phase, two-phase, and three-phase equilibria. This becomes advantageous when one tries to work out the phase boundaries using a VT flash algorithm. This is one of the motivations underlying the development of density-based algorithms for constructing phase envelopes, as attempted by Nichita (2019). The conventional PT flash calculations at constant pressure or constant temperature, however, do not have such advantage. **Figure 3-6** shows a projection of the two-phase and three-phase envelopes (shown in Figure 3-4) in the temperature-molar-volume space, while **Figure 3-7** shows the same projection in the temperature-density space. These phase boundaries are tracked based on the isochoric flash results calcualted using the VT flash algorithm developed in this study. Similar charts are displayed in the studies by Molina (2019) and Nichita (2019). Nichita (2019) showed that the density-based calculation method can be readily applied to generate two-phase boundaries in the temperature-density space.
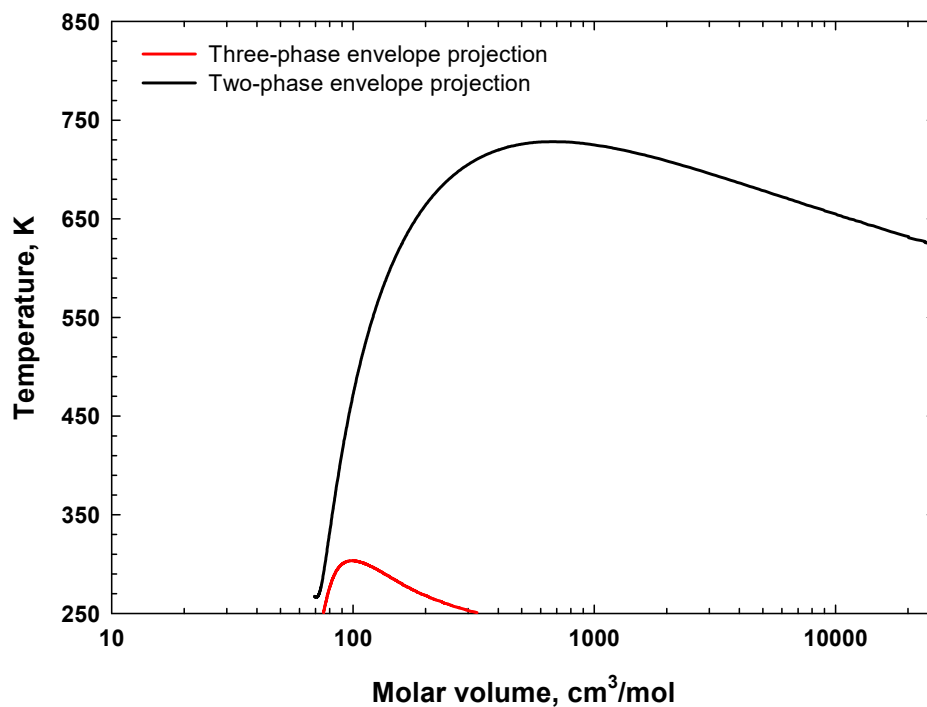
Figure 3-6 Projection of two-phase envelope and three-phase envelope in the temperature-molar-volume space calculated for the NWE oil mixed with 70 mol% injection gas.
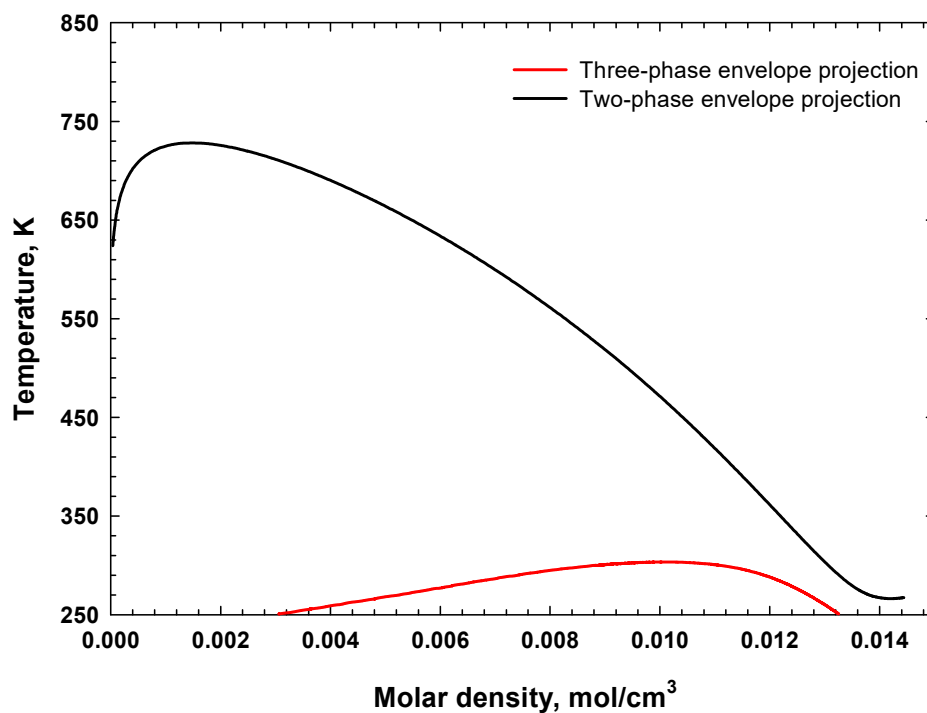
Figure 3-7 Projection of two-phase envelope and three-phase envelope in the temperature-density space calculated for the NWE oil mixed with 70 mol% injection gas.

Isochoric calculations can reveal how the phase fractions vary as a function of temperature in a fixed-volume cell. **Figure 3-8** illustrates how the phase fractions vary as temperature reduces along an isochoric line of 80 cm^3/mol. Along this isochoric line, the phase equilibria switch from single liquid-phase equilibria, to liquid-liquid two-phase equilibria, and finally to vapor-liquid-liquid three-phase equilibria. It can be seen from Figure 3-8 that the mixture remains as a single liquid phase at temperatures above 332 K. At temperatures lower than 332 K, a lighter liquid phase emerges. As temperature reduces, the phase fraction of the lighter phase first increases substantially, followed by a gentler increase before entering the three-phase zone. At 276 K, a vapor phase appears. After passing the three-phase boundary at 276 K, the phase fraction of the lighter phase starts to decrease, which is accompanied by an increase in the phase fractions of both the vapor phase and the heavier phase. **Figure 3-9** illustrates how the phase fractions vary as temperature reduces along an isochoric line with a much larger molar volume of 120 cm^3/mol. Along this isochoric line, the phase equilibria switch from single vapor-phase equilibria, to vapor-liquid two-phase equilibria, and finally to vapor-liquid-liquid three-phase equilibria. Figure 3-8 shows that the mixture remains as a single vapor phase at temperatures above 547 K. A heavier liquid phase emerges at temperatures lower than 547 K. At temperature reduces, the heavier liquid phase takes a larger fraction, which is accompanied by a decline in the phase fraction of the vapor phase. At 297 K, a third phase (*i.e.*, the lighter liquid phase) appears. As temperature further reduces, the phase fraction of the lighter liquid phase keeps increasing, while the phase fractions of the heavier liquid phase and the vapor phase keep

decreasing.
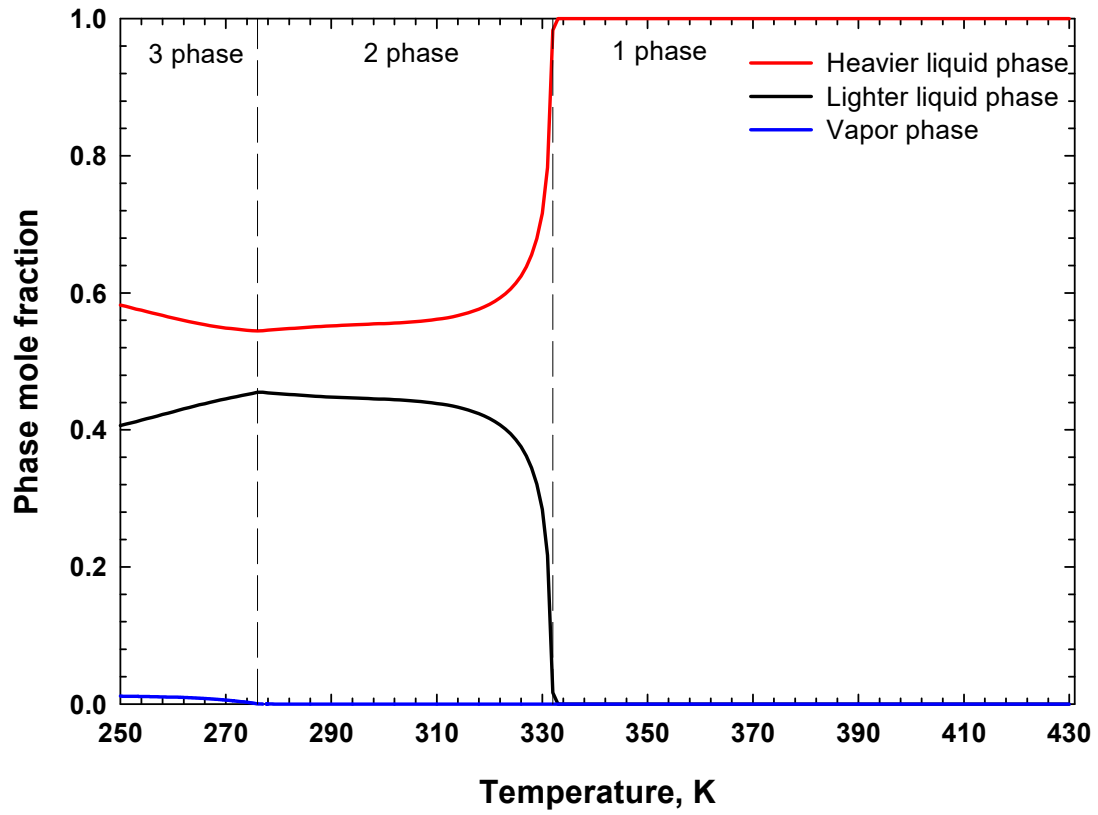
Figure 3-8 Variation of phase fractions vs. temperature along the isochore of 80 cm^3/mol calculated for the NWE oil mixed with 70 mol% injection gas.
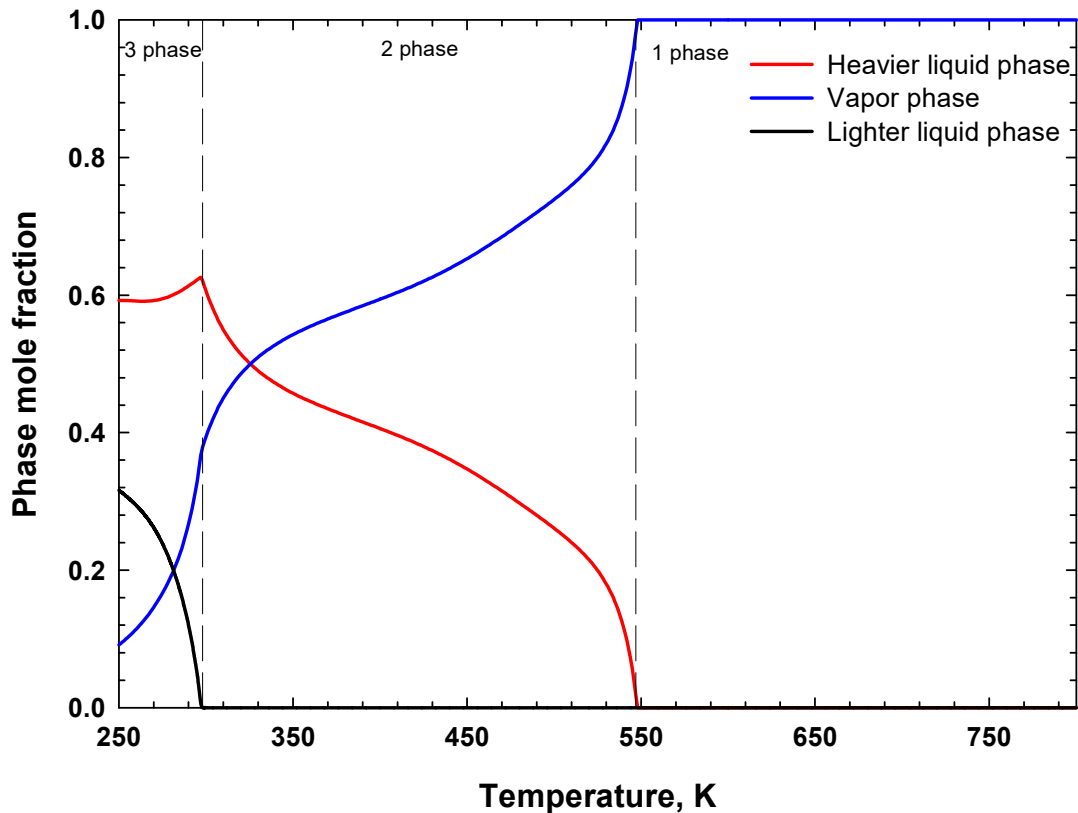
Figure 3-9 Variation of phase fractions vs. temperature along the isochore of 120 cm^3/mol for the NWE oil mixed with 70 mol% injection gas.

Figure 3-10 shows the number of calling the PT flash solver in the VT flash computations along the isochore of 120 cm^3/mol. It can be seen from Figure 3-10 that only one iteration is needed to call the PT flash solver to converge the solution. The number of calling the PT flash solver tends to increase when the number of equilibrating phases increases from one to two as well as from two to three. The maximum number of calling the PT flash solver is 15. **Figure 3-11** further shows a statistical summary of the number of calling the PT flash solvers during the VT flash computations for all the isochores shown in Figure 3-4. Figures 3-10 and 3-11 show that, on average, fewer than 10 iterations are required to converge the VT flashes, demonstrating a good overall efficiency of the VT flash algorithm.
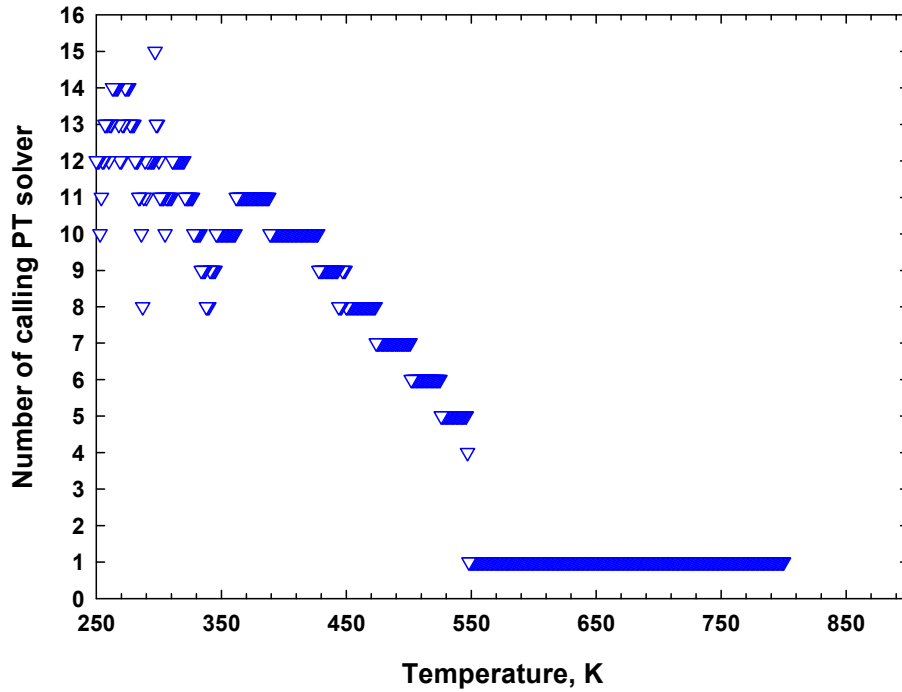
Figure 3-10 The number of calling the PT flash solver in the VT flash computations along the isochore of 120 cm^3/mol for the NWE oil mixed with 70 mol% injection gas.
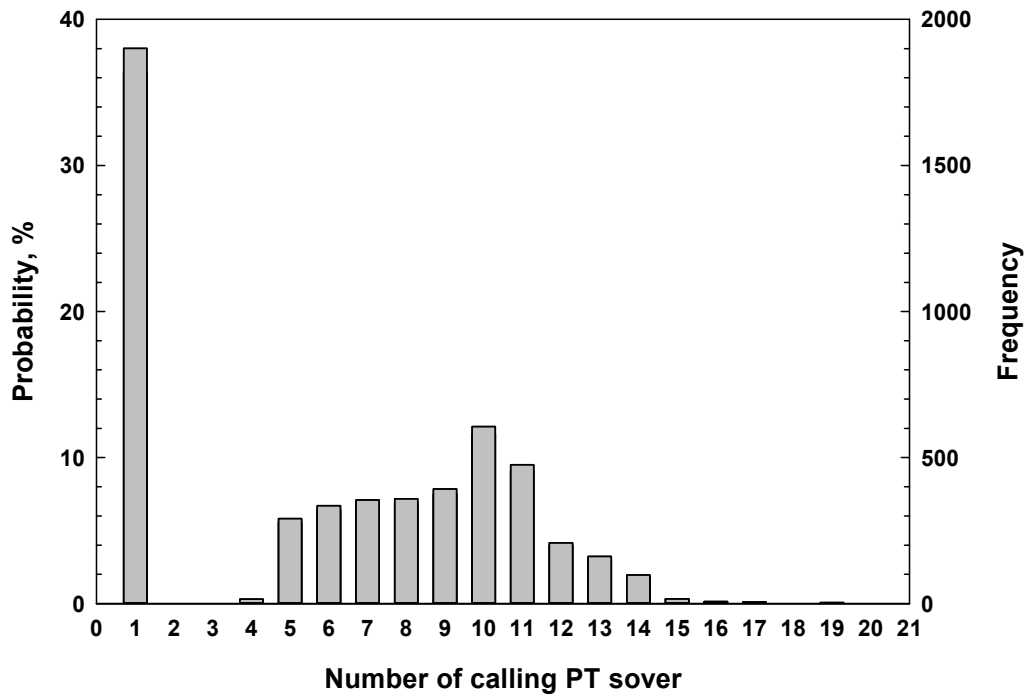
Figure 3-11 Statistical summary of the number of calling the PT flash solver in the VT flash computations along the isochores shown in Figure 3-4.

The application of the proposed VT flash algorithm is multifold. First of all, it can be

readily coupled into compositional reservoir-flow and wellbore-flow simulators that are more conducive to isochoric phase equilibrium computations. Secondly, it can be applied to aid engineering design calculations for constant-volume containers in the petroleum and chemical industry (such as storage tanks). Thirdly, our algorithm can be also applied to guide the phase equilibrium measurements in a fixed-volume PVT cell. In such fixed-volume phase behavior measurements, the temperature is either increased or decreased. Then, the resulting pressure and phase volume at equilibrium are measured. Sometimes, prior to the phase behavior experiments, we need to design a feed composition which can allow for the appearance of three-phase equilibria in the fixed-volume PVT cell. In such case, preliminary VT calculations can be conducted on a number of promising feeds. Based on the VT flash calculation results, we can confidently select the ones which can result in the appearance of three-phase equilibria. Last but not least, the VT flash algorithm presented in this study can be potentially leveraged to provide reliable initializations in the phase envelope construction algorithm (Michelsen, 1980; Aggar and Sørensen, 2018). For instance, when we try to calculate the three-phase boundary in a PT diagram for a given fluid, how to initialize the three-phase envelope construction algorithm is always a challenging task because we normally do not have good prior knowledge about under what conditions three-phase equilibria could appear. How can this be achieved? Herein, we can take the isochoric line corresponding to a molar volume of 100 cm^3/mol shown in Figure 3-4 for example. Multiple VT flash computations can be first conducted over the temperature range of interest (e.g., 250 K to 750 K). The intersection between the isochoric

line of 100 cm^3/mol and the three-phase boundary can be then easily detected from the VT flash computations. One can then use this intersection to conveniently initialize the three-phase envelope construction algorithm.

3.4 Conclusions

In this work, we develop a robust and simple VT flash algorithm for conducting three-phase equilibrium calculations for CO_2-inclusive mixtures. We draw the following conclusions from the present study:

1) The VT three-phase flash calculation algorithm is built using a nested approach. The PT three-phase flash code is used in the inner loop without any further modifications, while an effective equation-solving method, i.e., the Brent (1971) method, is applied in the outer loop to solve for the pressure corresponding to a given volume-temperature specification;

2) The robustness of the newly developed VT flash algorithm is safeguarded with the combined use of the trust-region-method-based PT flash solver and the Brent (1971) solver. These two solvers are shown to be very robust in previous studies as well as in the present study;

3) Our example calculations demonstrate that the new VT flash algorithm is always able to converge to the correct phase equilibria including one-phase equilibria,

vapor-liquid or liquid-liquid two-phase equilibria, and vapor-liquid-liquid three-phase equilibria;

4) The new algorithm is shown to be relatively efficient. On average, one time of calling the PT solver is needed to converge the VT flashes for one-phase equilibria, while fewer than 10 times of calling the PT solver are required to converge the VT flashes for two-phase and three-phase equilibria;

5) The potential applications of the developed VT flash algorithm are multifold. In particular, the VT flash algorithm presented in this study can be potentially leveraged to provide reliable initializations in the phase envelope construction algorithm. This opens the door of developing new robust phase-envelope construction algorithms based on the three-phase VT flash algorithm developed in this study.

Acknowledgments

3.5 References

Agarwal, R.K., Li, Y.K., Nghiem, L.X., and Coombe, D.A. 1991. Multiphase multicomponent isenthalpic flash calculations. *J. Can. Pet. Tech.* **30** (3): 69-75.

Agger, C.S. and Sørensen, H. 2018. Algorithm for constructing asphaltene PT and Px phase diagrams. *Ind. & Eng. Chem. Res.* **57** (1): 392-400.

Brent, R.P. 1971. An algorithm with guaranteed convergence for finding a zero of a function. *Comp. J.* **14** (4): 422-5.

Cismondi, M., Ndiaye, P.M., and Tavares, F.W. 2018. A new simple and efficient flash algorithm for T-v specifications. *Fluid Phase Equilibr.* 464: 32-39.

Connolly, M., Pan, H., and Tchelepi, H. 2019. Three-phase equilibrium computations for hydrocarbon-water mixtures using a reduced variables method. *Ind. Eng. Chem. Res.* **58**: 14954-14974.

Dekker, T.J. 1969. Finding a zero by means of successive linear interpolation, in *Constructive Aspects of the Fundamental Theorem of Algebra*, B. Dejon and P. Henrici (editors), Wiley-Interscience, New York, pp. 37–48.

Firoozabadi, A. 2015. *Thermodynamics and Applications of Hydrocarbon Energy Production*. McGraw Hill Professional.

Gao, J., Okuno, R., and Li, H. 2017. An experimental study of multiphase behavior for *n*-butane/bitumen/water mixtures. *SPE J.* **22** (3): 783-798.

Jindrova, T. and Mikyska, J. 2015. General algorithm for multiphase equilibria calculation

at given volume, temperature, and moles. *Fluid Phase Equilib.* **393**: 7-25.

Jindrova, T. and Mikyska, J. 2013. Fast and robust algorithm for calculation of two-phase equilibria at given volume, temperature, and moles. *Fluid Phase Equil.* **353**: 101-114.

Khan, S.A., Pope, G.A., and Sepehrnoori, K. 1992. Fluid characterization of three-phase CO_2/oil mixtures. Paper SPE 24130 presented at the *SPE/DOE Enhanced OilRecovery Symposium*, Tulsa, 22-24 April.

Li, R. and Li, H. 2017. A robust three-Phase isenthalpic flash algorithm based on free-water assumption. *J. Energy Res. Tech.* **140** (3): 032902.

Li, R. and Li, H. 2019a. Improved three-phase equilibrium calculation algorithm for water/hydrocarbon mixtures. *Fuel* **244** (15): 517-527.

Li. R. and Li, H. 2019b. Robust three-phase vapor–liquid–asphaltene equilibrium calculation algorithm for isothermal CO_2 flooding applications. *Ind. Eng. Chem. Res.* **58** (34): 15666-15680.

Lu, C., Jin, Z. and Li, H. 2019. A two-phase flash algorithm with the consideration of capillary pressure at specified mole numbers, volume and temperature. *Fluid Phase Equilibr.* **485**: 67-82.

Michelsen, M.L. 1982. The isothermal flash problem. Part I. Stability test. *Fluid Phase Equilibr.* **9** (1): 1-19.

Michelsen, M.L. 1982. The isothermal flash problem. Part II. Phase-split calculation. *Fluid*

Phase Equilibr. **9** (1): 21-40.

Michelsen, M.L. 1999. State function based flash specifications. *Fluid Phase Equilibr.* **158-160**: 617-626.

Michelsen, M.L. 1980. Calculation of phase envelopes and critical points for multicomponent mixtures. *Fluid Phase Equilibr.* **4** (1-2): 1-10.

Mikyska, J. and Firoozabadi, A. 2011. A new thermodynamic function for phase-splitting at constant temperature, moles, and volume. *AIChE J.* **57** (7): 1897-1904 .

Molina, M.J., Rodriguez-Reartes, S.B., and Zabaloy, M.S. 2019. Computation and analysis of binary multiphase isochors. *Fluid Phase Equilibri.* **500**: 112227.

Nichita, D.V. 2018. New unconstrained minimization methods for robust flash calculations at temperature, volume and moles specifications. *Fluid Phase Equilibr.* **466**: 31-47.

Nichita, D.V. 2019. A simple approximate density-based phase envelope construction method. *Fluid Phase Equilibr.* **499** (1): 112245.

Nocedal, J. and Wright, S.J. 2006. *Numerical Optimization*. Springer: New York.

Okuno, R., Johns, R., and Sepehrnoori, K. 2010. Three-phase flash in compositional simulation using a reduced method. *SPE J.* **15**: 689-703.

Pan, H., Chen, Y., Sheffield, J., Chang, Y., and Zhou, D. 2015. Phase-behavior modeling and flow simulation for low-temperature CO_2 injection. *SPE Res. Eval. Eng.* **18** (2): 250-263.

Pan, H., Connolly, M., and Tchelepi, H. 2019. Multiphase equilibrium calculation

framework for compositional simulation of CO_2 injection in low-temperature reservoirs. *Ind. Eng. Chem. Res.* **58**: 2052-2070.

Pang, W. and Li, H. 2017. An augmented free-water three-phase flash algorithm for CO_2/hydrocarbon/water mixtures. *Fluid Phase Equilibr.* **450**: 86-98.

Pasqualette, M.D., Carneiro, J., Johansen, S.T., Lovfall, B.T., Fonseca Jr., R., and Ciambelli, J. 2020. A numerical sssessment of carbon-dioxide-rich two-phase flows with dense phases in offshore production pipelines. *SPE J.* **25** (2): 712-731.

Peng, D.Y. and Robinson, D.B. 1976. A new two-constant equation of state. *Ind. Eng. Chem. Fund*. **15** (1): 59-64.

Petitfrere, M. and Nichita, D.V. 2014. Robust and efficient trust-region based stability analysis and multiphase flash calculations. *Fluid Phase Equilib.* **362**: 51−68.

Petitfrere, M., Nichita, D.V., Voskov, D., Zaydullin, R., and Bogdanov, I. 2020. Full-EoS based thermal multiphase compositional simulation of CO_2 and steam injection processes. *J. Pet. Sci. Eng.* **192:** 107241.

Rachford, H.Jr. and Rice, J. 1952. Procedure for use of electronic digital computers in calculating flash vaporization hydrocarbon equilibrium. *AIME Trans.* **195**: 327-328.

Appendix — Calculation results for the JEMA oil sample and injection gas (Khan *et al*., 1992; Okuno *et al*., 2010).
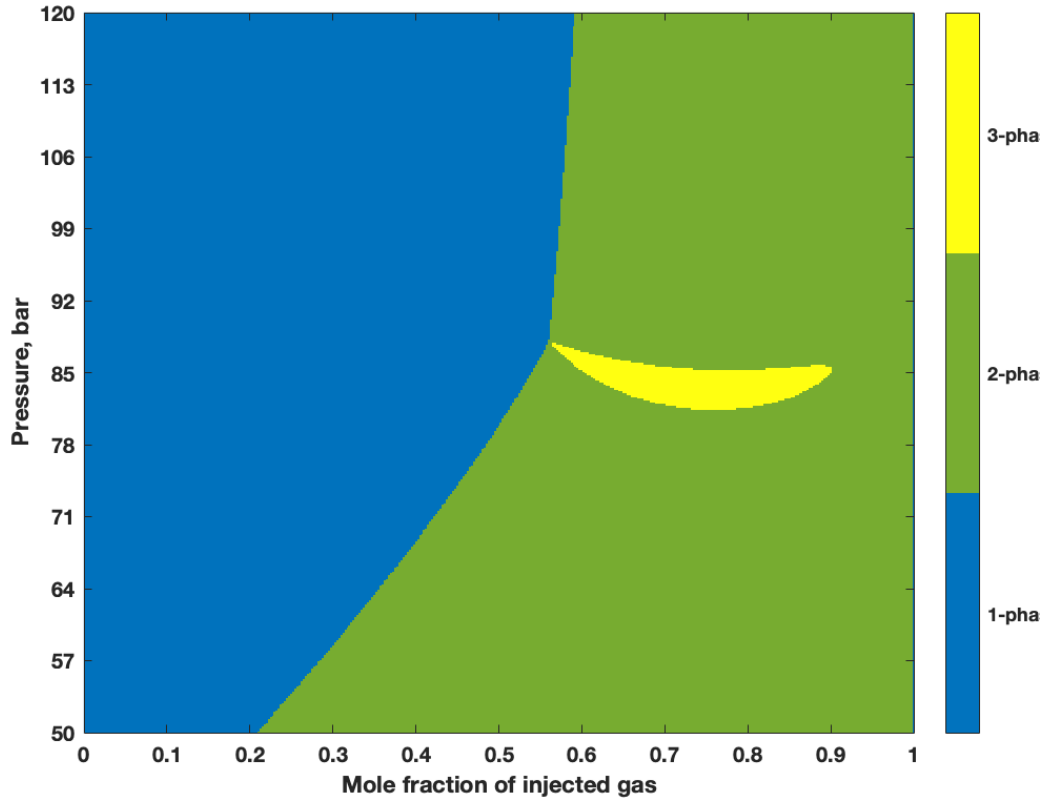
Figure 3-A1 *PX* diagram generated using the PT solver for the JEMA oil sample mixed with the injection gas at 316.48 K. The graph is generated by multiphase equilibrium calculations over a mole-fraction interval of 0.0025 and a pressure interval of 0.175 bar. A total of 160000 equilibrium calculations are involved.
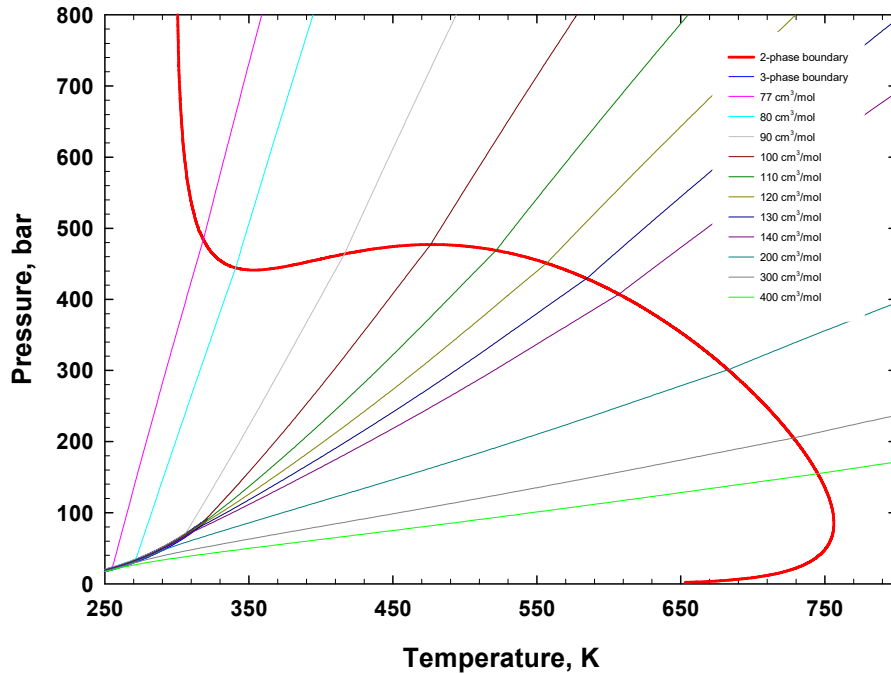
Figure 3-A2 Two-phase and three-phase envelope calculated for the JEMA oil mixed with 75 mol% injection gas as shown in Table A1. The isochoric lines are also calculated with the proposed algorithm and drawn in this figure.
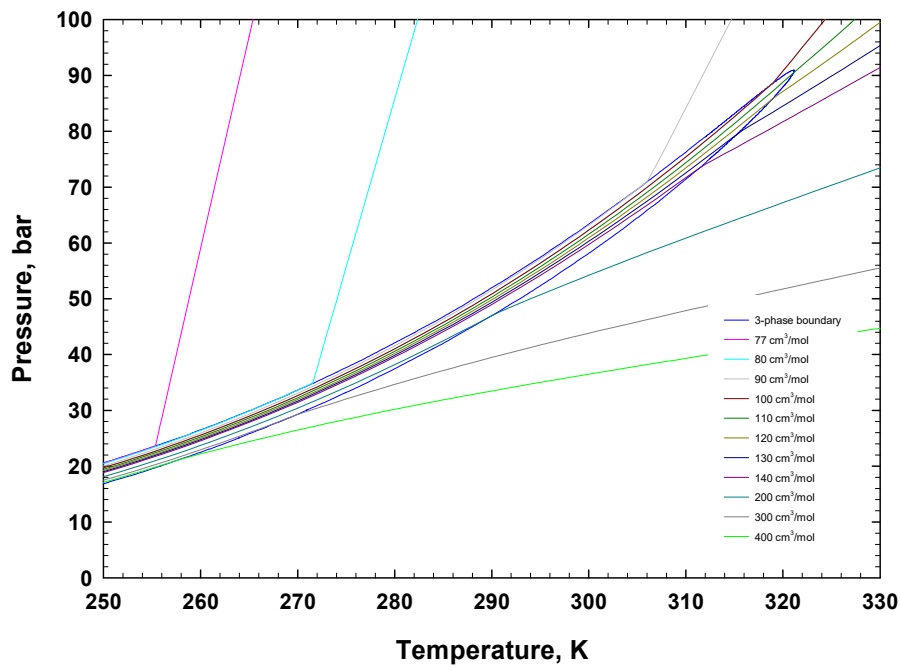
Figure 3-A3 A close-up view of the three-phase boundary shown in A2 together with the isochoric lines passing through the three-phase region.
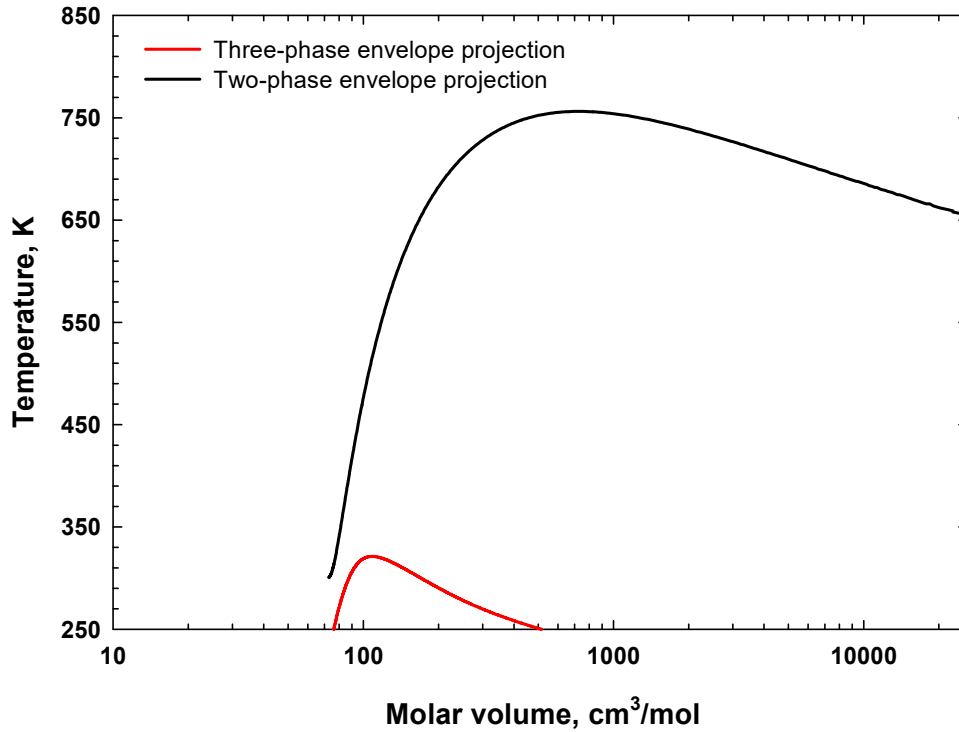
Figure 3-A4 Projection of two-phase envelope and three-phase envelope in the temperature-volume space calculated for the JEMA oil mixed with 75 mol% injection gas.
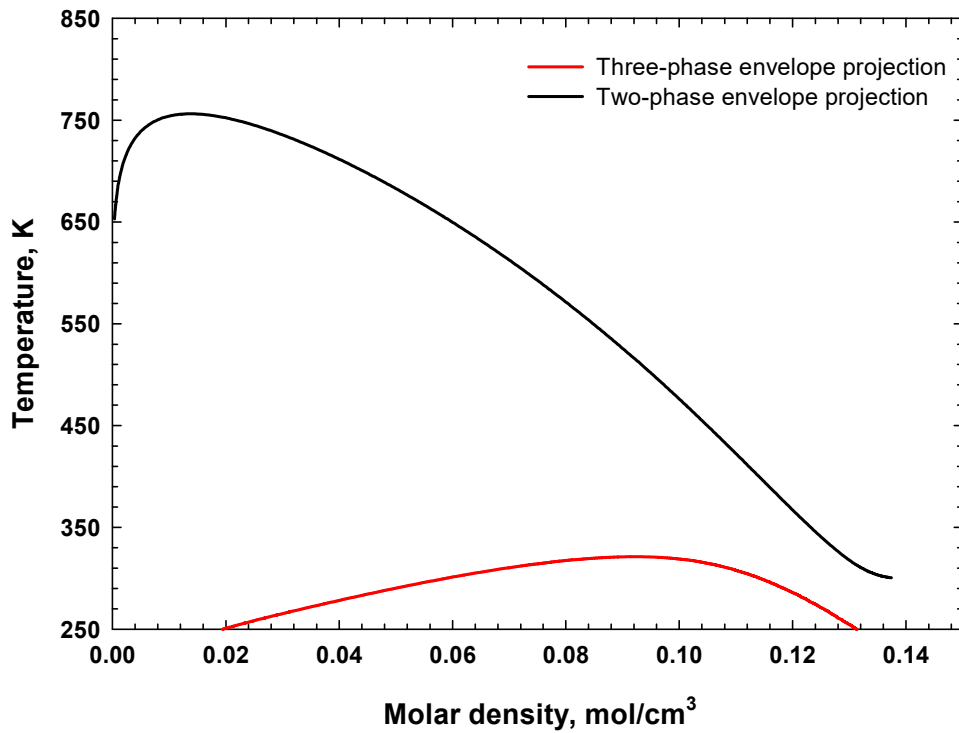
Figure 3-A5 Projection of two-phase envelope and three-phase envelope in the temperature-density space calculated for the JEMA oil mixed with 75 mol% injection gas.
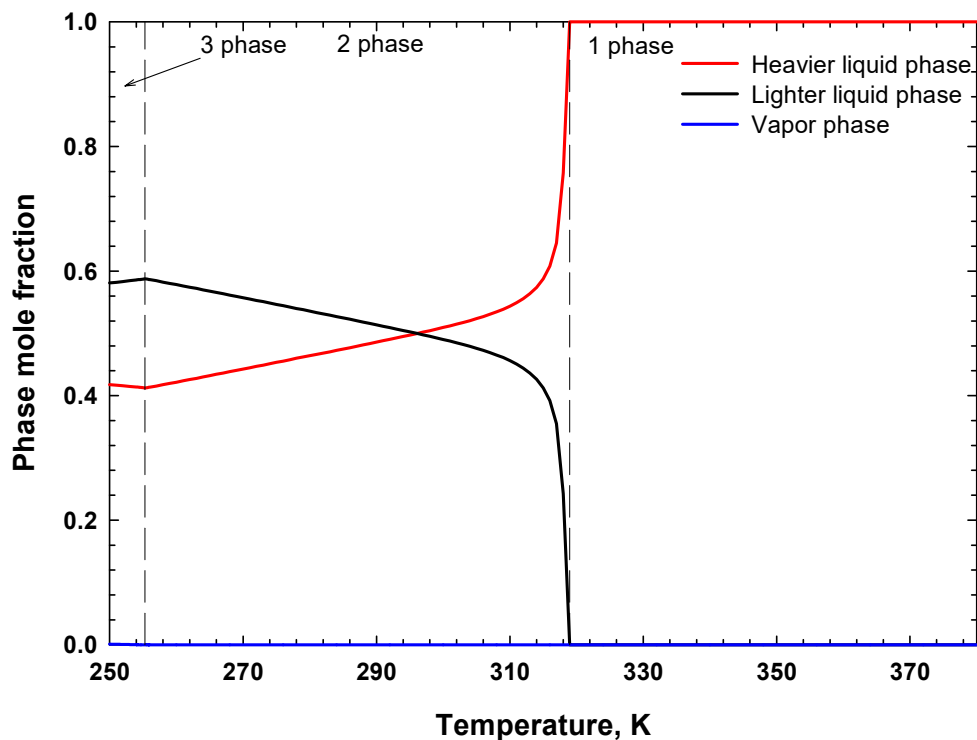
Figure 3-A6 Variation of phase fractions vs. temperature along the isochore of 77 cm^3/mol calculated for the JEMA oil mixed with 75 mol% injection gas.
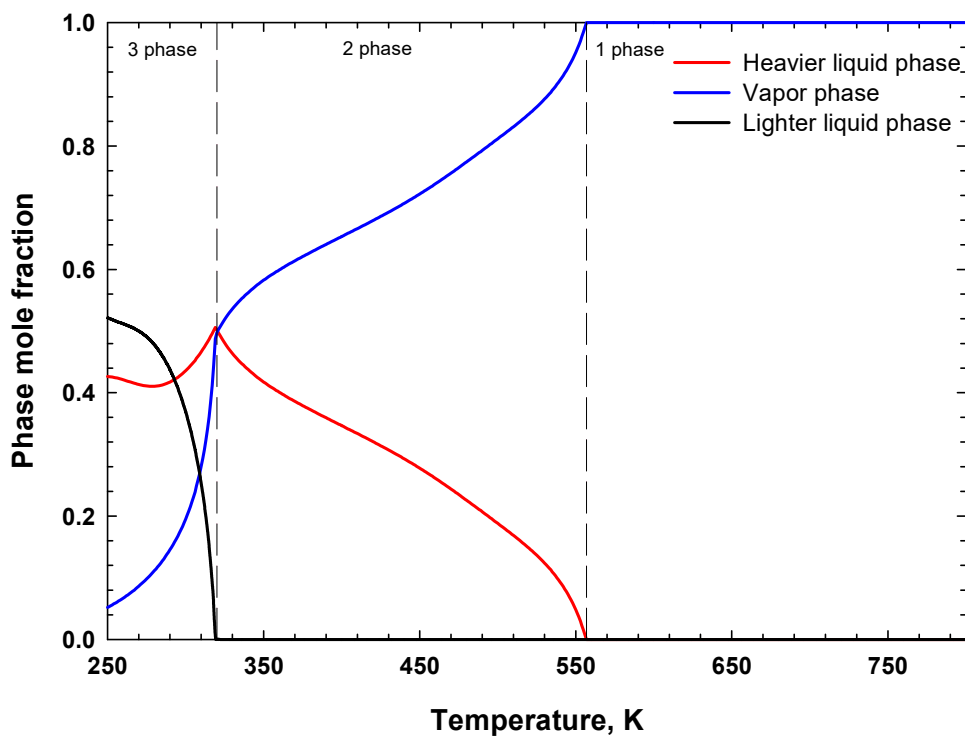
Figure 3-A7 Variation of phase fractions vs. temperature along the isochore of 120 cm^3/mol calculated for the JEMA oil mixed with 75 mol% injection gas.

Figure 3-A8 The number of calling the PT flash solver in the VT flash computations along the isochore of 120 cm³/mol for the JEMA oil mixed with 75 mol% injection gas.

Figure 3-A9 Statistical summary of the number of calling the PT flash solver in the VT flash computations along the isochores shown in Figure 3-A2.
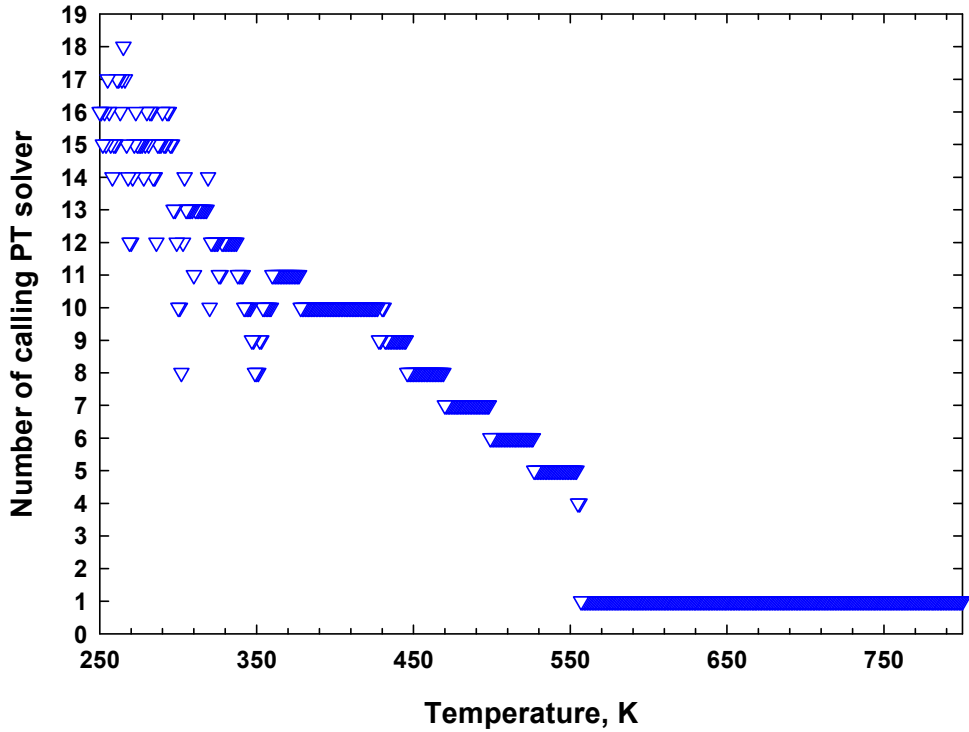
Table 3-A1 The fluid properties of the JEMA oil sample and injection gas (Khan *et al.*, 1992; Okuno *et al.*, 2010).

Components	Oil composition (mol%)	Gas composition (mol%)	Molecular weight	T_c, K	P_c, bar	ω	BIP with CO_2*
CO_2	1.92	100.0	44.01	304.20	73.76	0.225	0
C_1	6.93	0.0	16.04	166.67	46.00	0.008	0.05
C_{2-3}	17.42	0.0	36.01	338.81	45.53	0.126	0.05
C_{4-6}	19.44	0.0	70.52	466.12	33.68	0.244	0.05
C_{7-16}	31.38	0.0	147.18	611.11	20.95	0.639	0.09
C_{17-29}	15.49	0.0	301.48	777.78	15.88	1.000	0.09
C_{30+}	7.42	0.0	562.81	972.22	15.84	1.281	0.09

*All the other BIPs are zero.

CHAPTER 4 A PRACTICAL METHODOLOGY FOR INCORPORATING VOLUME-TRANSLATED EQUATION OF STATES IN ISOCHORIC-ISOTHERMAL PHASE EQUILIBRIUM CALCULATIONS

A version of this chapter will be submitted to *Fluid Phase Equilibria* for possible publication.

Abstract

Accurately predicting the phase behavior and properties of reservoir fluid plays an essential role in the simulation of petroleum recovery processes. Similar to the inaccurate liquid-density prediction issue in the isobaric-isothermal (PT) phase equilibrium calculations, an inaccurate pressure prediction issue can also be observed in isothermal-isochoric (VT) phase equilibrium calculations which involves a liquid phase. In this work, a practical methodology is proposed to incorporate a volume-translated equation of state in VT phase equilibrium calculations for more accurate pressure predictions. For this purpose, we adopt the state-of-art volume translation model recently proposed by Abudour *et al.* (2012; 2013). Single liquid phase calculations for 18 compounds and two hydrocarbon mixtures are conducted to demonstrate the soundness of the proposed methodology and evaluate the accuracy of pressure predictions. The calculated pressures by VT calculations with volume translated PR-EOS are compared to the actual pressures. The calculation results demonstrate that, by incorporating Abudour *et al.* (2012; 2013) volume translated PR-EOS models into the VT-based phase equilibrium calculation algorithm, the accuracy of pressure prediction in the single liquid phase region for both pure substances and mixtures can be significantly improved. Lastly, we apply the proposed algorithm to the two-phase VT phase equilibrium calculations for the oil sample MY10. We numerically replace the system pressure with the pressure corrected by applying the Abudour *et al.* VTPR-EOS [17] to the liquid phase only. The calculation results demonstrate that more accurate pressure

predictions can be obtained by applying the Abudour *et al.* VTPR-EOS [17] to the VT flash results compared to the scenario where only the original PR-EOS is used. To our knowledge, this study is the first one to investigate the issue of how to incorporate the volume translation concept in VT phase equilibrium calculations.

4.1 Introduction

Accurately predicting the phase behavior of reservoir fluid plays an essential role in the simulation of petroleum recovery processes. Due to its simplicity and computational efficiency, Peng-Robinson equation of state (PR-EOS) [1] is one of the most widely used cubic EOS (CEOS) in the petroleum industry to perform reservoir simulations. This kind of semi-empirical EOS is developed by fitting the pure-substance PVT data. However, subject to the inherent limitations of the two-parameter nature of CEOS (e.g., it yields a constant critical compressibility factor (z_c) for all substances, although the actual z_c values vary from one substance to another), significant error in liquid-phase density prediction is observed under specified pressure, temperature and composition conditions [2].

The concept of "volume translation" was first introduced by Martin [2] to improve the liquid density prediction. The translation is along the volume axis to improve the liquid density prediction without causing changes in the vapor-liquid equilibrium predictions [3]. A constant volume translation parameter was proposed by Peneloux *et al.* [3] in 1982 for SRK EOS [4]. Later, many researchers [5-9] have developed various types of temperature-dependent volume translations in two-parameter CEOS to accommodate the effect of temperature. One should be cautious that most of the temperature-dependent volume translations in PR-EOS are found to be thermodynamically inconsistent, which can lead to pressure-volume isotherm crossing phenomenon at relatively low pressures [10-13]. The volume translation models based on the distance function (both temperature and volume-

dependent) were also developed. They will only bear an isotherm crossover issue at an extremely high pressure, showing a great potential of having wide application in the chemical and petroleum industry [14-17] . One of the most commonly used one is Abudour *et al.* volume translation model [16]. It can be used to obtain reliable predictions of liquid densities in both saturated and single-phase regions. Later, Abudour *et al.* also extended their volume translation model to liquid mixtures in both the vapor-liquid equilibrium region and the liquid phase region [17].

Pressure-temperature (PT) based formulation of the phase behavior calculations has been widely used in reservoir simulations. Recently, a promising alternative approach, using volume-temperature (VT) based formulations to predict the reservoir fluid phase behavior, becomes increasingly attractive [18-24]. In such a framework, one conducts the equilibrium calculation by specifying volume, temperature, and composition. As such, pressure becomes one of the outputs. Similar to the inaccurate liquid density prediction issue in the PT-based phase behavior calculations, pressure may fail to be predicted accurately by VT-based phase behavior calculations. Due to a large slope of pressure-volume curve in the liquid phase region, a small difference in volume may lead to very inaccurate pressure prediction by VT-based calculations using the original PR-EOS. It is also an obstruction for VT-flash to by employed in the reservoir simulations, which may cause the collapse of the simulators when a very inaccurate pressure is predicted. But this issue has been overlooked in previous studies. To improve the pressure prediction results,

in this work, we propose to apply the volume translation models into the VT-based phase behavior calculations. The volume translated PR-EOS (VTPR-EOS) proposed by Abudour *et al.* [16-17] is adopted due to its excellent performance. To our knowledge, a comprehensive evaluation of the pressure prediction by incorporating the volume translation model into VT-based phase behavior calculations has not been reported in the past.

In this work, we propose a practical methodology to incorporate the volume translation model into VT-based equilibrium calculations in order to obtain a better performance of pressure prediction in both the liquid phase region and the vapor-liquid equilibrium region. This chapter is structured as follows. In section 4.2, we introduce the methodology and flow chart of our algorithm that incorporates Abudour *et al.* [16-17] volume translation model into VT calculations. The algorithms for the single liquid phase and vapor-liquid equilibrium calculations are both presented. In section 4.3, various example fluids are used to examine the performance of this method. The single-phase PVT data of 18 pure substances (as retrieved from NIST Chemistry Webbook) and two mixtures (i.e., the C_2-C_3 mixture and the C_3-nC_4 mixture) (as reported in the literature) are employed for such purpose. In addition, we conduct two-phase VT equilibrium calculations on one oil sample with and without incorporating the volume translation strategy. The VT-based two-phase equilibrium calculation results are compared to the PT-based ones. The conclusions are presented in Section 4.4.

4.2 Methodology

4.2.1 Volume translation proposed by Abudour *et al.* [16-17]

4.2.1.1 Abudour *et al.* [16] VTPR-EOS for pure substances

The PR-EOS is given by [1],

$$P = \frac{RT}{v-b} - \frac{a}{v^2 + 2vb - b^2} \tag{4.1}$$

where P is the pressure, bar; T is the temperature, K; v is the molar volume, L/mol; R is the gas constant, 8.314 J/(mol·K); a is the attraction parameter and b is the repulsion parameter.

For pure components, a and b can be expressed in term of critical temperature T_c (K), critical pressure P_c (bar), and acentric factor ω [1,25],

$$a = 0.45724 \frac{RT_c^2}{P_c} \alpha(T, \omega) \tag{4.2}$$

$$b = 0.0778 \frac{RT_c}{P_c} \tag{4.3}$$

$$\alpha = \left[1 + m \left(1 - \sqrt{\frac{T}{T_c}} \right) \right]^2 \tag{4.4}$$

$$m = \begin{cases} 0.37464 + 1.54226\omega - 0.26992\omega^2, \text{for } \omega < 0.5 \\ 0.3796 + 1.485\omega - 0.1644\omega^2 + 0.01667\omega^3, \text{for } \omega \geq 0.5 \end{cases} \tag{4.5}$$

The Abudour *et al.* volume-translation function is defined as [16],

$$v_t = v + c_0 - \delta_c \left(\frac{0.35}{0.35 + d} \right) \tag{4.6}$$

where v_t and v are the translated and untranslated molar volumes and c_0 is the volume translation term expressed by [16],

$$c_0 = \left(\frac{RT_c}{P_c} \right) \left(c_1 - \left(0.004 + c_1 \right) \exp(-2d) \right) \tag{4.7}$$

where c_1 is a constant for a given pure substance, z_c^{exp} is the critical compressibility factor, d is the dimensionless distance function given by [16],

$$d = \frac{1}{RT_c} \left(\frac{\partial P^{PR}}{\partial \rho} \right)_T \tag{4.8}$$

where ρ is the molar density, mol/L, which is the inverse of molar volume v, L/mol. δ_c appearing in Eq. (4.6) is the volume correction at the critical temperature [16],

$$\delta_c = \left(\frac{RT_c}{P_c} \right) \left(z_c^{EOS} - z_c^{\text{exp}} \right) \tag{4.9}$$

where z_c^{EOS} is the compressibility factor calculated by PR-EOS (i.e., 0.3074).

4.2.1.2 Abudour *et al.* volume translated PR-EOS for mixtures [17]

The mixing rule employed to calculate the values of a and b for mixtures is given by [17]

$$a = \sum_i \sum_j x_i x_j a_{ij} \tag{4.10}$$

$$b = \sum_i \sum_j x_i x_j b_{ij} \tag{4.11}$$

where x_i is the mole fraction of compound i, and a_{ij} and b_{ij} can be calculated by the following combining rules [17],

$$a_{ij} = \sqrt{a_i a_j}\left(1 - C_{ij}\right) \tag{4.12}$$

$$b_{ij} = \frac{\left(b_i + b_j\right)}{2}\left(1 + D_{ij}\right) \tag{4.13}$$

where C_{ij} and D_{ij} are empirical binary interaction parameters (BIPs). The volume translation parameter for mixtures given by Abudour *et al.* [17] is shown as,

$$v_t = v + c_m - \delta_{cm}\left(\frac{0.35}{0.35 + d_m}\right) \tag{4.14}$$

The subscript *m* represents the parameters for mixtures. c_m is given by [17],

$$c_m = \left(\frac{RT_{cm}}{P_{cm}}\right)\left(c_{1m} - (0.004 + c_{1m})\exp(-2d_m)\right) \tag{4.15}$$

where c_{1m} is calculated following a linear mixing rule [3],

$$c_{1m} = \sum x_i c_{1i} \tag{4.16}$$

where c_{1i} is a species-dependent parameter for component *i*. The dimensionless distance function for a binary mixture, d_m, is calculated by [17],

$$d_m = \frac{1}{RT_{cm}}\left(\frac{\partial P^{PR}}{\partial \rho_m}\right)_T - \left(\frac{1}{RT_{cm}\rho_m^2}\right)\frac{a_{v1}^2}{a_{11}} \tag{4.17}$$

where T_{cm} and ρ_m are the critical temperature and the molar density of the mixture. The expressions for a_{v1} and a_{11} were derived based on the Helmholtz energy equations. In our work, the Helmholtz term is neglected, since, based on the study of Matheis *et al.* [15], the contribution of this term to the volume correction is insignificant but the influence of this

term to the computation efficiency becomes significant with an increasing number of species.

In Eq. (4.14), the volume correction for a mixture at critical temperatures δ_m is given as [17],

$$\delta_{cm} = v_{cm}(x) - v_{cm}^{\exp}(x) \tag{4.18}$$

where $v^{\exp}_{cm}(x)$ is the true critical volume and $v_{cm}(x)$ is the mixture critical volume predicted from PR-EOS. $v^{\exp}_{cm}(x)$ is calculated as [26],

$$v_{cm}^{\exp}(x) = \sum_i \theta_i v_{ci}^{\exp} \tag{4.19}$$

$$\theta_i = \frac{x_i v_{ci}^{2/3}}{\sum_i x_i v_{ci}^{2/3}} \tag{4.20}$$

where $v^{\exp}_{ci}$ is the true critical volume of pure compound i and θ_i is the surface fraction of compound i. The mixture critical volume $v_{cm}(x)$ is calculated as [27],

$$v_{cm}(x) = \left(\frac{RT_{cm}}{P_{cm}} \right) z_c^{EOS} \tag{4.21}$$

$$T_{cm} = \sum_i \theta_i T_{ci} \tag{4.22}$$

$$P_{cm} = \frac{(0.2905 - 0.085\omega_m)RT_{cm}}{v_{cm}} \tag{4.23}$$

$$\omega_m = \sum_i x_i \omega_i \tag{4.24}$$

where T_{cm} and P_{cm} are the mixture critical temperature and pressure, T_{ci} and ω_i are the

critical temperature and acentric factor of component *i*.

4.2.2 Proposed methodology for incorporating VTPR-EOS in VT equilibrium calculations

In VT-based equilibrium calculations, volume, temperature and feed composition are the inputs, while pressure, phase fractions, and phase composition are the outputs. In order to give a better prediction of pressure, we desire to find the relation between the translated pressure P_t and given volume v:

$$P_t = P_t\left(v,\ T\right). \tag{4.25}$$

Instead of directly shifting the pressure that is calculated by PR-EOS, we calculate the translated pressure (P_t) indirectly also by shifting the volume. At constant v and T conditions, the translated pressure P_t is the PR-EOS-calculated pressure which allows the translated volume to equate with the given volume. **Figure 4-1** shows the ρ-P curve of CO_2 in the liquid phase region at 280 K. Figure 4-1 also illustrates how we can find the translated pressure P_t. The problem is to properly predict the pressure at the molar density ρ. We treat the given molar density ρ as the translated one, i.e., ρ_t. By using the original PR-EOS, we can output the pressure P at the point (a). We next calculate $\rho_{PR,}$ based on ρ and the Abudour *et al.* volume translation model [16-17]. To shift the pressure to P_t, we calculate the pressure at point (b) based on $\rho_{PR,}$ by using the original PR-EOS.
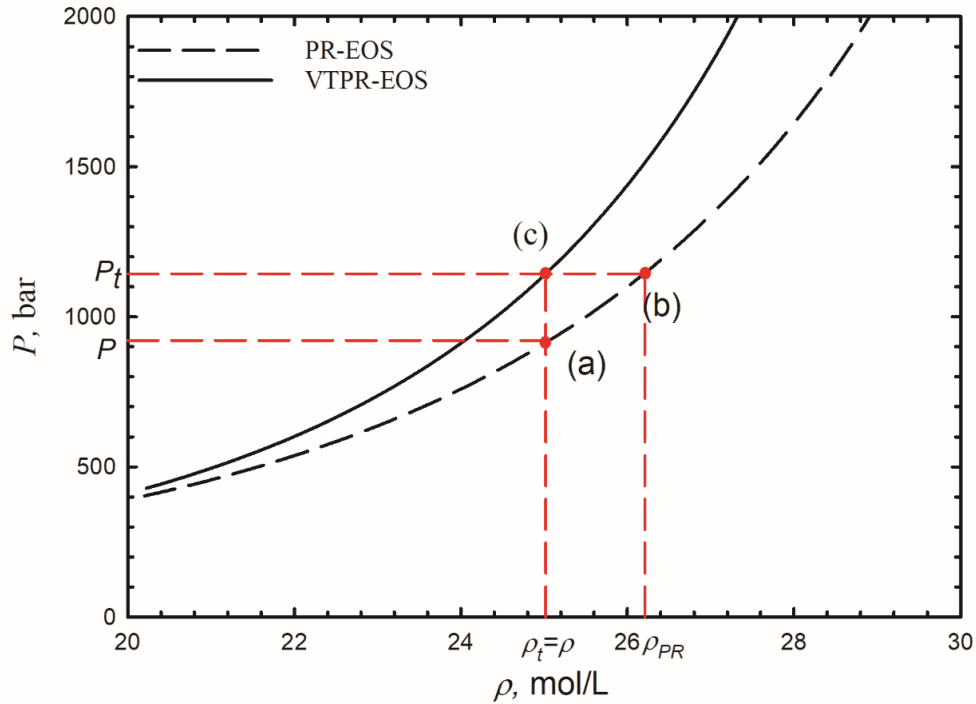
Figure 4-1 Schematic diagram of the ρ-P curve of CO_2 in the single liquid phase region at T=280 K. This diagram shows how we calculate the shifted pressure by applying the volume translation concept. Note that ρ_{PR} is the untranslated density, ρ_t=$1/v_t$ is the translated density, P is the calculated pressure by PR-EOS, and P_t is the translated pressure.

If the volume translation model is a constant or a temperature dependent one, its incorporation into the VT equilibrium calculations is much easier. We can shift ρ to ρ_{PR} first, and substitute ρ_{PR} into PR-EOS directly, because, at a given temperature, the volume shift parameter remains a constant at any density levels. However, the Abudour *et al.* volume translation model [16] is not only temperature dependent but also volume dependent, implying that the volume shift parameter at different density conditions is also different. Practically, we need to calculate the translated pressure by using a numerical method when adopting the Abudour *et al.* volume translation model [16].

4.2.2.1. Algorithm of pressure prediction in the single liquid phase region

To calculate the pressure in the single liquid phase region, we need to first find the ρ_{PR} by iterative calculations, and then determine the shifted P_t with PR-EOS. We develop an effective algorithm to achieve such purpose for both pure substances and mixtures. The flow chart of the developed algorithm is shown in **Figure 4-2**. The procedure of the algorithm is briefly explained as follows:

1) Input molar density (ρ), temperature (T) and compositions (note that composition is not necessary for pure substances), and other fluid properties (critical temperature (T_c), critical pressure (P_c), acentric factors (ω), binary interaction parameters (BIPs: C_{ij} and D_{ij}), molecular weight (MW), critical compressibility factor (z_c^{exp}) and the constant (c_l).

2) Use ρ as an initial guess of the molar density (ρ_0).

3) Calculate the translated molar density ρ_t using Abudour *et al.* volume translation model at ρ_0.

4) Calculate the tolerance $error = abs(\rho_t - \rho_0)$ and check the criterion $error = abs(\rho_t - \rho_0) \leq tol = 10^{-6}$. If the termination condition is not satisfied, update ρ_0 by applying the bisection method over the interval of $\left(\rho, \rho + 2abs(\rho - \rho_{0t})\right)$ (where ρ_{0t} is the translated density at ρ_0), and go back to step 3.

5) Otherwise, calculate the pressure at ρ_0 and output P_t.
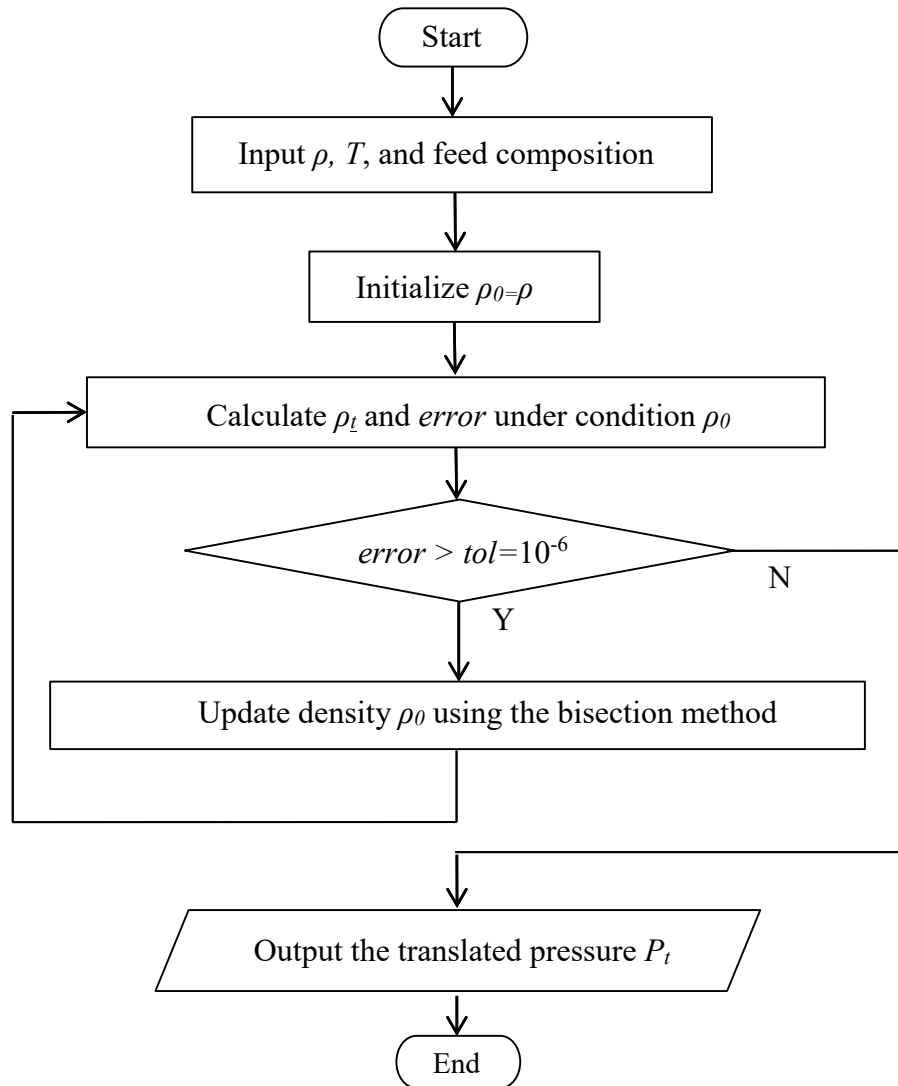
Figure 4-2 Flow chart of the proposed pressure prediction algorithm in the single liquid phase region.

4.2.2.2 Algorithm of pressure prediction in two-phase VT equilibrium calculations

In VT equilibrium calculations, temperature (T), the overall molar density ($\rho_{overall}$) and feed composition are the inputs, while pressure, phase fractions, and phase compositions are the outputs. To force the fugacity-equality condition at equilibrium, the equilibrium calculation should be conducted first. Then, the molar density of each phase can be calculated. Without

incorporating volume translation into the VT flash, the pressure can be calculated based on that of either vapor or liquid phase, which will lead to the same value. However, Abudour *et al.*'s study shows that the prediction of liquid phase density in the vapor-liquid equilibrium region by PR-EOS is also unsatisfactory and can be improved by applying volume translation [17]. Hence, assuming that the predicted ρ_{liquid}-P relation of the liquid phase described by the Abudour *et al.* volume translation model is more accurate than that described by the original PR-EOS, we can more accurately determine the equilibrium pressure by applying the Abudour *et al.* volume translation to the resulting liquid phase [17].

Figure 3 shows the flow chart of the algorithm that incorporates the Abudour *et al.* volume translation model [17] into the VT equilibrium calculations. The flow chart shown inside the dashed frame is the basic VT equilibrium calculation algorithm, which was firstly proposed by Mikyška and Firoozabadi [21] and also used in our previous work [24]. The detailed description of the stepwise procedure of the basic VT equilibrium calculation algorithm can be found in Ref. [24]. The basic VT equilibrium calculation algorithm will output the fractions, the compositions and the molar densities of the vapor and liquid phases. The translated pressure (P_t) can be calculated based on the properties of the liquid phase by following the same procedure for the single-liquid phase regions as demonstrated in **Section 4.2.2.1**. Last but not least, it should be emphasized that the above methodology for incorporating the Abudour *et al.* volume translation model [16][17] applies the Abudour *et*

al. volume translation model [16][17] directly to the resulting liquid phase only. This is achieved based on the assumption that the volume translation does not affect the actual phase equilibrium.
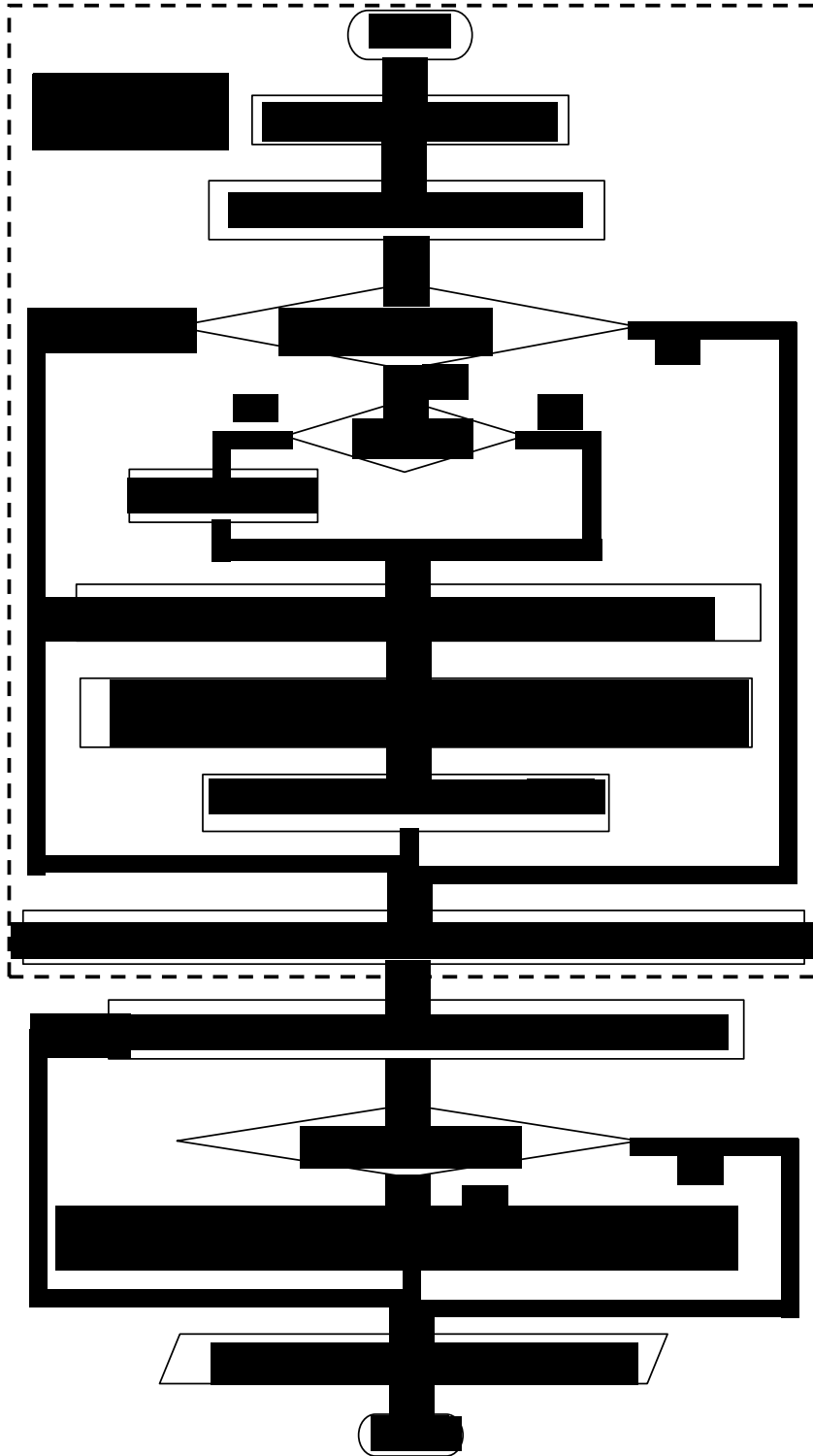
Figure 4-3 Flow chart of the algorithm that incorporates the Abudour *et al.* volume translation model [16-17] into the two-phase VT phase equilibrium calculations

4.3 Results and Discussion

4.3.1 Single liquid phase VT calculations using VTPR-EOS

In this study, we use the algorithm shown in **Section 4.2.2.1** to predict the liquid phase pressure for both pure substances and mixtures under specified volume and temperature conditions. To illustrate the accuracy of pressure prediction and validate the correctness of the developed algorithm, we compare the calculated results for 18 pure substances and two mixture systems with the NIST Chemistry Webbook data [28].

The 18 pure substances including several classes of chemical compounds: n-alkanes, alkenes, alcohols, ketones, aromatics, cyclic hydrocarbons and inorganic compounds. The benchmark data are taken from the National Institute of Standards and Technology (NIST) Chemistry Webbook [28]. The two mixture systems are C_2H_6-C_3H_8 mixtures and C_3H_8-n-C_4H_{10} mixtures. For these mixture systems, the experimental data for C_2H_6-C_3H_8 mixtures and C_3H_8-n-C_4H_{10} mixtures measured by Parrish [29] and Miyamoto and Uematsu [30] are employed, respectively. The pure-compound properties (including critical temperature (T_c), critical pressure (P_c), acentric factors (ω), molar weight (MW), critical compressibility factor (z_c^{exp}) and the constant c_1 constitute the necessary input variables for the Abudour *et al.* VTPR-EOS. **Table 4-1** shows all these properties for all the substances involved in this work.

Table 4-1 Physical properties of the pure substances and the parameters of Abudour *et al.* volume translation model [16-17,28]

Substance	T_c, K	P_c, bar	ω	MW, g/mol	z_c	c_1
Carbon dioxide	304.13	73.773	0.22394	44.0100	0.2746	0.00652
Nitrogen	126.19	33.958	0.03700	28.0140	0.2894	0.01386
Methane	190.56	45.992	0.01100	16.0430	0.2863	0.01313
Ethane	305.33	48.718	0.09930	30.0700	0.2776	0.00993
Propane	369.83	42.477	0.15240	44.0970	0.2769	0.00778
n-Butane	425.13	37.960	0.20100	58.1240	0.2738	0.00642
n-Pentane	469.70	33.700	0.25100	72.1510	0.2684	0.00434
n-Hexane	507.82	30.340	0.29900	86.1780	0.2656	0.00306
n-Heptane	540.13	27.360	0.349	100.2050	0.2632	0.00095
n-Octane	569.32	24.970	0.393	114.2320	0.2565	0.000195
n-Nonane	594.55	22.810	0.44300	128.2590	0.2550	-0.00196
n-Decane	617.70	21.030	0.48800	142.2860	0.2501	-0.00230
n-Dodecane	658.10	18.170	0.57400	170.3400	0.2492	-0.00428
n-Tetradecane	693.00	15.700	0.64300	198.3940	0.2400	-0.00772
Ethylene	282.35	50.418	0.08660	28.0540	0.2813	0.00995
Cyclohexane	553.64	40.750	0.20926	84.1620	0.2729	0.00711
Benzene	562.05	48.940	0.20921	78.1118	0.2686	0.00526
Toluene	591.75	48.263	0.26600	92.1410	0.2647	0.00288
Tetrafluoromethane	227.51	37.750	0.17850	88.0000	0.2807	0.01152
Acetone	508.20	47.010	0.30650	58.0800	0.2330	−0.00880
Ethanol	513.92	61.480	0.64900	46.0690	0.2430	−0.00424

4.3.1.1 Pure substances

18 pure substances are studied in this section. We compare the pressure prediction results by using the Abudour *et al.* VTPR-EOS [17] and the results by PR-EOS [1] under four different temperatures for each pure substance. The benchmark data from NIST Chemistry

Webbook are used as reference data to evaluate the prediction results. We use the following equation to quantify the average percentage absolute deviation (*AAD%*) in the pressure prediction by the Abudour *et al.* VTPR and the original PR-EOS,

$$AAD(\%) = \frac{100}{NDP} \sum_{i=1}^{NDP} \frac{\left|P_{cal,i} - P_{exp,i}\right|}{P_{exp,i}} \qquad (4.26)$$

where $P_{cal,i}$ is the calculated pressure, $P_{exp,i}$ is the actual pressure corresponding to given density and temperature as given by NIST Chemistry Webbook [28], and *NDP* is the number of data points. **Table 4-2** compares the average percentage absolute deviation (*AAD%*) of the predicted pressures yielded by the two different models for the 18 pure substances. As seen from Table 2, by applying the Abudour *et al.* VTPR-EOS [17], the accuracy of pressure prediction can be significantly improved. The overall AAD% decreases from 109.76% to 18.47%.

Table 4-2 *AAD%* of pressure predictions by PR-EOS [1] and Abudour *et al.* VTPR-EOS [17].

Substance	*T*, K	Range of ρ, mol/L	*%ADD* by PR-EOS [1]	*%ADD* By VTPR-EOS [17]	*NDP*
Carbon dioxide	250	23.0-30.0	96.79	9.57	80
	280	20.0-30.0			
	310	18.0-28.5			
	340	15.0-28.0			
Nitrogen	80	26.0-31.0	134.30	13.19	80
	90	25.0-31.0			
	100	24.0-30.5			
	120	18.5-30.0			
Methane	120	25.5-27.5	104.56	11.41	80
	140	23.5-27.5			
	160	21.0-27.0			
	180	17.5-26.5			
Ethane	180	18.0-19.0	160.35	18.03	100
	200	17.5-19.0			
	250	15.0-19.0			
	300	12.0-19.0			

Propane	220	13.5-14.5	122.69	15.13	100
	240	13.0-14.5			
	300	11.0-14.3			
	360	9.0 -14.3			
n-Butane	260	10.6-11.4	90.33	17.14	100
	300	9.9 -11.3			
	360	8.5 -11.3			
	420	7.5 -11.2			
n-Pentane	300	8.6-9.5	56.53	14.63	80
	350	7.9-9.3			
	400	7.0-9.1			
	450	6.1-9.0			
n-Hexane	350	7.0-8.0	40.21	15.86	80
	400	6.5-7.8			
	450	5.8-7.6			
	500	4.8-7.4			
n-Nonane	430	4.7-5.6	42.14	20.12	100
	480	4.5-5.6			
	530	4.0-5.6			
	580	3.6-5.6			
n-Decane	440	4.3-5.0	71.57	18.16	80
	500	3.9-5.0			
	560	3.6-5.0			
	610	3.4-5.0			
n-Dodecane	460	3.6-4.1	145.19	15.77	80
	520	3.3-4.1			
	580	3.1-4.1			
	650	2.8-4.1			
Ethylene	160	20.6-21.5	135.39	28.17	100
	200	18.6-20.5			
	240	15.6-19.2			
	280	12.0-17.8			
Cyclohexane	350	8.5-9.3	87.14	19.99	80
	400	8.0-9.0			
	500	6.2-8.5			
	550	4.5-8.3			
Benzene	400	9.7-11.2	66.32	23.93	100
	450	8.9-11.2			
	500	8.4-11.2			
	550	7.1-11.2			
Toluene	380	8.5-9.1	36.02	14.09	80
	450	7.7-9.1			
	520	7.0-9.1			
	580	6.0-9.1			
Tetrafluoromethane	160	17.4-19.2	84.98	14.59	80
	180	16.0-18.5			
	200	13.9-17.8			
	220	12.6-17.0			
Acetone	350	12.5-13.9	230.44	19.98	100
	400	11.5-13.5			
	450	10.0-13.0			
	500	9.0-12.6			

	380	15.3-16.2			
Ethanol	420	14.1-15.5	270.69	42.659	80
	460	12.4-14.6			
	500	10.2-14.6			
Overall			109.75	18.47	1580

The pressure prediction results of carbon dioxide, methane, n-hexane and acetone are shown in **Figures 4-7** for illustration purposes. Under four different temperatures for each substance, the pressure was calculated at a specified volume by both the PR-EOS [1] and the VTPR-EOS [17]. From these figures, we can clearly observe that the pressures calculated by the VTPR-EOS [17] are much more accurate than the pressures calculated by PR-EOS [1]. However, the pressure-prediction accuracy at relatively larger density conditions tends to deteriorate as the density increases. As shown in Figures 4-7, the slope of the density-pressure curve becomes larger as the molar density increases, which means, at a relatively high density, a small change in density will result in a large difference in the calculated pressure. The Abudour *et al.* volume translation model [17] was originally developed to correct the liquid phase density at relatively lower pressures (e.g., pressures in close proximity to the critical pressure). Thus, the prediction of pressure under high-density conditions by this model becomes less accurate.
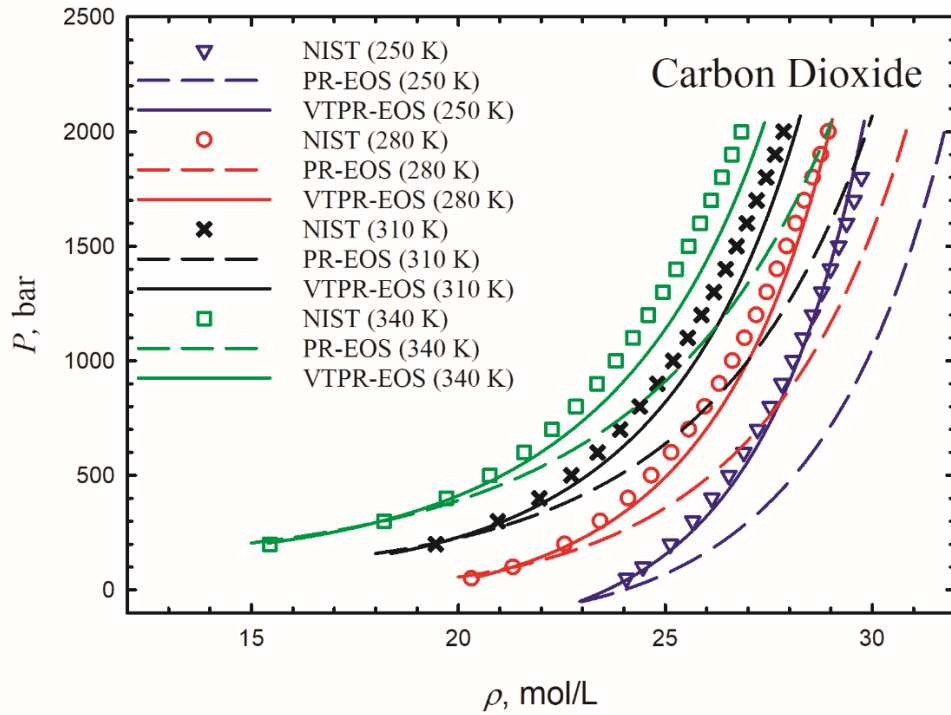
Figure 4-4 Pressure prediction for pure CO_2 at specified volume and temperature by using both PR-EOS [1] and VTPR-EOS [17].
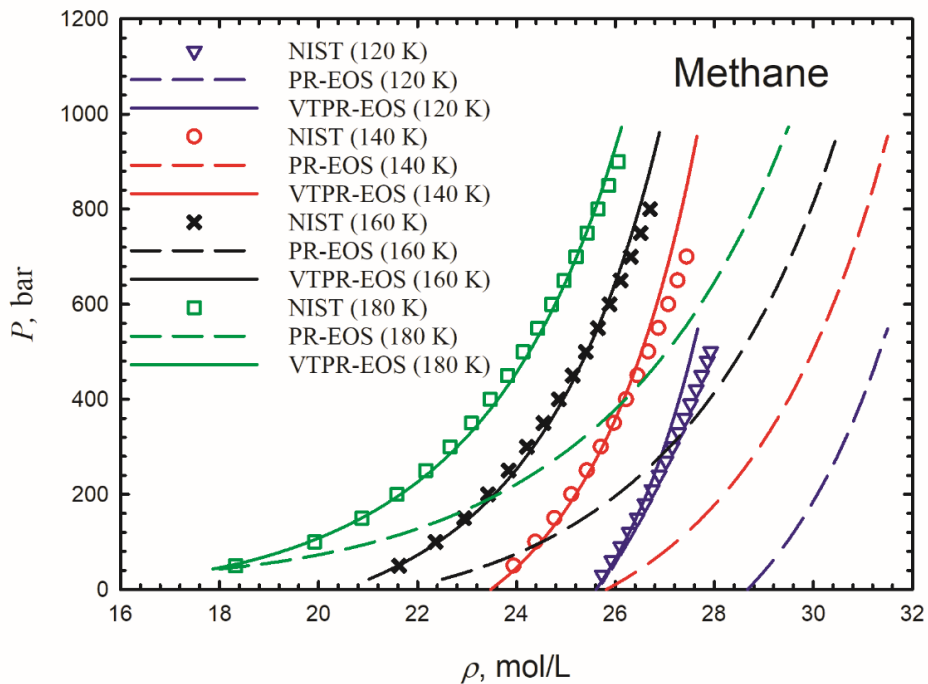
Figure 4-5 Pressure prediction of pure CH_4 at specified volume and temperature by using both PR-EOS [1] and VTPR-EOS [17].

125
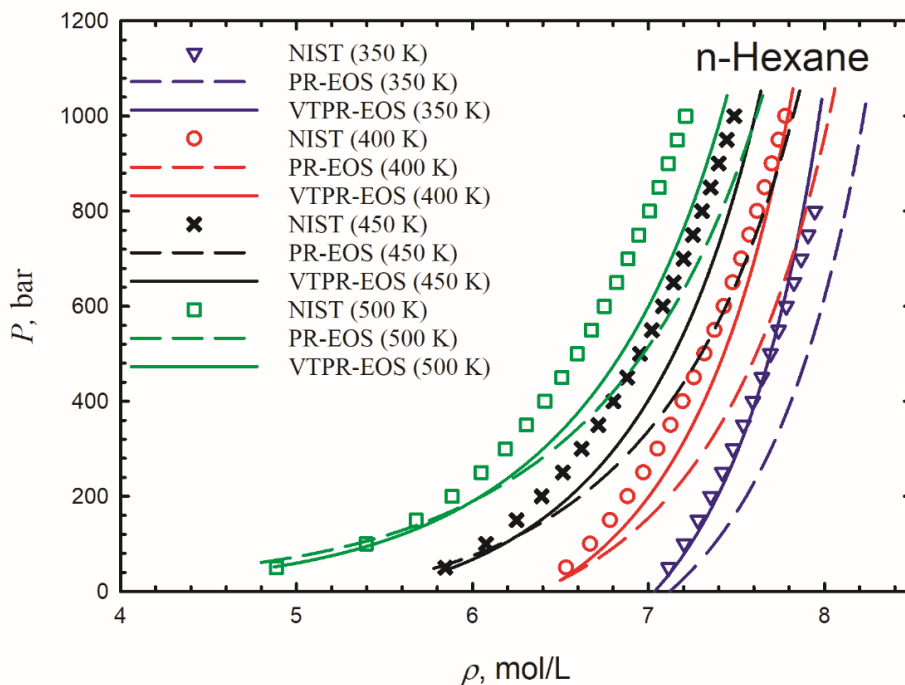
Figure 4-6 Pressure prediction of n-hexane at specified volume and temperature by using both PR-EOS [1] and VTPR-EOS [17].
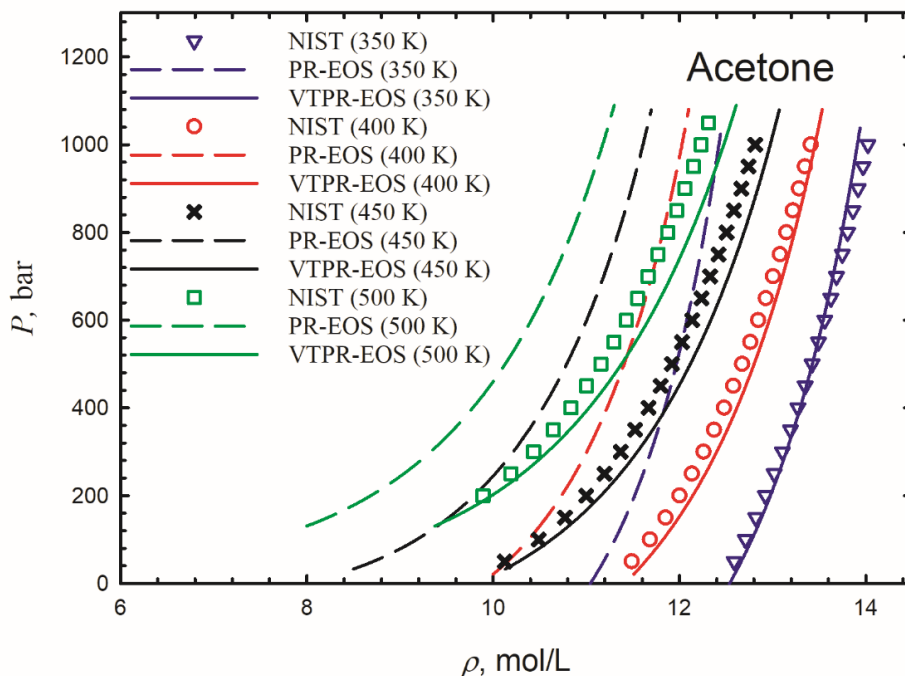
Figure 4-7 Pressure predictions for acetone at specified volume and temperature by using both PR-EOS [1] and VTPR-EOS [17].

4.3.1.2 Mixtures

Two binary mixture systems (C_2H_6-C_3H_8 mixtures and C_3H_8-n-C_4H_{10} mixtures) are used in this section to illustrate the improvement of pressure prediction by applying the Abudour *et al* volume translation model [17]. The experimental data from Parrish's work [29] and Miyamoto and Uematsu's work [30] are employed as the reference data.

Figure 4-8 shows the pressure prediction results for C_2H_6-C_3H_8 mixtures as a function of the weight density (g/cm^3) by both PR-EOS [1] and Abudour *et al.* VTPR-EOS [17]. The calculations are done under four different temperatures. Under each temperature, four different compositions are used (a: T=283.15 K, x_{C2} = 0.9006, 0.7007, 0.4981 and 0.2978; b: T=288.71 K, x_{C2} = 0.9060, 0.7045, 0.5151 and 0.3103; c: T=299.82 K, x_{C2} = 0.9497, 0.6976, 0.4973 and 0.2982; d: T=310.95 K, x_{C2}= 0.8994, 0.6992, 0.4954 and 0.2993). The BIPs between C_2H_6 and C_3H_8 are C_{ij} = 0.0090 and D_{ij} = 0 [31]. **Figure 4-9** shows the pressure prediction results for C_3H_8-n-C_4H_{10} mixtures as a function of density by both PR-EOS [1] and Abudour *et al.* VTPR-EOS [17]. The calculations are conducted under four different temperatures (T=280 K, 320 K, 360 K and 400 K) and three different compositions (x_{C3} = 0.2729, 0.5021, and 0.7308) for each temperature. The BIPs between C_3H_8 and n-C_4H_{10} are C_{ij} = 0.0220 and D_{ij} = 0 [31]. It is obviously seen from both Figures 4-8 and 4-9 that by applying the Abudour *et al.* VTPR-EOS [17], the accuracy of pressure prediction is improved significantly. However, the same problem that appears for pure substances also appears for the mixtures. At higher density conditions, the pressure

prediction accuracy starts to deteriorate with an increase in density.
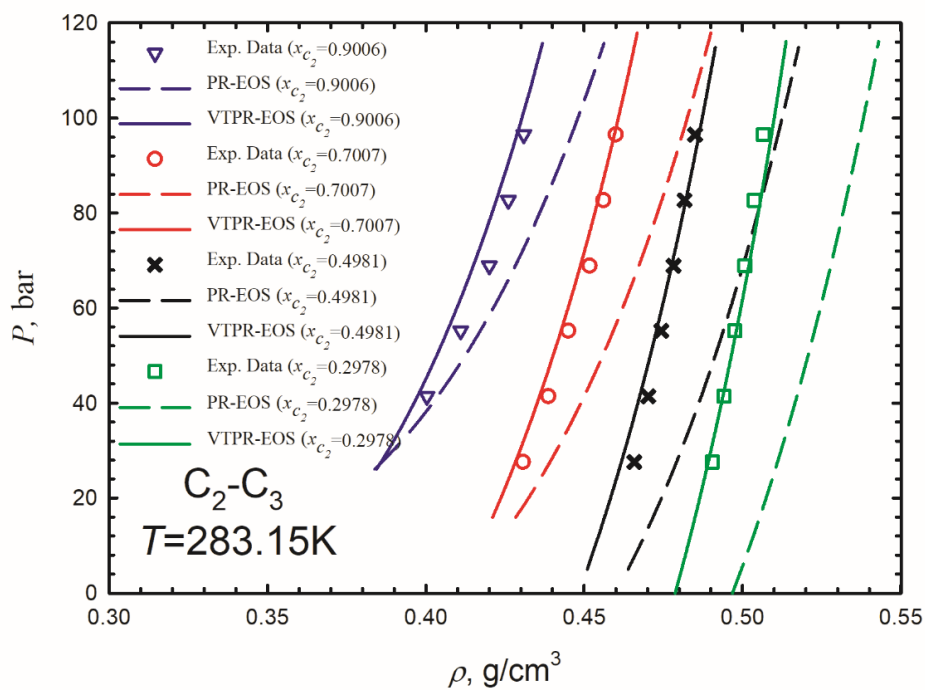
(a)
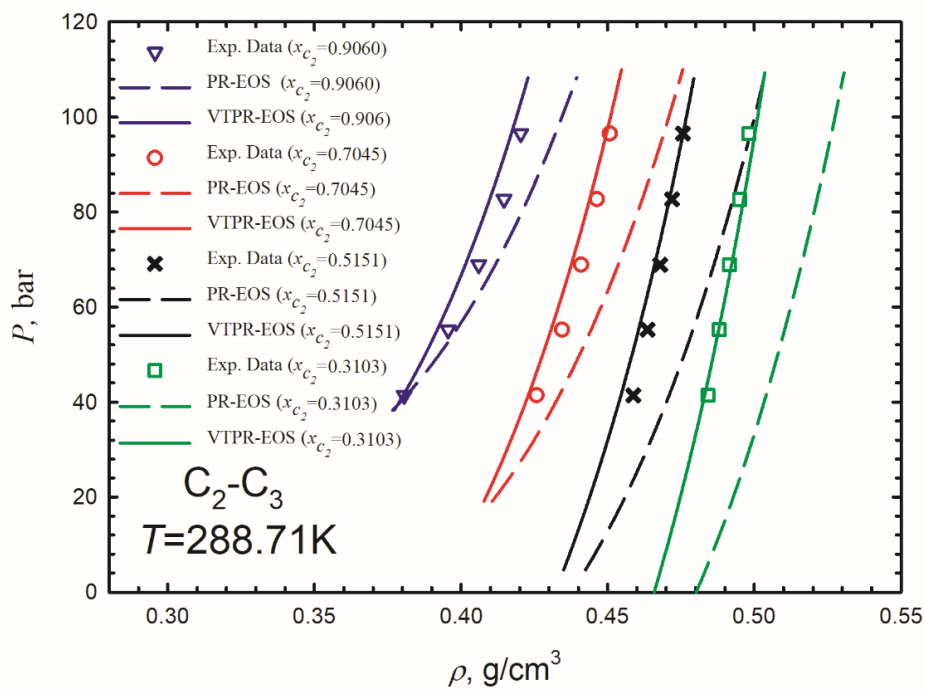
(b)
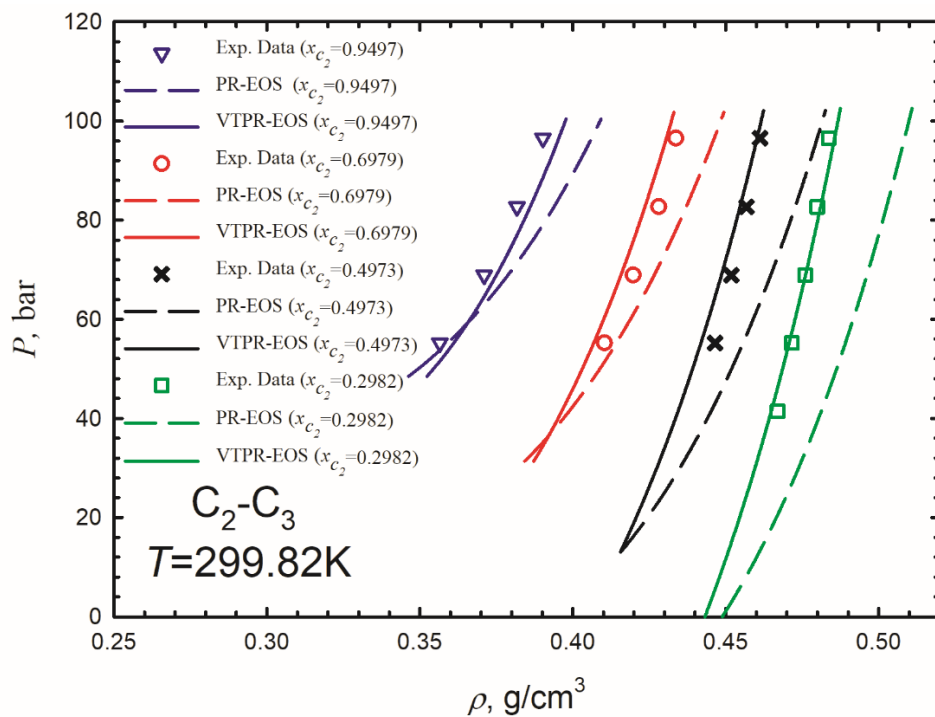
(c)
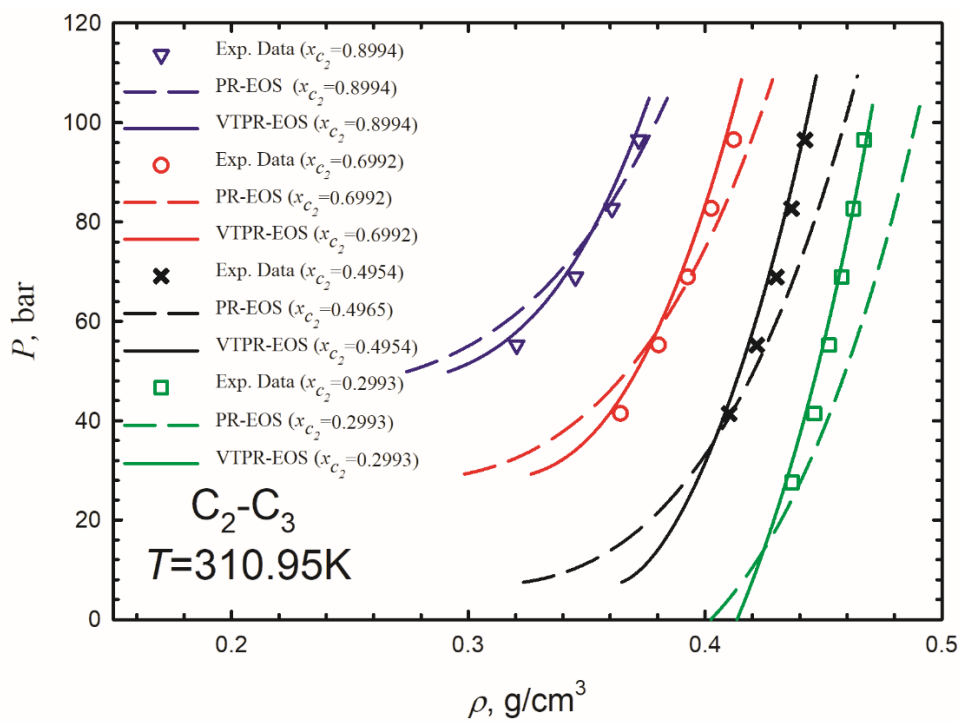
(d)

Figure 4-8 Pressures predicted for C_2H_6-C_3H_8 mixtures using both PR-EOS [1] and VTPR-EOS [17] at specified density (volume) and temperature: (a): T=283.15 K; (b): T=288.71 K; (c): T=299.82 K; (d): T=310.95 K. The experimental data are obtained from Parrish [29].
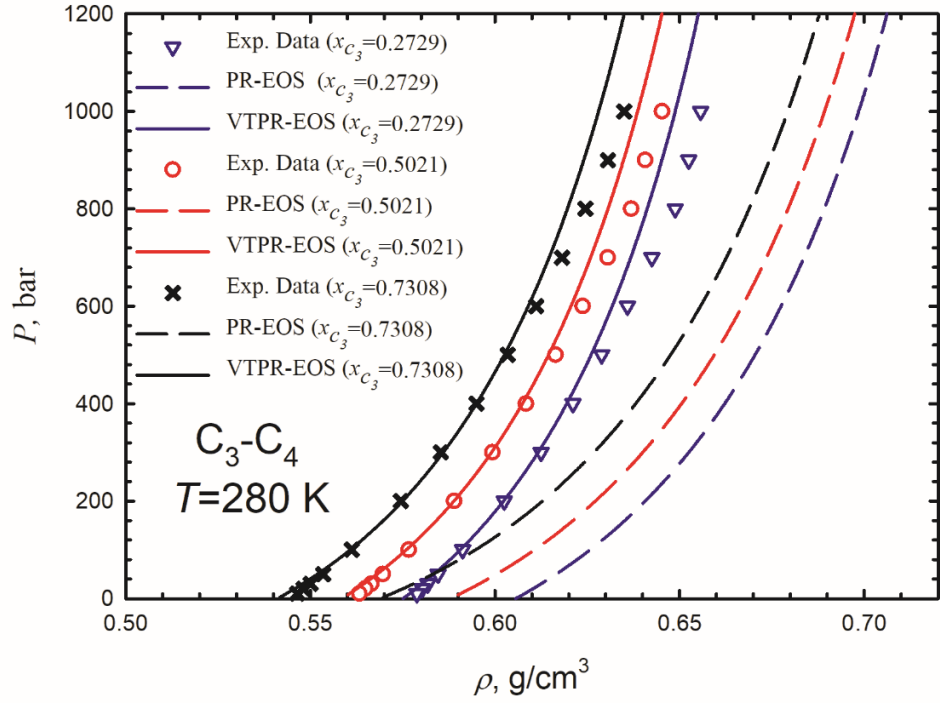
(a)
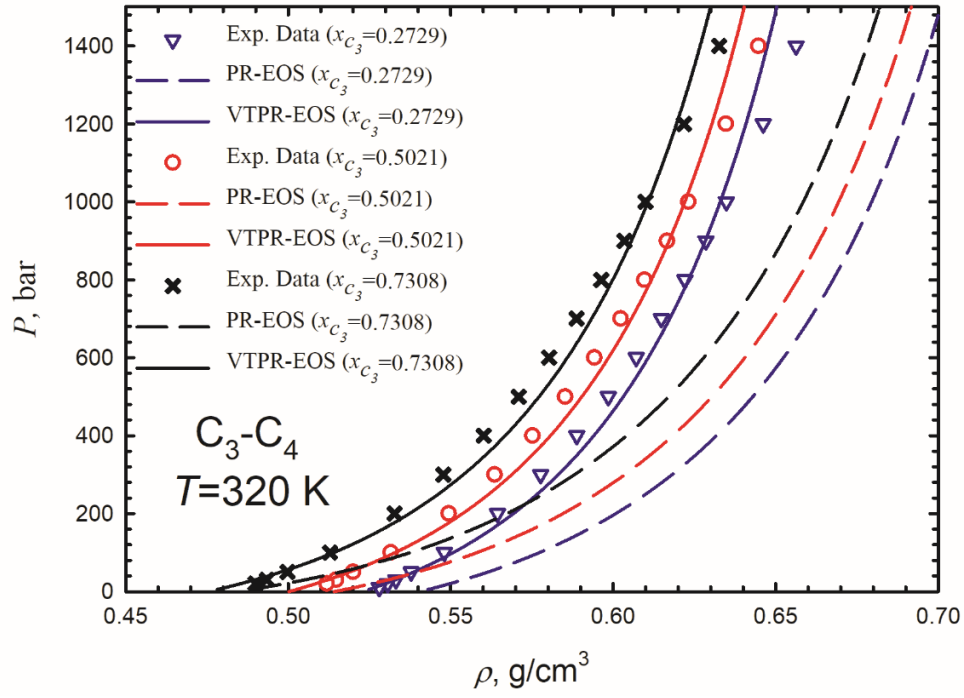
(b)
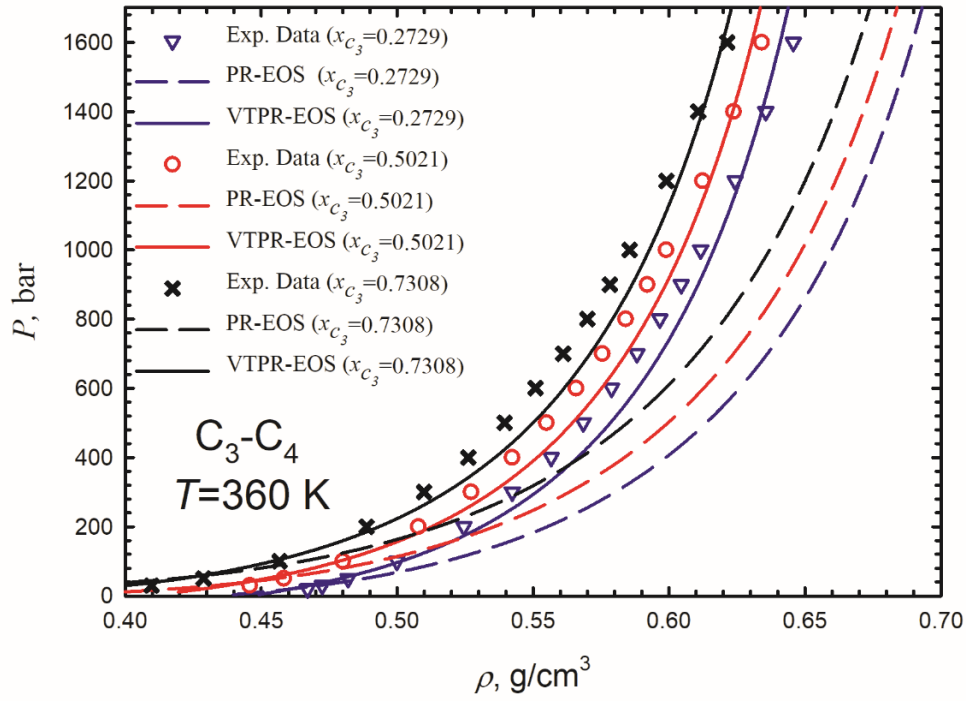
(c)
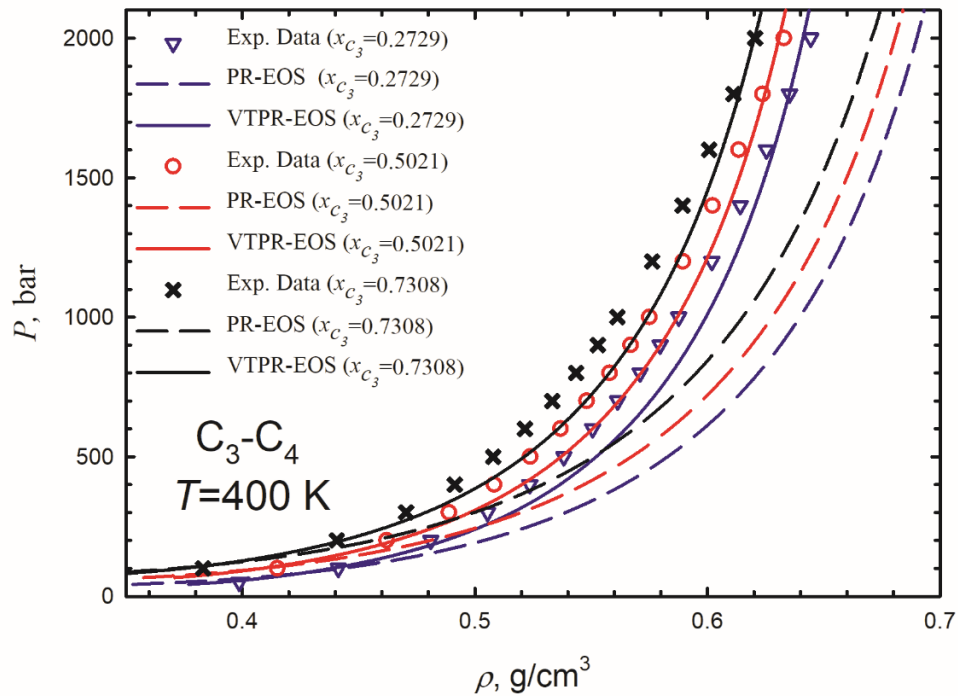
(d)

Figure 4-9 Pressures predicted for C_3H_8-n-C_4H_{10} mixtures using both PR-EOS [1] and VTPR-EOS [17] at specified density (volume) and temperature: (a): T=280 K; (b): T=320 K; (c): T=360 K; (d): T=400 K. The experimental data are obtained from Miyamoto and Uematsu [30].

4.3.2 Two-phase VT equilibrium calculations using VTPR-EOS

In this section, we incorporate Abudour *et al.* VTPR [17] into the VT phase equilibrium calculations for one oil sample MY10 [32]. The oil sample MY10 [32] is a mixture containing ten kinds of normal alkanes. Feed composition and the physical properties of this oil sample are obtained from [33] and shown in **Table 4-3**. Only the C_{ij} between methane and other components are considered, and all the D_{ij} are set to be 0. The example calculations are conducted in the two-phase vapor-liquid equilibrium region under 500 K.

Table 4-3 Feed composition and physical properties of the MY10 oil sample [16, 33]

Comp.	Feed	T_c, K	P_c, bar	ω	MW, g/mol	z_c	c_1	C_{ij} (C_1)
C_1	0.35	190.56	45.99	0.011	16.04	0.2863	0.0131	0
C_2	0.03	305.33	48.72	0.099	30.07	0.2776	0.0099	0
C_3	0.04	369.83	42.48	0.152	44.1	0.2769	0.0078	0
nC_4	0.06	425.13	37.96	0.201	58.12	0.2738	0.0064	0
nC_5	0.04	469.7	33.7	0.251	72.15	0.2684	0.0043	0.02
nC_6	0.03	507.82	30.34	0.299	86.18	0.2656	0.0031	0.02
nC_7	0.05	540.13	27.36	0.349	100.21	0.2632	0.00095	0.025
nC_8	0.05	569.32	24.97	0.393	114.23	0.2565	0.000195	0.025
nC_{10}	0.3	617.7	21.03	0.488	142.29	0.2501	-0.0023	0.035
nC_{14}	0.05	693	15.7	0.643	198.39	0.24	-0.0077	0.045

Figure 4-10 shows the pressure prediction results for this oil sample as a function of molar density (mol/L). We try two methodologies for incorporating the Abudour *et al.* volume translation into the two-phase VT equilibrium calculations, i.e., applying it to the liquid

132

phase (Figure 4-10a) and applying it to the vapor phase (Figure 4-10b). The ρ_{liquid}-P and ρ_{vapor}-P curves calculated by the PT equilibrium calculation algorithms (with or without incorporating volume translation) are used for comparison. The calculation results for both the liquid phase and vapor phase by using our algorithm without the volume translation match very well with the ones calculated by the PT equilibrium calculation algorithms. Without applying the volume shift model, the pressures in the liquid phase and vapor phase are exactly the same. However, by applying the volume translation method, the pressures calculated by different phases become different. By applying Abudour *et al.* VTPR-EOS, the pressures predicted based on the liquid phase are shifted downwards significantly. Using the predicted results from PR-EOS as the references, the differences in the calculated pressure can reach over 30%. As a contrast, the pressures predicted by applying the volume translation to the vapor phase only are only slightly shifted. This problem does not appear when we predict the pressure in the liquid phase region. Abudour *et al.* [17] already proved that their volume translation function for mixtures is capable of providing reliable predictions of liquid densities in both the vapor-liquid equilibrium region and single liquid phase region. Here we also show that we can obtain more accurate pressure predictions by applying the volume translation method to the liquid phase. Overall, it is *a posteriori* effective approach to replace the system pressure with the pressure corrected by applying the Abudour *et al.* VTPR-EOS [17] to the liquid phase only.
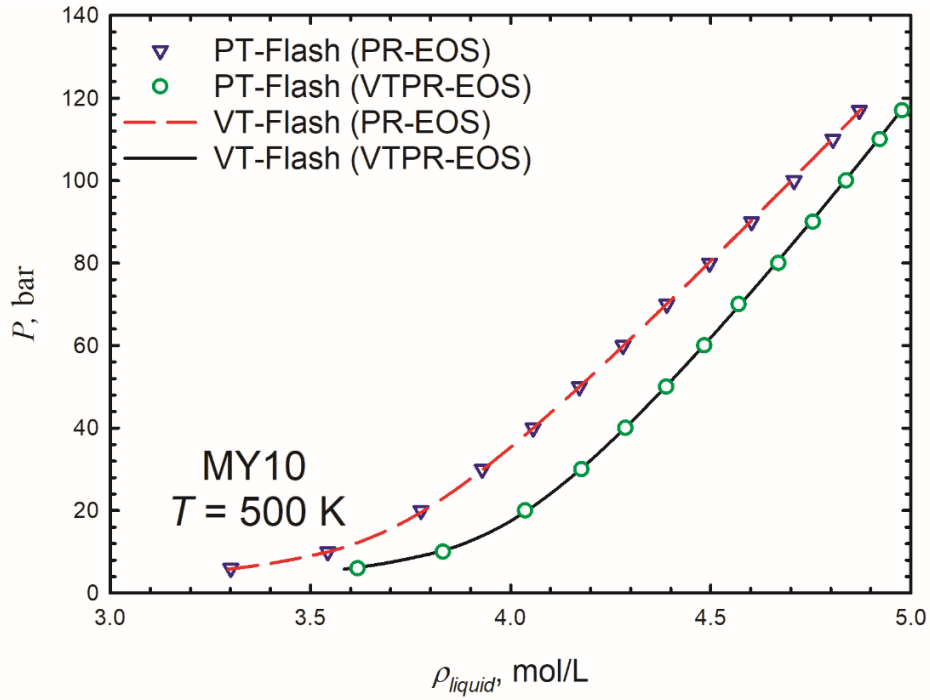
(a)
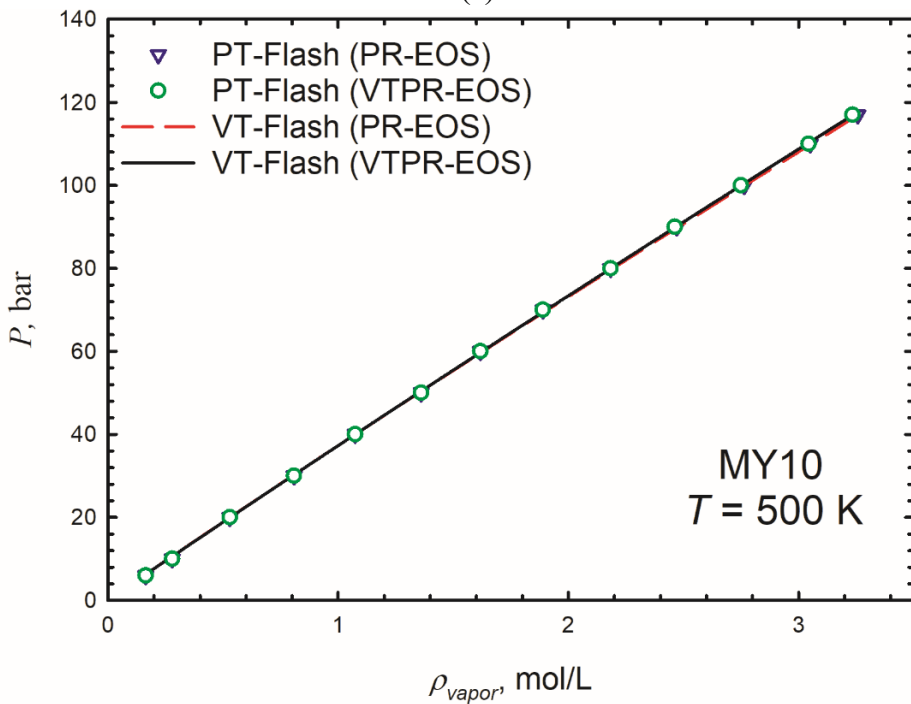
(b)

Figure 4-10 Comparison of the pressure calculation results for the oil sample MY10 obtained by the PR-EOS-based [1] PT equilibrium calculation algorithm and the VTPR-EOS-based [17] VT equilibrium calculation algorithm at 500 K : (a) liquid phase; (b) vapor phase.

4.4 Conclusions

In this work, to obtain a better prediction of pressure, a practical methodology is proposed by applying the Abudour *et al.* VTPR-EOS [17] in VT-based equilibrium calculations. We test the performance of the proposed methodology in predicting the pressures in the single liquid phase and the two-phase vapor-liquid regions. Algorithms are developed to predict the pressures of the single liquid phase equilibria and the two-phase equilibria by incorporating the Abudour *et al.* VTPR-EOS model [17] to the VT-based phase equilibrium calculation algorithm. Single liquid phase pressures for 18 pure substances and two hydrocarbon mixtures are predicted using the developed algorithms and compared to the calculated pressures using the original PR-EOS. The comparison results show that the accuracy of pressure predictions for both the pure substances and the mixtures can be significantly improved by incorporating the Abudour *et al.* VTPR-EOS model [17] to the VT-based phase equilibrium algorithm. The overall *ADD%* of pressure prediction for the 18 pure substance decreases from 109.75% (using PR-EOS [1]) to 18.46% (using VTPR-EOS [17]). Lastly, we apply the proposed algorithm to the two-phase VT phase equilibrium calculations for the oil sample MY10. We replace the system pressure with the pressure corrected by applying the Abudour *et al.* VTPR-EOS [17] to the liquid phase only. The calculation results demonstrate that we can obtain more accurate pressure predictions by applying the Abudour *et al.* VTPR-EOS [17] to the VT flash results compared to the scenario where only the original PR-EOS is used.

Due to the fact that more accurate pressure predictions for both single liquid phase

equilibria and vapor-liquid equilibria are achieved by our method, the collapse risk of the

reservoir simulator that employs the VT-flash is significantly reduced. However, as we use

the liquid phase to represent the vapor-liquid two-phase equilibrium pressure, pressure

discontinuity may be observed at the phase boundary, posing a negative influence on the

performance of the reservoir simulator that incorporates our VT-flash methodology. Future

works are needed to address this issue.

Nomenclature

a	attraction parameter, $L^2 \cdot bar \cdot mol^{-2}$
$AAD\%$	average percentage absolute deviation, %
b	repulsion parameter, L
c_0	volume translation term
c_1	constant in Abudour *et al.* model [17]
C_{ij}, D_{ij}	binary interaction parameters
d	distance function, unit, cm
err	tolerance
MW	molecular weight, g/mol
NDP	number of data points
P	pressure, bar
P_c	critical pressure, bar
P_{cal}	calculated pressure, bar
P_{exp}	measured pressure, bar

P_t	pressure after translation
R	gas constant, 8.314 J/(mol·K)
T	temperature, K
T_c	critical temperature, K
v	molar volume calculated by PR-EOS, L/mol
v_c	critical volume predicted from PR-EOS, L/mol
v^{exp}_c	true critical volume, L/mol
v_t	molar volume after volume translation, L/mol
x	mole fraction of substance
z_c^{exp}	experimental critical compressibility factor
z_c^{EOS}	compressibility factor calculated by PR-EOS, 0.3074
α	alpha function
δ	volume correction at critical temperature
ω	acentric factor
ρ	molar density, mol/L
$\rho_{overall}$	overall molar density, mol/L
$\rho_{liquid}, \rho_{vapor}$	molar density of liquid/vapor phase, mol/L
θ	surface fraction of compound

Subscripts

i, j	component indicator
m	parameters for mixtures

4.5 References

[1]   Peng, D. Y., and Robinson, D. B. (1976). A new two-constant equation of state. *Industrial & Engineering Chemistry Fundamentals*, 15(1), 59-64.

[2]   Martin, J. J. (1967). Equations of state - Applied thermodynamics symposium. *Industrial & Engineering Chemistry*, 59(12), 34-52.

[3]   Péneloux, A., Rauzy, E., and Fréze, R. (1982). A consistent correction for Redlich-Kwong-Soave volumes. *Fluid Phase Equilibria*, 8(1), 7-23.

[4]   Soave, G. (1972). Equilibrium constants from a modified Redlich-Kwong equation of state. *Chemical Engineering Science*, 27(6), 1197-1203.

[5]   Magoulas, K., and Tassios, D. (1990). Thermophysical properties of n-alkanes from C1 to C20 and their prediction for higher ones. *Fluid Phase Equilibria*, 56, 119-140.

[6]   Ungerer, P., and Batut, C. (1997). Prédiction des propriétés volumétriques des hydrocarbures par une translation de volume améliorée. *Revue de l'institut français du pétrole*, 52(6), 609-623.

[7]   Pellegrini, L. A., Moioli, S., Gamba, S., and Ceragioli, P. (2012). Prediction of volumetric properties of fluids for oil and gas applications. *Fluid Phase Equilibria*, 317, 52-58.

[8]   Baled, H., Enick, R. M., Wu, Y., McHugh, M. A., Burgess, W., Tapriyal, D., and Morreale, B. D. (2012). Prediction of hydrocarbon densities at extreme conditions

using volume-translated SRK and PR equations of state fit to high temperature, high pressure PVT data. *Fluid Phase Equilibria*, 317, 65-76.

[9]   Shi, J., Li, H., and Pang, W. (2018). An improved volume translation strategy for PR EOS without crossover issue. *Fluid Phase Equilibria*, 470, 164-175.

[10]   Pfohl. O. (1999) Letter to the editor: Evaluation of an improved volume translation for the prediction of hydrocarbon volumetric properties. *Fluid Phase Equilibria*, 163, 157–159.

[11]   Ungerer, P., and de Sant'Ana, H. B. (1999). Evaluation of an improved volume translation for the prediction of hydrocarbon volumetric properties. *Fluid Phase Equilibria*, 1(163), 161-162.

[12]   Jaubert, J. N., Privat, R., Le Guennec, Y., and Coniglio, L. (2016). Note on the properties altered by application of a Péneloux–type volume translation to an equation of state. *Fluid Phase Equilibria*, 419, 88-95.

[13]   Shi, J., and Li, H. (2016). Criterion for determining crossover phenomenon in volume-translated equation of states. *Fluid Phase Equilibria*, 430, 1-12.

[14]   Chou, G. F., and Prausnitz, J. M. (1989). A phenomenological correction to an equation of state for the critical region. *AIChE Journal*, 35(9), 1487-1496.

[15]   Matheis, J., Müller, H., Lenz, C., Pfitzner, M., and Hickel, S. (2016). Volume translation methods for real-gas computational fluid dynamics simulations. *The*

Journal of Supercritical Fluids, 107, 422-432.

[16]   Abudour, A. M., Mohammad, S. A., Robinson Jr, R. L., and Gasem, K. A. (2012). Volume-translated Peng–Robinson equation of state for saturated and single-phase liquid densities. *Fluid Phase Equilibria*, 335, 74-87.

[17]   Abudour, A. M., Mohammad, S. A., Robinson Jr, R. L., and Gasem, K. A. (2013). Volume-translated Peng-Robinson equation of state for liquid densities of diverse binary mixtures. *Fluid Phase Equilibria*, 349, 37-55.

[18]   Castier, M. (2014). Helmholtz function-based global phase stability test and its link to the isothermal–isochoric flash problem. *Fluid Phase Equilibria*, 379, 104-111.

[19]   Mikyška, J., and Firoozabadi, A. (2012). Investigation of mixture stability at given volume, temperature, and number of moles. *Fluid Phase Equilibria*, 321, 1-9.

[20]   Nichita, D. V. (2017). Fast and robust phase stability testing at isothermal-isochoric conditions. *Fluid Phase Equilibria*, 447, 107-124.

[21]   Mikyška, J., and Firoozabadi, A. (2011). A new thermodynamic function for phase-splitting at constant temperature, moles, and volume. *AIChE Journal*, 57(7), 1897-1904.

[22]   Jindrová, T., and Mikyška, J. (2015). General algorithm for multiphase equilibria calculation at given volume, temperature, and moles. *Fluid Phase Equilibria*, 393, 7-25.

[23] Nichita, D. V. (2018). A volume-based approach to phase equilibrium calculations at pressure and temperature specifications. *Fluid Phase Equilibria*, 461, 70-83.

[24] Lu, C., Jin, Z., and Li, H. (2019). A two-phase flash algorithm with the consideration of capillary pressure at specified mole numbers, volume and temperature. *Fluid Phase Equilibria*, 485, 67-82.

[25] Robinson, D. B., and Peng, D. Y. (1978). The characterization of the heptanes and heavier fractions for the GPA Peng-Robinson programs. *Gas Processors Association*.

[26] Chueh, P. L., and Prausnitz, J. M. (1967). Vapor-liquid equilibria at high pressures: Calculation of critical temperatures, volumes, and pressures of nonpolar mixtures. *AIChE Journal*, 13(6), 1107-1113.

[27] Aalto, M., Keskinen, K. I., Aittamaa, J., and Liukkonen, S. (1996). An improved correlation for compressed liquid densities of hydrocarbons. Part 2. Mixtures. *Fluid Phase Equilibria*, 114(1-2), 21-35.

[28] NIST Standard Reference Database Number 69, National Institute of Standards and Technology. http://webbook.nist.gov.

[29] Parrish, W. R. (1984). Compressed liquid densities of ethane-propane mixtures between 10 and 49 ℃ at pressures up to 9.6 MPa. *Fluid Phase Equilibria*, 18(3), 279-297.

[30] Miyamoto, H., and Uematsu, M. (2008). The (p, ρ, T, x) properties of (x1 propane+

x2 n-butane) with x1= (0.0000, 0.2729, 0.5021, and 0.7308) over the temperature range from (280 to 440) K at pressures from (1 to 200) MPa. *The Journal of Chemical Thermodynamics*, 40(2), 240-247.

[31] Abudour, A. M., Mohammad, S. A., Robinson Jr, R. L., and Gasem, K. A. (2013). Supplementary Material for 'Volume-translated Peng-Robinson equation of state for liquid densities of diverse binary mixtures'. *Fluid Phase Equilibria*, 349, 37-55.

[32] Yarborough, L. (1972). Vapor-liquid equilibrium data for multicomponent mixtures containing hydrocarbon and nonhydrocarbon components. *Journal of Chemical and Engineering Data*, 17(2), 129-133.

[33] Firoozabadi, A., and Pan, H. (2002). Fast and robust algorithm for compositional modeling: Part I-stability analysis testing. *SPE Journal*, 7(1), 78-89.

CHAPTER 5 CONCLUSIONS, CONTRIBUTIONS AND RECOMMENDATIONS

5.1 Conclusions and Scientific Contributions to the Literature

In this dissertation, we develop robust and efficient two-phase equilibrium calculation algorithms by taking the consideration of capillary pressure in confined pores, and three-phase equilibrium calculation algorithms at specified volume, temperature and mole numbers. Moreover, to increase the pressure prediction accuracy, a practical methodology for incorporating the volume-translated equation of states in VT phase equilibrium calculations is proposed. The main conclusions of this thesis are summarized as follows:

Chapter 2:

In this chapter, we develop an alternative two-phase split algorithm by considering the effect of capillary pressure at constant volume, temperature and mole numbers of components based on Mikyška and Firoozabadi's theory (2011). To improve the robustness of our algorithm, the following measures are proposed:

1) Firstly, we propose a method to determine the correct root of volume fraction by selecting the one leading to the minimum Helmholtz free energy (Michelsen, 1999), which ensures the robustness of our algorithm near the dewpoint at low temperatures.

2) Secondly, an improved scheme of updating k_i values is adopted to resolve the convergence issue that is encountered when conducting two-phase VT under low temperature and high overall molar density conditions.

We use four examples to test the robustness and correctness of our algorithms, leading to the following conclusions:

1) Using the first example, it is shown that our VT flash algorithm with capillarity can give the same flash results as the PT flash algorithm with capillarity (Liu *et al.*, 2017);

2) As for the vapor-liquid phase boundary, under the effect of capillarity, the bubble point occurs at a larger overall molar density, but the dew point occurs at either a larger or smaller overall molar density, depending on the location of the phase envelope. The phase envelopes calculated under different pore sizes intersect with the bulk phase envelope at the critical point, where the capillary pressure is zero due to zero IFT. We can also detect a higher cricondentherm point in the *c-T* plot when capillarity is considered in the VT flash.

3) As for the vapor-liquid equilibria, the capillarity effect results in a smaller equilibrium pressure, smaller mass densities of both phases, a smaller liquid-phase saturation and a larger vapor-phase saturation. Capillarity also leads to higher mole fractions of the relatively lighter component, but lower mole fractions of the relatively heavier component in both phases.

4) Our algorithm can be also used to model the liquid-liquid equilibrium. However, in our example, due to the small IFT between the two liquid phases, we hardly see the noticeable effect of the capillary pressure on the phase boundary and the fluid properties.

Chapter 3:

In this chapter, we develop a robust and simple VT flash algorithm for conducting three-phase equilibrium calculations for CO_2-inclusive mixtures. We draw the following conclusions in this chapter:

1) The VT three-phase flash calculation algorithm is built using a nested approach. The PT three-phase flash code is used in the inner loop without any further modifications, while an effective equation-solving method, i.e., the Brent (1971) method, is applied in the outer loop to solve for the pressure corresponding to a given volume-temperature specification.

2) The robustness of the newly developed VT flash algorithm is safeguarded with the combined use of the trust-region-method-based PT flash solver and the Brent (1971) solver. These two solvers are shown to be very robust in previous studies as well as in the present study.

3) Our example calculations demonstrate that the new VT flash algorithm is always able to converge to the correct phase equilibria including one-phase equilibria,

vapor-liquid or liquid-liquid two-phase equilibria, and vapor-liquid-liquid three-phase equilibria.

4) The new algorithm is shown to be relatively efficient. On average, one time of calling the PT solver is needed to converge the VT flashes for one-phase equilibria, while fewer than 10 times of calling the PT solver are required to converge the VT flashes for two-phase and three-phase equilibria.

5) The potential applications of the developed VT flash algorithm are multifold. In particular, the VT flash algorithm presented in this study can be potentially leveraged to provide reliable initializations in the phase envelope construction algorithm. This opens the door of developing new robust phase-envelope construction algorithms based on the three-phase VT flash algorithm developed in this study.

Chapter 4:

In this chapter, we proposed a practical methodology by applying the Abudour *et al.* VTPR-EOS (Abudour *et al.*, 2012; Abudour *et al.*, 2013) in VT-based equilibrium calculations to obtain a better prediction of pressure.

1) We test the performance of the proposed methodology in predicting the pressures in the single liquid phase and the two-phase vapor-liquid regions. Algorithms are developed to predict the pressures of the single liquid phase equilibria and the two-

phase equilibria by incorporating the Abudour *et al.* VTPR-EOS model (2012; 2013) to the VT-based phase equilibrium calculation algorithm.

2) Single liquid phase pressures for 18 pure substances and two hydrocarbon mixtures are predicted using the developed algorithms and compared to the calculated pressures using the original PR-EOS (Peng and Robinson, 1976). The comparison results show that the accuracy of pressure predictions for both the pure substances and the mixtures can be significantly improved by incorporating the Abudour *et al.* VTPR-EOS model (2012; 2013) to the VT-based phase equilibrium algorithm. The overall ADD% of pressure prediction for the 18 pure substance decreases from 109.75% (using PR-EOS (Peng and Robinson, 1976)) to 18.46% (using VTPR-EOS (2012; 2013)).

3) We apply the proposed algorithm to the two-phase VT phase equilibrium calculations for the oil sample MY10 (Yarborough, 1972). We replace the system pressure with the pressure corrected by applying the Abudour *et al.* VTPR-EOS (2012; 2013) to the liquid phase only. The calculation results demonstrate that we can obtain more accurate pressure predictions by applying the Abudour *et al.* VTPR-EOS (2012; 2013) to the VT flash results compared to the scenario where only the original PR-EOS is used.

4) Since we achieve more accurate pressure predictions for both liquid phase and vapor-liquid equilibrium phase using our method, the collapse risk of the reservoir

simulator that employs the proposed VT-flash methodology is significantly reduced. However, as we use the liquid phase to represent the two-phase equilibrium pressure, pressure discontinuity may be observed at the phase boundary. Such issue needs to be addressed in future works.

5.2 Suggested Future Work

- In this thesis, we developed robust and efficient two-phase equilibrium calculation algorithms by consideration of capillary pressure in confined pores, and three-phase equilibrium calculation algorithms at specified volume, temperature and mole numbers. In the future, firstly, we can couple them into compositional reservoir-flow and wellbore-flow simulators that are more conducive to isochoric phase equilibrium computations. Secondly, we can apply them to aid engineering design calculations for constant-volume containers in the petroleum and chemical industry (such as storage tanks). Thirdly, we can also apply our algorithm to guide the phase equilibrium measurements in a fixed-volume PVT cell.

- As mentioned in Chapter 2, the unconventional reservoirs, such as shale and tight reservoirs, play very important roles in fulfilling the global energy supply nowadays. Besides the vapor-liquid equilibria residing in the nanopores, previous studies have shown that there is a considerable quantity of shale oil existing in the dissolved state in the organic matters in shale reservoirs (Ertas, 2006). Kerogen is the key component in these organic matters and shows a dissolving effect for

hydrocarbons. The dissolution and liberation of hydrocarbons in kerogen will change the composition of shale oil that is equilibrating with kerogen, and thereby may impose a significant impact on the phase behavior of shale oil. VT-based equilibrium calculation algorithm can be developed to model the three-phase gas-oil-kerogen equilibria in shale oil reservoirs.

- Moreover, four-phase vapor-liquid-liquid-aqueous or vapor-liquid-aqueous-asphaltene equilibria can commonly appear in reservoirs containing water and asphaltenic oil. It is worthwhile of developing a suite of robust and efficient four-phase vapor-liquid-aqueous-asphaltene equilibrium calculation algorithms at given volume, temperature and composition. This task is, however, much more complex and requires a much more careful design of the algorithm configurations.

5.3 References

Abudour, A. M., Mohammad, S. A., Robinson Jr, R. L., and Gasem, K. A. (2012). Volume-translated Peng–Robinson equation of state for saturated and single-phase liquid densities. *Fluid Phase Equilibria*, **335**, 74-87.

Abudour, A. M., Mohammad, S. A., Robinson Jr, R. L., and Gasem, K. A. (2013). Volume-translated Peng-Robinson equation of state for liquid densities of diverse binary mixtures. *Fluid Phase Equilibria,* **349**, 37-55.

Brent, R.P. (1971). An algorithm with guaranteed convergence for finding a zero of a function. *The Computer Journal,* **14**(4), 422-5.

Ertas, D., Kelemen, S. R., and Halsey, T. C. (2006). Petroleum expulsion part 1. Theory of kerogen swelling in multicomponent solvents. *Energy & Fuels*, **20**(1), 295-300.

Liu, Y., Jin, Z., and Li, H. (2017). Comparison of PR-EOS with capillary pressure model with engineering density functional theory on describing the phase behavior of confined hydrocarbons. *SPE Journal*, **23**(5), 1784-1797.

Michelsen, M. L. (1999). State function based flash specifications. *Fluid Phase Equilibria,* **158-160**, 617-626.

Mikyska, J. and Firoozabadi, A. (2011). A new thermodynamic function for phase-splitting at constant temperature, moles, and volume. *AIChE Journal*, **57**(7), 1897-1904.

Peng, D. Y., and Robinson, D. B. (1976). A new two-constant equation of state. *Industrial*

& Engineering Chemistry Fundamentals, **15**(1), 59-64.

Yarborough, L. (1972). Vapor-liquid equilibrium data for multicomponent mixtures containing hydrocarbon and nonhydrocarbon components. *Journal of Chemical and Engineering Data*, **17**(2), 129-133.

BIBLIOGRAPHY

Aalto, M., Keskinen, K. I., Aittamaa, J., and Liukkonen, S. (1996). An improved correlation for compressed liquid densities of hydrocarbons. Part 2. Mixtures. *Fluid Phase Equilibria*, **114**(1-2), 21-35.

Abudour, A. M., Mohammad, S. A., Robinson Jr, R. L., and Gasem, K. A. (2012). Volume-translated Peng–Robinson equation of state for saturated and single-phase liquid densities. *Fluid Phase Equilibria*, **335**, 74-87.

Abudour, A. M., Mohammad, S. A., Robinson Jr, R. L., and Gasem, K. A. (2013). Volume-translated Peng-Robinson equation of state for liquid densities of diverse binary mixtures. *Fluid Phase Equilibria*, **349**, 37-55.

Agarwal, R.K., Li, Y.K., Nghiem, L.X., and Coombe, D.A. (1991). Multiphase multicomponent isenthalpic flash calculations. *Journal of Canadian Petroleum Technology*, **30**(3), 69-75.

Agger, C.S. and Sørensen, H. (2018). Algorithm for constructing asphaltene PT and Px phase diagrams. *Industrial & Engineering Chemistry Research*, **57**(1), 392-400.

Alfi, M., Nasrabadi, H., and Banerjee, D. (2016). Experimental investigation of confinement effect on phase behavior of hexane, heptane and octane using lab-on-a-chip technology. *Fluid Phase Equilibria*, **423**, 25-33.

Baled, H., Enick, R. M., Wu, Y., McHugh, M. A., Burgess, W., Tapriyal, D., and Morreale,

B. D. (2012). Prediction of hydrocarbon densities at extreme conditions using volume-translated SRK and PR equations of state fit to high temperature, high pressure PVT data. *Fluid Phase Equilibria*, **317**, 65-76.

Brent, R.P. (1971). An algorithm with guaranteed convergence for finding a zero of a function. *The Computer Journal*, **14**(4), 422-425.

Castier, M. (2014). Helmholtz function-based global phase stability test and its link to the isothermal–isochoric flash problem. *Fluid Phase Equilibria*, **379**, 104-111.

Chou, G. F., and Prausnitz, J. M. (1989). A phenomenological correction to an equation of state for the critical region. *AIChE Journal*, **35**(9), 1487-1496.

Chueh, P. L., and Prausnitz, J. M. (1967). Vapor-liquid equilibria at high pressures: Calculation of critical temperatures, volumes, and pressures of nonpolar mixtures. *AIChE Journal*, **13**(6), 1107-1113.

Cismondi, M., Ndiaye, P.M., and Tavares, F.W. (2018). A new simple and efficient flash algorithm for T-v specifications. *Fluid Phase Equilibria*, **464**, 32-39.

Connolly, M., Pan, H., and Tchelepi, H. (2019). Three-phase equilibrium computations for hydrocarbon-water mixtures using a reduced variables method. *Industrial & Engineering Chemistry Research*, **58**, 14954-14974.

Dekker, T.J. (1969). Finding a zero by means of successive linear interpolation, in *Constructive Aspects of the Fundamental Theorem of Algebra*, B. Dejon and P.

Henrici (editors), Wiley-Interscience, New York, 37–48.

Ertas, D., Kelemen, S. R., and Halsey, T. C. (2006). Petroleum expulsion part 1. Theory of kerogen swelling in multicomponent solvents. *Energy & Fuels*, **20**(1), 295-300.

Firoozabadi, A. (2015). *Thermodynamics and Applications of Hydrocarbon Energy Production,* McGraw Hill Professional.

Firoozabadi, A., and Pan, H. (2000). Fast and robust algorithm for compositional modeling: Part I-stability analysis testing. *SPE Journal*, **7**(1), 78-89.

Gao, J., Okuno, R., and Li, H. (2017). An experimental study of multiphase behavior for n-butane/bitumen/water mixtures. *SPE Journal*, **22**(3), 783-798.

Jaubert, J. N., Privat, R., Le Guennec, Y., and Coniglio, L. (2016). Note on the properties altered by application of a Péneloux–type volume translation to an equation of state. *Fluid Phase Equilibria*, **419**, 88-95.

Jin, Z., and Firoozabadi, A. (2016). Thermodynamic modeling of phase behavior in shale media. *SPE Journal*, **21**(1), 190-207.

Jin, Z. (2018). Bubble/dew point and hysteresis of hydrocarbons in nanopores from molecular perspective. *Fluid Phase Equilibria*, **458**, 177-185.

Jindrova, T., and Mikyska, J. (2013). Fast and robust algorithm for calculation of two-phase equilibria at given volume, temperature, and moles. *Fluid Phase Equilibria*, **353**, 101-114.

Jindrova, T., and Mikyska, J. (2015). General algorithm for multiphase equilibria calculation at given volume, temperature, and moles. *Fluid Phase Equilibra*, **393**, 7-25.

Khan, S.A., Pope, G.A., and Sepehrnoori, K. (1992). Fluid characterization of three-phase CO_2/oil mixtures. Paper SPE 24130 presented at the *SPE/DOE Enhanced Oil Recovery Symposium*, Tulsa, 22-24 April.

Kou, J., and Sun, S. (2018). A stable algorithm for calculating phase equilibria with capillarity at specified moles, volume and temperature using a dynamic model. *Fluid Phase Equilibria*, **456**, 7-24.

Kuila, U., and Prasad, M. (2013). Specific surface area and pore-size distribution in clays and shales. *Geophysical Prospecting*, **61**, 341-362.

Leibovici, C. F., and Neoschil, J. (1992). A new look at the Rachford-Rice equation. *Fluid Phase Equilibria*, **74**, 303-308.

Li, R., and Li, H. (2017). A robust three-Phase isenthalpic flash algorithm based on free-water assumption. *Journal of Energy Resources Technology,* **140**(3), 032902.

Li, R., and Li, H. (2018). New two-phase and three-phase Rachford-Rice algorithms based on free-water assumption. *The Canadian Journal of Chemical Engineering,* **96**(1), 390-403.

Li, R., and Li, H. (2019a). Improved three-phase equilibrium calculation algorithm for

water/hydrocarbon mixtures. *Fuel*, **244**(15), 517-527.

Li. R., and Li, H. (2019b). Robust three-phase vapor–liquid–asphaltene equilibrium calculation algorithm for isothermal CO_2 flooding applications. *Industrial & Engineering Chemistry Research*, **58**(34), 15666-15680.

Liu, Y., Jin, Z., and Li, H. (2018). Comparison of PR-EOS with capillary pressure model with engineering density functional theory on describing the phase behavior of confined hydrocarbons. *SPE Journal*, **23**(5), 1784-1797.

Lu, C., Jin, Z., and Li, H. (2019). A two-phase flash algorithm with the consideration of capillary pressure at specified mole numbers, volume and temperature. *Fluid Phase Equilibria*, **485**, 67-82.

Magoulas, K., and Tassios, D. (1990). Thermophysical properties of n-alkanes from C1 to C20 and their prediction for higher ones. *Fluid Phase Equilibria,* **56**, 119-140.

Martin, J. J. (1967). Equations of state—Applied thermodynamics symposium. *Industrial & Engineering Chemistry*, **59**(12), 34-52.

Matheis, J., Müller, H., Lenz, C., Pfitzner, M., and Hickel, S. (2016). Volume translation methods for real-gas computational fluid dynamics simulations. *The Journal of Supercritical Fluids*, **107**, 422-432.

Michelsen, M.L. (1980). Calculation of phase envelopes and critical points for multicomponent mixtures. *Fluid Phase Equilibria*, **4**(1-2), 1-10.

Michelsen, M. L. (1982a). The isothermal flash problem. Part I. Stability. *Fluid Phase Equilibria*, **9**(1), 1-19.

Michelsen, M. L. (1982b). The isothermal flash problem. Part II. Phase-split calculation. *Fluid Phase Equilibria*, **9**(1), 21-40.

Michelsen, M. L. (1994). Calculation of multiphase equilibrium. *Computers & Chemical Engineering*, **18**(7), 545-550.

Michelsen, M. L. (1999). State function based flash specifications. *Fluid Phase Equilibria.* **158-160**, 617-626.

Miyamoto, H., and Uematsu, M. (2008). The (p, ρ, T, x) properties of (x1 propane+ x2 n-butane) with x1=(0.0000, 0.2729, 0.5021, and 0.7308) over the temperature range from (280 to 440) K at pressures from (1 to 200) MPa. *The Journal of Chemical Thermodynamics*, **40**(2), 240-247.

Mikyska, J., and Firoozabadi, A. (2011). A new thermodynamic function for phase-splitting at constant temperature, moles, and volume. *AIChE Journal*, **57**(7), 1897-1904.

Mikyška, J., and Firoozabadi, A. (2012). Investigation of mixture stability at given volume, temperature, and number of moles. *Fluid Phase Equilibria*, **321**, 1-9.

Molina, M.J., Rodriguez-Reartes, S.B., and Zabaloy, M.S. (2019). Computation and analysis of binary multiphase isochors. *Fluid Phase Equilibria,* **500**, 112227.

Nelson, P. H. (2009). Pore-throat sizes in sandstones, tight sandstones, and shales. *AAPG Bulletin*, **93**(3), 329-340.

Nichita, D. V. (2017). Fast and robust phase stability testing at isothermal-isochoric conditions. *Fluid Phase Equilibria*, **447**, 107-124.

Nichita, D.V. (2018). New unconstrained minimization methods for robust flash calculations at temperature, volume and moles specifications. *Fluid Phase Equilibria*, **466**, 31-47.

Nichita, D.V. (2019). A simple approximate density-based phase envelope construction method. *Fluid Phase Equilibria*, **499**(1), 112245.

NIST Standard Reference Database Number 69, National Institute of Standards and Technology http://webbook.nist.gov.

Nocedal, J., and Wright, S.J. (2006). *Numerical Optimization*. Springer: New York.

Nojabaei, B., Johns, R. T., and Chu, L. (2013). Effect of capillary pressure on phase behavior in tight rocks and shales. *SPE Reservoir Evaluation & Engineering*, **16**(03), 281-289.

Okuno, R., Johns, R. T., and Sepehrnoori, K. (2009). Three–phase flash in compositional simulation using a reduced method. *SPE Journal*, **15**(3), 689-703.

Pan, H., Chen, Y., Sheffield, J., Chang, Y. B., and Zhou, D. (2015). Phase-behavior modeling and flow simulation for low-temperature CO_2 injection. *SPE Reservoir*

Evaluation & Engineering, **18**(02), 250-263.

Pan, H., Connolly, M., and Tchelepi, H. (2019). Multiphase equilibrium calculation framework for compositional simulation of CO_2 injection in low-temperature reservoirs. *Industrial & Engineering Chemistry Research,* **58**, 2052-2070.

Pang, W., and Li, H. (2017). An augmented free-water three-phase flash algorithm for CO_2/hydrocarbon/water mixtures. *Fluid Phase Equilibria,* **450**, 86-98.

Parrish, W. R. (1984). Compressed liquid densities of ethane-propane mixtures between 10 and 49° C at pressures up to 9.6 MPa. *Fluid Phase Equilibria*, **18**(3), 279-297.

Parsa, E., Yin, X., and Ozkan, E. (2015). Direct observation of the impact of nanopore confinement on petroleum gas condensation. In *SPE Annual Technical Conference and Exhibition*. Society of Petroleum Engineers.

Pasqualette, M. D., Carneiro, J., Johansen, S. T., Lovfall, B. T., Fonseca Jr., R., and Ciambelli, J. (2020). A numerical assessment of carbon-dioxide-rich two-phase flows with dense phases in offshore production pipelines. *SPE Journal*, **25**(2), 712-731.

Pellegrini, L. A., Moioli, S., Gamba, S., and Ceragioli, P. (2012). Prediction of volumetric properties of fluids for oil and gas applications. *Fluid Phase Equilibria*, **317**, 52-58.

Péneloux, A., Rauzy, E., and Fréze, R. (1982). A consistent correction for Redlich-Kwong-Soave volumes. *Fluid Phase Equilibria*, **8**(1), 7-23.

Peng, D. Y., and Robinson, D. B. (1976). A new two-constant equation of state. *Industrial & Engineering Chemistry Fundamentals*, **15**(1), 59-64.

Petitfrere, M. and Nichita, D.V. (2014). Robust and efficient trust-region based stability analysis and multiphase flash calculations. *Fluid Phase Equilibria*, **362**, 51−68.

Petitfrere, M., Nichita, D.V., Voskov, D., Zaydullin, R., and Bogdanov, I. (2020). Full-EOS based thermal multiphase compositional simulation of CO_2 and steam injection processes. *Journal of Petroleum Science and Engineering*, **192**, 107241.

Pfohl. O. (1999). Letter to the editor: Evaluation of an improved volume translation for the prediction of hydrocarbon volumetric properties. *Fluid Phase Equilibria*, **163**, 157–159.

Qiao, S. Z., Bhatia, S. K., and Nicholson, D. (2004). Study of hexane adsorption in nanoporous MCM-41 silica. *Langmuir*, **20**(2), 389-395.

Quayle, O. R. (1953). The Parachors of organic compounds. An interpretation and catalogue. *Chemical Reviews*, **53**(3), 439-589.

Rachford Jr, H. H., and Rice, J. D. (1952). Procedure for use of electronic digital computers in calculating flash vaporization hydrocarbon equilibrium. *Journal of Petroleum Technology*, **4**(10), 19-3.

Robinson, D. B., and Peng, D. Y. (1978). The characterization of the heptanes and heavier fractions for the GPA Peng-Robinson programs. *Gas Processors Association*.

Sandoval, D. R., Yan, W., Michelsen, M. L., and Stenby, E. H. (2016). The phase envelope of multicomponent mixtures in the presence of a capillary pressure difference. *Industrial & Engineering Chemistry Research*, **55**(22), 6530-6538.

Sherafati, M., and Jessen, K. (2017). Stability analysis for multicomponent mixtures including capillary pressure. *Fluid Phase Equilibria*, **433**, 56-66.

Shi, J., and Li, H. (2016). Criterion for determining crossover phenomenon in volume-translated equation of states. *Fluid Phase Equilibria*, **430**, 1-12.

Shi, J., Li, H., and Pang, W. (2018). An improved volume translation strategy for PR EOS without crossover issue. *Fluid Phase Equilibria*, **470**, 164-175.

Soave, G. (1972). Equilibrium constants from a modified Redlich-Kwong equation of state. *Chemical Engineering Science*, **27**(6), 1197-1203.

Stimpson, B. C., and Barrufet, M. A. (2016). Thermodynamic modeling of pure components including the effects of capillarity. *Journal of Chemical & Engineering Data*, **61**(8), 2844-2850.

Ungerer, P., and Batut, C. (1997). Prédiction des propriétés volumétriques des hydrocarbures par une translation de volume améliorée. *Revue de L'institut Français du Pétrole*, **52**(6), 609-623.

Ungerer, P., and de Sant'Ana, H. B. (1999). Evaluation of an improved volume translation for the prediction of hydrocarbon volumetric properties. *Fluid Phase*

Equilibria, **1**(163), 161-162.

Walton, J. P. R. B., and Quirke, N. P. R. B. (1989). Capillary condensation: a molecular simulation study. *Molecular Simulation*, **2**(4-6), 361-391.

Weinaug, C. F., and Katz, D. L. (1943). Surface tensions of methane-propane mixtures. *Industrial & Engineering Chemistry*, **35**(2), 239-246.

Wilson, G. M. (1969). A modified Redlich-Kwong equation of state, application to general physical data calculations. In *65th National AIChE Meeting*, Cleveland, OH, USA.

Young, T. (1805). III. An essay on the cohesion of fluids. *Philosophical Transactions of the Royal Society of London*, **95**, 65-87.

Yarborough, L. (1972). Vapor-liquid equilibrium data for multicomponent mixtures containing hydrocarbon and nonhydrocarbon components. *Journal of Chemical and Engineering Data*, **17**(2), 129-133.